



UNIVERSITÄT  
BAYREUTH

# **Complex Polymer Electrospun Nanofibers for Drug Delivery Applications**

DISSERTATION

zur Erlangung des akademischen Grades einer Doktorin der

Naturwissenschaften (Dr. rer. nat.)

in der Bayreuther Graduiertenschule für Mathematik und Naturwissenschaften

(BayNAT)

der Universität Bayreuth

vorgelegt von

**Mina Heidari**

Aus Isfahan, Iran

Bayreuth, 2021

Die vorliegende Arbeit wurde in der Zeit von Juni 2017 bis Oktober 2021 am Lehrstuhl Makromolekulare Chemie II der Universität Bayreuth unter Betreuung von Herrn Professor Dr. Andreas Greiner angefertigt.

Vollständiger Abdruck der von der Bayreuther Graduiertenschule für Mathematik und Naturwissenschaften (BayNat) der Universität Bayreuth genehmigten Dissertation zur Erlangung des akademischen Grades einer Doktorin der Naturwissenschaften (Dr. rer. Nat.).

Dissertation eingereicht am: 27.10.2021

Zulassung durch das Leitungsgremium: 22.11.2021

Wissenschaftliches Kolloquium: 15.02.2022

Amtierender Direktor: Prof. Dr. Hans Keppler

Prüfungsausschuss:

Prof. Dr. Andreas Greiner (Gutachter)

Dr. Sahar Salehi (Gutachterin)

Prof. Dr. Anna Schenk (Vorsitz)

Prof. Dr. Ruth Freitag

Die vorliegende Arbeit ist als Monographie verfasst.

Teile der Arbeit sind bereits in den folgenden Publikationen erscheinen:

**Direct electrospinning of cellulose in the DBU-CO<sub>2</sub> switchable solvent system.**

Mina, Kelechukwu N. Onwukamike, Etienne Grau, Stéphane Grelier, Henri Cramail, Michael AR Meier, and Andreas Greiner. (2021). *Cellulose*, 1-12.

**DOI:** 10.1007/s10570-021-03967-8

Diese Publikation ist in der vorliegenden Arbeit mit der Literaturstelle [175] zitiert.

**Meeting the needs of a potent carrier for malaria treatment: Encapsulation of artemisone in poly(lactide-co-glycolide) micro- and nanoparticles.**

Mina Heidari, Jacob Golenser, and Andreas Greiner. accepted.

**To my beautiful mom**

## List of Symbols and Abbreviations

<b>°C</b>	Degree Celcius
<b>CA</b>	Cellulose Acetate
<b>μl</b>	Microliters
<b>ml</b>	Mililiters
<b>μm</b>	Micrometers
<b>nm</b>	Nanometers
<b>h</b>	Hours
<b>g</b>	Gram
<b>ART</b>	Artemisone
<b>ACT</b>	Artemisinin-based Combination Therapy
<b>Expt.</b>	Experiment
<b>RSM</b>	Response Surface Methodology
<b>SLN</b>	Solid Lipid Nanoparticles
<b>AuNPs</b>	Gold Nanoparticles
<b>PLGA</b>	Poly (lactide-co-glycolide)
<b>CNT</b>	Carbon Nanotubes
<b>BBD</b>	Box-Benkhen Design
<b>DOE</b>	Design of Experiment
<b>DHA</b>	Dihydroxyartemisinin
<b>mPEG</b>	α-methoxy-ω-hydroxy-poly (ethylene glycol)
<b>PCL</b>	Polycaprolactone
<b>PLA</b>	Poly (lactic acid)
<b>PGA</b>	Poly (glycolic acid)
<b>PEG</b>	Polyethylene Glycole
<b>MCC</b>	Microcrystalline Cellulose

<b>PVP</b>	Polyvinylpyrrolidone
<b>EC</b>	Ethyl Cellulose
<b>CP</b>	Cellulose Pulp
<b>SDS</b>	Sodium Dodecyl Sulfate
<b>BSA</b>	Bovine Serum Albumin
<b>DDS</b>	Drug Delivery Systems
<b>TCH</b>	Tetracycline Hydrochloride
<b>FDA</b>	(US) Food and Drug Administration
<b>EDX</b>	Energy-dispersive X-ray Spectroscopy
<b>HPLC</b>	High-performance Liquid Chromatography
<b>GPC</b>	Gel Permeation Chromatography
<b>NMR</b>	Nuclear Magnetic Resonance Spectroscopy
<b>SEM</b>	Scanning Electron Microscopy
<b>TEM</b>	Transmission Electron Microscopy
<b>DLS</b>	Dynamic Laser Scattering
<b>AF4</b>	Asymmetric Field Flow Fractionation
<b>XRD</b>	X-ray Diffraction Spectroscopy
<b>DSC</b>	Differential Scanning Calorimetry
<b>TGA</b>	Thermogravimetric Analysis

# Inhaltsverzeichnis

<b>List of Symbols and Abbreviations .....</b>	<b>5</b>
<b>1 Introduction .....</b>	<b>10</b>
<b>1.1 Theoretical background .....</b>	<b>12</b>
1.1.1 Nanofibers and electrospinning .....	12
1.1.2 Co-electrospinning .....	14
1.1.3 Side-by-side electrospinning .....	14
1.1.4 Emulsion electrospinning .....	15
1.1.5 Suspension electrospinning .....	17
1.1.6 Core-shell electrospinning .....	20
<b>1.2 Studies of release mechanisms .....</b>	<b>24</b>
1.2.1 Release profile shape.....	24
1.2.2 Drug release mechanisms.....	27
1.2.3 Drug diffusion through water filled pores .....	28
1.2.4 Drug diffusion through polymer matrix .....	28
1.2.5 Osmotic pumping .....	29
1.2.6 Surface erosion .....	29
1.2.7 Bulk erosion .....	29
<b>1.3 Factors influencing drug release from PLGA-based DDSs.....</b>	<b>30</b>
1.3.1 Physiochemical processes occurring in PLGA-based DDSs.....	30
1.3.2 Factors influencing the physiochemical behavior of PLGA .....	31
<b>1.4 Development of different drug-loaded carriers .....</b>	<b>33</b>
1.4.1 Polymer-drug conjugates.....	33
1.4.2 Micelles.....	34
1.4.3 Liposome.....	36
1.4.4 Nanocapsules.....	37
1.4.5 Nanoparticles.....	39
<b>1.5 Nanomedicines .....</b>	<b>42</b>
<b>1.6 Methods for preparing drug-loaded nano and microparticles .....</b>	<b>43</b>
1.6.1 Solvent displacement method.....	43
1.6.2 Spray drying .....	47
<b>1.7 Malaria .....</b>	<b>50</b>
<b>1.8 Available treatments for Malaria .....</b>	<b>52</b>
<b>1.9 Stability of Artemisinin and its derivatives .....</b>	<b>54</b>
<b>1.10 Artemisone .....</b>	<b>54</b>
1.10.1 ART decomposition at different pHs .....	56
1.10.2 Overcoming shortcomings of ART .....	56
<b>1.11 Cellulose electrospinning.....</b>	<b>57</b>
<b>1.12 Aim and concept .....</b>	<b>60</b>
<b>2 Results and discussion .....</b>	<b>63</b>
<b>2.1 Synthesis of ART-loaded PLGA nanoparticles using solvent displacement method .....</b>	<b>63</b>
<b>2.2 Preparation of ART-loaded PLGA microparticles by spray drying method .....</b>	<b>72</b>
<b>2.3 Drug release from ART-loaded micro- and nanoparticles .....</b>	<b>81</b>
<b>2.4 Synthesis of PCL-mPEG as a biocompatible biodegradable polymer .....</b>	<b>82</b>

<b>2.5</b>	<b>Immobilization of ART-loaded PLGA nanoparticles prepared by solvent displacement into PCL-mPEG electrospun nanofibers .....</b>	<b>85</b>
2.5.1	Characterizations of electrospun nanofibers immobilized with ART-loaded nanoparticles .....	86
2.5.2	Determination of drug content in nanoparticles and in electrospun nanofibers by HPLC.....	90
2.5.3	Studies on drug release behaviors of ART from nanoparticles and electrospun nanofibers.....	92
<b>2.6</b>	<b>Immobilization of ART-loaded PLGA micro and nanoparticles into PCL-mPEG electrospun nanofibers by suspension electrospinning .....</b>	<b>99</b>
2.6.1	Characterization of electrospun nanofibers immobilized with ART-loaded PLGA micro and nanoparticles by suspension electrospinning.....	100
2.6.2	Release behavior of electrospun nanofibers immobilized with ART-loaded PLGA micro and nanoparticles by suspension electrospinning.....	104
<b>2.7</b>	<b>Immobilization of ART into PCL-mPEG electrospun nanofibers by coaxial electrospinning</b>	<b>105</b>
2.7.1	Preparation and characterization of core-shell nanofibers .....	106
2.7.2	Determination of the amount of ART in core-shell nanofibers.....	109
2.7.3	Release behavior from core-shell nanofibers.....	110
<b>2.8</b>	<b>Cellulose electrospinning using DBU-CO<sub>2</sub> switchable solvent system .....</b>	<b>111</b>
2.8.1	Investigation on microcrystalline cellulose (MCC) .....	112
2.8.2	Investigation on using cellulose pulp (CP) .....	123
<b>3</b>	<b>Experimental part.....</b>	<b>131</b>
<b>3.1</b>	<b>Materials .....</b>	<b>131</b>
<b>3.2</b>	<b>Methods .....</b>	<b>132</b>
3.2.1	Characterizations .....	132
3.2.2	Preparation of nanoparticles through solvent displacement method .....	134
3.2.3	Preparation of ART-loaded microparticles using spray drying technique.....	135
3.2.4	Determining calibration curve of ART for validating HPLC for determining the amount of ART. ....	136
3.2.5	Determination of drug loading and encapsulation efficiency .....	136
3.2.6	Release behavior of ART-loaded micro and nanoparticles using HPLC.....	137
3.2.7	Synthesis of PCL <sub>15000</sub> -b-MPEG <sub>5000</sub> .....	138
3.2.8	Preparation of ART-loaded electrospun nanofibers immobilized with ART-loaded nanoparticles	138
3.2.9	Preparation of ART-loaded electrospun nanofibers.....	139
3.2.10	Quantification of ART in ART-loaded PLGA nanoparticles and electrospun nanofibers immobilized with ART-loaded PLGA nanoparticles .....	139
3.2.11	Release behavior of different electrospun nanofibers using HPLC .....	140
3.2.12	Preparation of suspension electrospinning immobilized with ART-loaded PLGA micro and nanoparticles.....	140
3.2.13	Core-shell electrospinning .....	141
3.2.14	Solubilization of MCC and CP.....	142
3.2.15	Electrospinning of cellulose solutions .....	143
<b>4</b>	<b>Summary.....</b>	<b>145</b>
<b>5</b>	<b>Zusammenfassung.....</b>	<b>148</b>
<b>6</b>	<b>Acknowledgements .....</b>	<b>151</b>
<b>7</b>	<b>References.....</b>	<b>154</b>



# **Chapter 1**

## Introduction

# 1 Introduction

The aim of this work was to develop biodegradable electrospun polymeric nanofiber. Electrospun nanofibers have gained a lot of interest due to their high surface to volume ratio, high porosity, their ability to load different biomolecules as well as ease of functionalization. If a drug is loaded into nanofibers, there would be the possibility that the drug is located on the surface of the nanofibers and in most cases it results in a burst release, where most of the drug is released immediately after being exposed to the physiological medium. The hypothesis was to design a nanofibrous structure, in which the drug is immobilized into micro and nanoparticles to verify, whether this results in a much more prolonged release as well as protecting the drug from being degraded. For this purpose, we used Artemisone (ART), a hydrophobic drug, which could find application in cancer therapy, malaria treatment. For immobilizing the ART-loaded particles into electrospun nanofibers, different electrospinning techniques were used including co-electrospinning, suspension electrospinning as well as core-shell electrospinning.

One of the underlying concepts was to fabricate a system, which consists of electrospun nanofibers along with ART-loaded polymeric micro and nanoparticles to merit both the characteristics of nanoparticles and nanofibers as well as providing the system with a more sustained drug release in comparison to both single systems.

In the first part, two different methods were used to encapsulate ART into micro and nanoparticles namely spray drying and solvent displacement method. Both methods were investigated in order to attain the highest encapsulation and loading efficiencies using Design-expert software. Release studies were done using HPLC to compare the release behavior from both micro and nanoparticles. In the second part, nanoparticles prepared by solvent displacement method

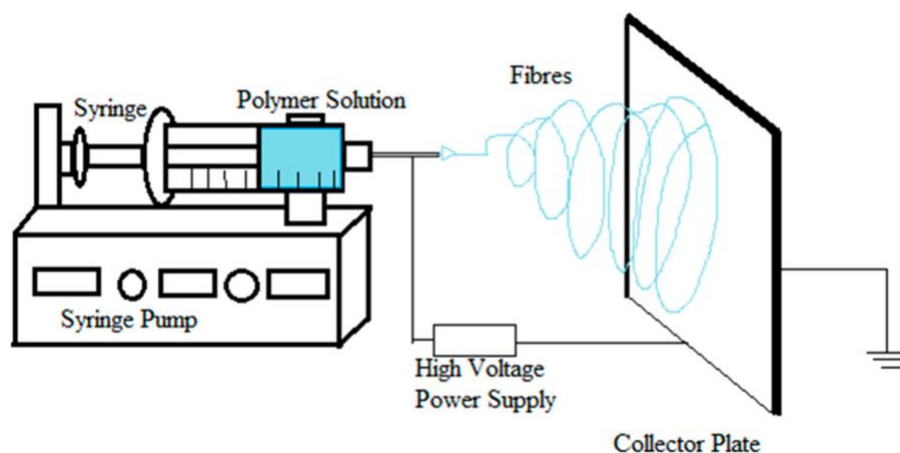
were immobilized into electrospun nanofibers to compare the release behavior with nanoparticles alone, as well as electrospun nanofibers, which are loaded with ART. Our hypothesis was to evaluate, whether the encapsulation of ART first in particles and then in nanofibers results in a more sustained release. In the third part suspension electrospinning was used in order to fabricate two different particle sizes in electrospun nanofibers including micro and nanoparticles and to compare release from them. In the fourth part, core-shell electrospun nanofibers were made, in which ART was encapsulated in the core and PCL-mPEG was used as the shell material and the release of ART from these nanofibers was studied. In the fifth part, direct electrospinning of cellulose under DBU-CO<sub>2</sub> solvent system was conducted, which could be potentially used in drug delivery applications. Two types of cellulose namely Microcrystalline cellulose (MCC) as well as cellulose pulp (CP) were employed. Cellulose as the most abundant renewable carbon-based material was used, as its well known for being a key raw material for the pulp and paper industry as well its application in various areas from textile, coating, nonwovens to drug release and filter.

## 1.1 Theoretical background

### 1.1.1 Nanofibers and electrospinning

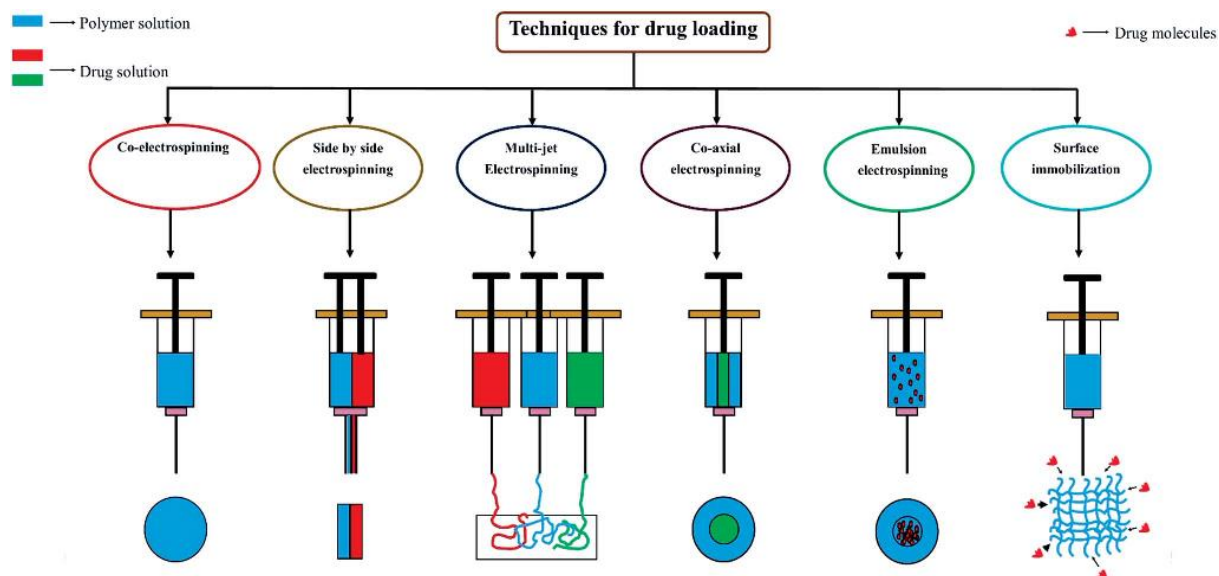
Nanofibers have attracted a lot of interest due to their high surface area, unique structure and high porosity, which makes them suitable for potential applications in filtration, <sup>[1]</sup> tissue engineering, drug delivery, smart materials, reinforcing composites, adhesives, wound dressing, biosensors, etc. <sup>[2,3]</sup> Nanofibers have the advantage that their properties can be controlled by changing different factors including environmental (humidity and temperature), process (applied voltage, feed rate and electrospinning distance) and polymer solution parameters (concentration, viscosity and electrical conductivity). <sup>[4]</sup> Various therapeutic agents can be encapsulated into nanofibers such as drugs, proteins, peptide and DNA. Electrospinning is considered as one of the most conventional techniques for fabrication of nanofibers from a polymer solution containing drugs. Over the years monolithic and blended nanofibers loaded with different types of drugs have been investigated as a potential promising drug delivery system. <sup>[5]</sup> Electrospinning is a technique for producing micro- and nanofibers from a liquid, which could be a polymer solution in which the solvent evaporates as it moves toward the collector. Figure 1 presents the schematic of electrospinning process. A liquid is charged by an electric field and stretched to form a thin liquid jet that is ejected toward a collector. If a repulsive charge is sufficient and the repulsive force overcomes the surface tension, the drop surface starts to form a so-called Taylor cone. <sup>[6]</sup> The formation of a continuous jet instead of droplets, as observed in electrospraying, which is ensured by the presence of entanglements in the polymer solution that is spun. The fiber forming from the Taylor cone travels towards the collector, and during the process, the solvent evaporates, resulting in the deposition of a solid fiber onto the collector. The fiber diameters are usually between 10 nm and 10  $\mu\text{m}$  and can

be controlled by the electrospinning parameters and polymer concentration. <sup>[7]</sup>



**Figure 1.** Schematic of electrospinning. <sup>[6]</sup>

There would be different techniques of encapsulating drug into electrospun nanofibers namely co-electrospinning, side by side, multi-jet, coaxial, emulsion electrospinning and surface immobilization. <sup>[8,9]</sup> Electrospinning provides not only but also different methods for loading various medications and biomolecules. Schematic of these encapsulation methods is brought in Figure 2.



**Figure 2.** Different techniques for encapsulation drugs into electrospun nanofibers. <sup>[9]</sup>

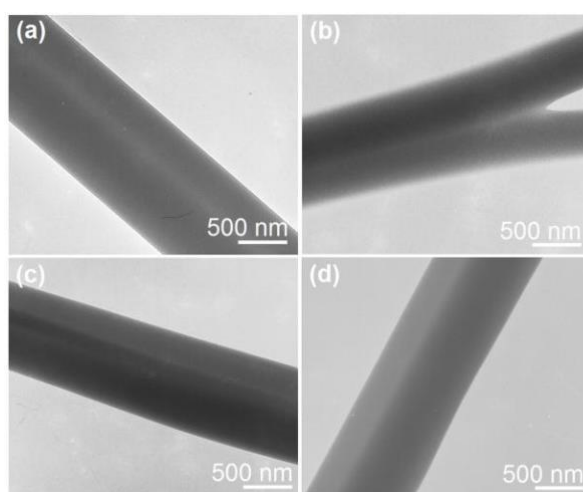
### 1.1.2 Co-electrospinning

The co-electrospinning method is simple and cost-effective, through which the polymer solution and the drug are mixed prior to electrospinning. It enables high drug loadings, homogenous distribution of drug molecules, but on the other hand it suffers from an increased initial burst, which is defined as the process of dissolution of drugs from the particle surfaces into the bulk aqueous phase. Furthermore, the direct exposure of drugs to the electric field might influence their bioactivity. As the nanofiber surface is predominantly inhibited by loaded bioactive agents, the total drug release is accomplished within few days owing to diffusion and polymer degradation. <sup>[9]</sup>

### 1.1.3 Side-by-side electrospinning

If the drug molecule cannot be dissolved in a certain solvent, it can be electrospun to nanofibers using side by side electrospinning. Using this method,

the polymer solution and the biomolecules are loaded into different spinnerets. By applying an electric field, fibers with a distinct upper and lower layer are collected on the same target, which could be used for delaying the burst release of the drug. <sup>[9]</sup> Using side by side fibers is interesting in order to provide a platform for designing multifunctional materials and to develop novel nanostructures for application in different fields from biodegradation studies to cell culture and drug release. <sup>[10]</sup> Yu et al. conducted side by side electrospinning, using PVP and ethyl cellulose (EC) as raw materials and ketoprofen as an active biomolecule. Electron microscopy proved the formation of side-by-side structure. A biphasic drug release pattern was observed and they concluded that by changing the amount of PVP loaded on the EC side, the release rate could be modified. <sup>[11]</sup> Figure 3 shows the transmission electron microscopy (TEM) of the electrospun nanofibers.



**Figure 3.** TEM images containing 40 mg KET in (a) 360 mg, (b) 370 mg, (c) 381 mg, (d) 460 mg fiber. <sup>[11]</sup>

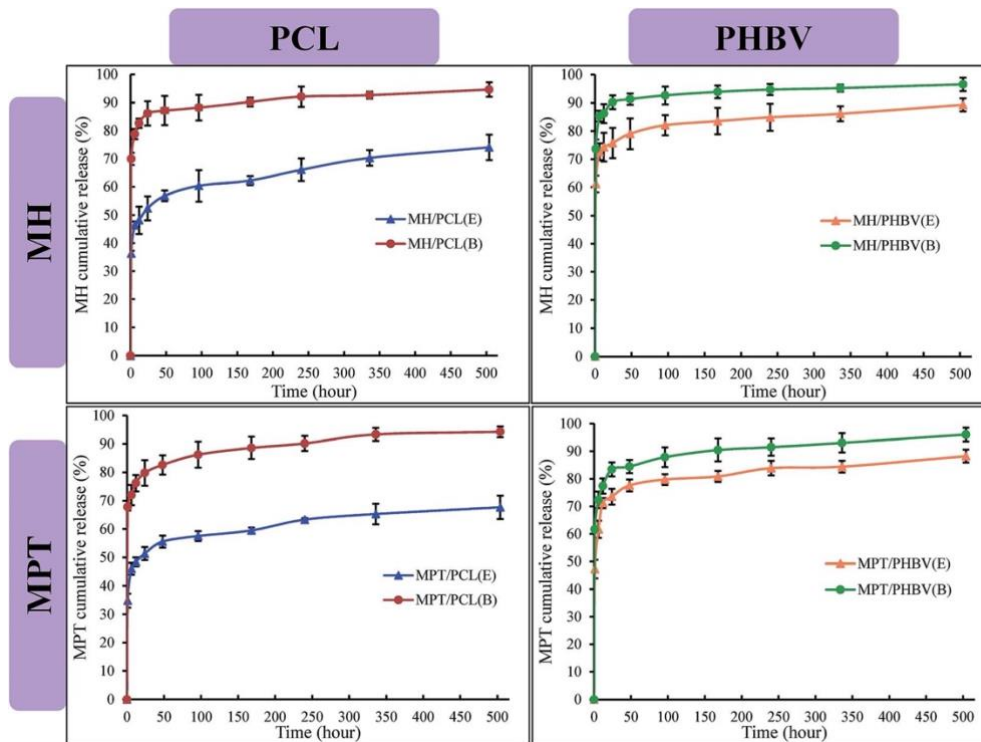
#### 1.1.4 Emulsion electrospinning

Emulsion electrospinning is a facile method, which provides encapsulation of

biomedical additives including drugs, proteins and growth factors into the core of nanofibers for sustained release. <sup>[12]</sup> It has attracted lots of interest due to its capability to protect biologically active agents as well as reducing the initial burst release effect. Using this method, the resultant nanofiber will show a core-shell structure and thus the drug molecules are protected from the electric field. Nevertheless, in most cases the formation of a core-shell structure is not observed. <sup>[9]</sup> In the emulsification process, the hydrophilic drug is dissolved in water (aqueous phase), whereas the hydrophobic polymer is dissolved in the organic solvent (oil phase). While the oil phase evaporates, most of the hydrophilic drug is encapsulated into the fibers rather than being deposited on the fiber surface, thereby reducing the probability of burst release. <sup>[12,13]</sup>

Hu et al. <sup>[12]</sup> loaded metformin hydrochloride (MH) or metoprolol tartrate (MPT) into PCL or poly(3-hydroxybutyric acid-co-3-hydroxyvaleric acid) (PHBV) using emulsion electrospinning. From drug release curves (Figure 4), they concluded that of the two polymers, PCL was considered a better drug delivery carrier than PHBV and the nanofibers which were loaded with MPT exhibited less burst release compared to other fibers.





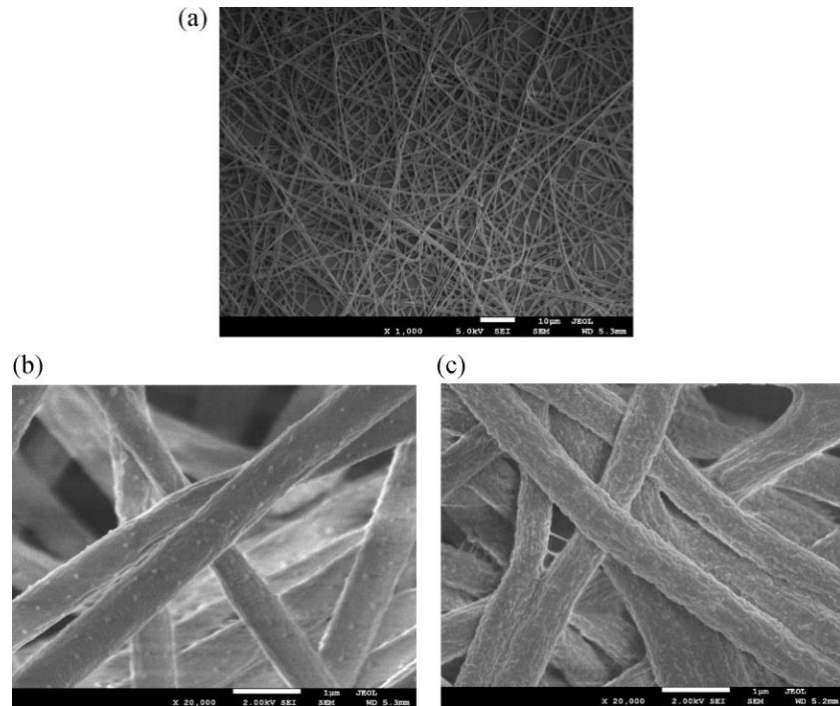
**Figure 4.** Release profile of MH and MPT from emulsion nanofibers. <sup>[12]</sup>

### 1.1.5 Suspension electrospinning

Suspension electrospinning is regarded as a rather novel method, in which an aqueous dispersion of a water-insoluble polymer is used. It is considered as green electrospinning and overcomes the limitations of solution and melt electrospinning. Suspensions are comprised of mixtures of a liquid, which is mostly water and finely dispersed solid particles. Compared to emulsion electrospinning, which could be critical for in vivo medical applications, suspension electrospinning enables the electrospinning of polymers from water, without requiring a further crosslinking step, <sup>[14]</sup> resulting in less toxicity and environmental safety concerns. <sup>[15]</sup>

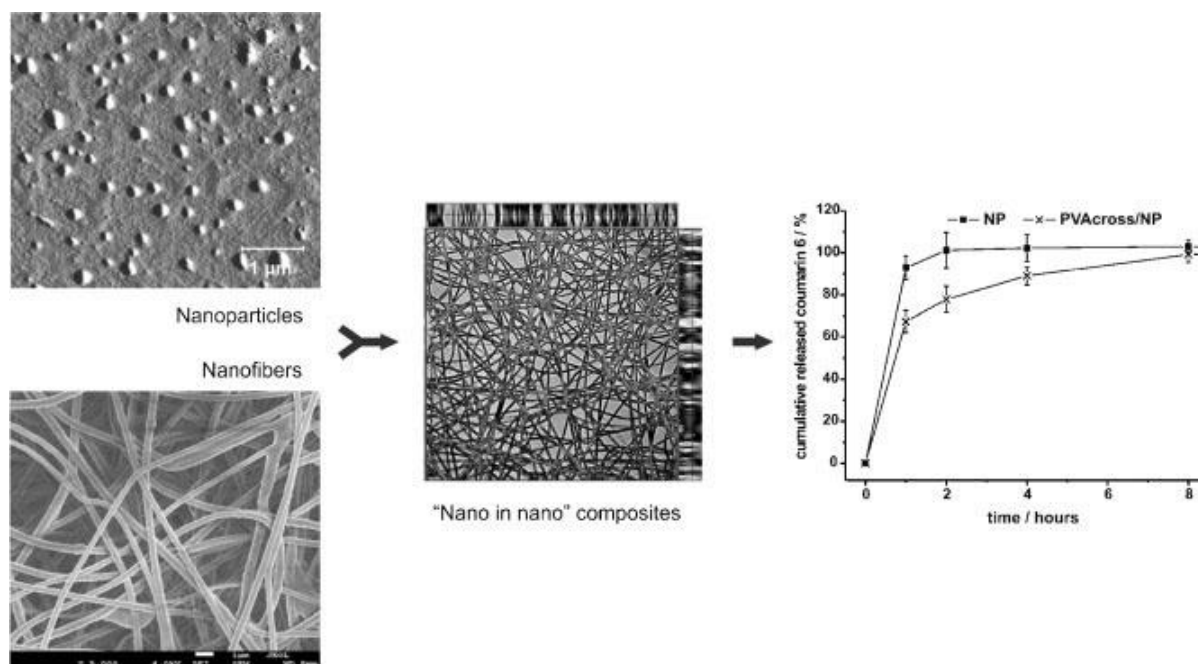
Electrospinning of secondary suspensions of biodegradable polyesters has gained a lot of attention, which could offer novel applications in medicine, pharmacy and agriculture. Polymer suspensions can be prepared by dispersion

of any water-insoluble polymer in water, which is termed a secondary latex suspension. This could be achieved if, firstly, a water-insoluble biodegradable polyester with a relatively low melting point is chosen and, secondly, a block of a water-soluble polymer is chemically attached to a polyester block to guarantee the polyester can be suspended in water for fiber formation. However, there is a specific required concentration of polymer and conditions to be able to successfully prepare the secondary suspension. <sup>[16]</sup> Aqueous suspensions of biodegradable polyesters, like PLA and PLGA nanoparticles are of interest and can be prepared by different methods including emulsion, double emulsion and salting out. These secondary suspensions use a very low solids content of the polymer. <sup>[17]</sup> Sun et al. <sup>[17]</sup> produced nanofibers by green electrospinning of aqueous suspensions of poly(hexamethylene adipate)-PEO block copolymers (PHA-b-PEO). Figure 5 shows the scanning electron microscopy (SEM) of the nanofibers with 4 wt. % PEO before and after water treatment for 2 days at 25 °C. The resultant nanofibers kept their structural integrity upon contact with water without using any surfactant or other additional template polymer.



**Figure 5.** SEM of electrospun fibers of PHA-b-PEO-2b with 4% PEO, after (a) water treatment (b) and (c) are before and after water treatment for 2 d at 25 °C at higher magnifications. <sup>[17]</sup>

Beck-Broicheter et al. electrospun aqueous suspensions of dye-loaded PLGA nanoparticles, which were immobilized into PVA or PEO fibers. <sup>[18]</sup> The dye-loaded nanoparticles immobilized into electrospun nanofibers showed a significantly retarded release (Figure 6). They concluded that the first diffusion step through the polymeric nanoparticle matrix followed by the second diffusion from polymeric nanofiber matrix accounts for the sustained release of the model drug.

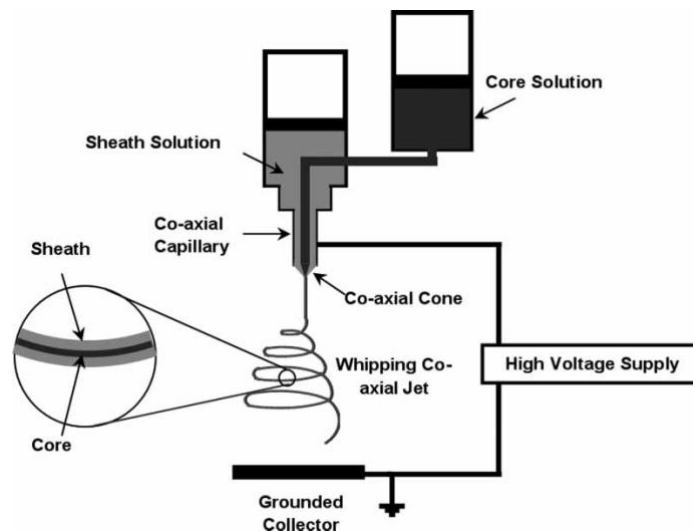


**Figure 6.** schematic of the immobilization of nanoparticles into electrospun nanofibers and their drug release behavior. <sup>[18]</sup>

### 1.1.6 Core-shell electrospinning

Coaxial electrospinning was introduced in 2003 as an alternative for fabricating electrospun nanofibers. <sup>[19]</sup> In core-shell electrospinning two dissimilar materials, previously dissolved or molten, are injected separately into a coaxial capillary, and drawn by a strong electrostatic field. <sup>[3,20]</sup> The spinneret consists of two nozzles, which are located concentrically, and the core and shell solutions are fed at a controlled rate through the inner and outer nozzle, respectively. This results in the accumulation of the charges which occurs predominantly on the surface of the sheath solution. The droplet is elongated and stretched due to bending instability, forming a conical shape. As the accumulation of the charges reaches a threshold, a jet appears at the tip of the droplet, which is guided towards the counter electrode. <sup>[21]</sup> During this process the solvent evaporates and the resulting jet will solidify, contributing to the fabrication of core-shell

nanofibrous structure. <sup>[19]</sup> Using this method, the polymer shell and the drug would come in contact, only when the nanofiber are formed. This phenomenon keeps away unfavorable reactions between the polymer and drug prior to electrospinning. <sup>[9]</sup> The core-shell electrospinning apparatus is shown in the Figure 7.

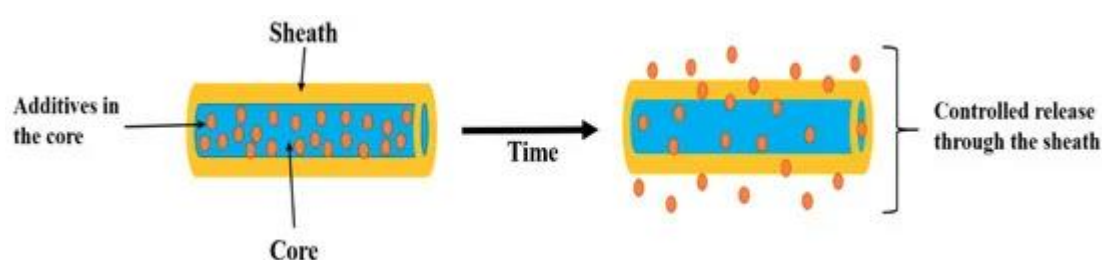


**Figure 7.** Schematic of core-shell electrospinning. <sup>[20]</sup>

Core-shell nanofibers have gained great attention due to the following reasons:

- ❖ Protecting unstable components and reducing the chance of decomposition. <sup>[9,20,21]</sup>
- ❖ Enhancing mechanical properties by reinforcing a material. <sup>[20]</sup>
- ❖ Possibility of preparing nanofibers from unspinnable solutions. <sup>[21]</sup>
- ❖ Releasing a bioactive molecule in a more sustained controlled way, suppressing the drug from burst release. <sup>[5,21]</sup>
- ❖ More opportunities to be used as a scaffold for tissue engineering due to the possibility of a less biocompatible polymer to be surrounded by a more biocompatible material. <sup>[20]</sup>

Core-shell nanofibers, which are fabricated either by coaxial or emulsion electrospinning have gained applications in tissue engineering, drug delivery, wound dressings, etc. <sup>[3]</sup> Sustained drug release is of prominent importance in order to have more successful treatment yields in case of several diseases, which reduces the fluctuation of the drug in blood, decreases the adverse effects as well as dosing frequency thus enhancing patient compliance. <sup>[5]</sup> In the case of drug-loaded core-shell nanofibers, the shell protects the drug from being immediately dissolved and prevents the drug from migrating toward the surface of the nanofiber. On the other hand, the shell enhances the diffusion path (Figure 8).



**Figure 8.** Schematic showing the encapsulation and release procedure. <sup>[21]</sup>

The release behavior is strongly influenced by the amount of drug loading, the thickness of the shell, shell hydrophilicity and interactions between the core and shell polymer as well as their flow rates. <sup>[5,22]</sup> Nevertheless, it should be emphasized that coaxial electrospinning does not necessarily result in the formation of core-shell nanofibers. <sup>[5]</sup> It is noteworthy to mention that the process of co-electrospinning should be fast enough to prevent mixing of the core and shell solutions as well as any other available compound in the system and is particularly of interest for core materials, which are not themselves electrospinnable. <sup>[19]</sup> A variety of different polymers have been used for the fabrication of electrospun nanofibers by coaxial electrospinning. These include

synthetic materials (polyesters, polyurethane, polycarbonates, etc), natural materials (chitosan, silk, collagen, gelatin, etc.) as well as synthetic biodegradable polymers for example (poly(lactic acid), poly(glycolic acid), PCL, poly(lactide-co-glycolide)).<sup>[3]</sup> These polymers belong to the typically most used biocompatible stable polymers with suitable mechanical properties.<sup>[23]</sup> Different conductive and magnetic nanomaterials can be incorporated into the core, which make them appropriate candidates for electronic and smart clothing applications.<sup>[3]</sup> Furthermore, bioactive agents nanofibers including drugs, enzymes and proteins can be loaded into core-shell fibers for biomedical applications,<sup>[23]</sup> which gives rise to improved biological and cell proliferation characteristics.<sup>[5]</sup>

Different release profiles could be obtained using core-shell electrospinning, which are listed below.

- i. Sustained drug release at a predetermined rate with the drug concentration being kept constant over a specific time.
- ii. Biphasic (multiphase) release, providing drug delivery at two different rates such as immediate followed by a constant drug release.
- iii. Targeted drug release, which enables a higher drug efficacy by delivering the drug in way that enhances its concentration in some parts of the body rather than others.<sup>[24]</sup>

He et al.<sup>[25]</sup> fabricated core-shell nanofibers with PLLA as a shell and tetracycline hydrochloride as core. The resulting core-shell nanofibers showed a decreased amount of burst release, where only 22.9 % of the TCH was released after 144 h, compared to blended PLLA/TCH nanofibers, prepared by single nozzle electrospinning, where more than 30 % of the drug was released after 8 h. In work reported by Jiang et al.,<sup>[26]</sup> PCL nanofibers were fabricated with protein

containing PEG as the core, which could find applications for controlled release of proteins and tissue engineering. In another work, Zhang et al.<sup>[27]</sup> incorporated bovine serum albumin (BSA) and PEG into PCL nanofibers by coaxial electrospinning technique for tissue engineering applications. Song et al.<sup>[28]</sup> incorporated iron-platinum nanoparticles into a PCL nanofiber mat to induce magnetic properties in a PCL nanofiber. Ranjbar-Mohammadi et al.<sup>[29]</sup> co-electrospun PLGA/gum tragacanth and used TCH as a model drug, which resulted in a prolonged release of TCH with low burst releases.

As a drug carrier, the large surface-to-volume ratio of the electrospun nanofibers enhances the drug solubility in aqueous medium and improves drug delivery efficiency as well as higher drug encapsulation efficiencies. Additionally, drug release rate could be substantially controlled by modifying the various physical and chemical parameters, structure and morphology of nanofibers. The drug release mechanism could be interpreted through a combination of diffusion processes, polymer degradation, drug partitioning in polymeric carrier, drug solubility, and water uptake (swellability).<sup>[4]</sup>

## **1.2 Studies of release mechanisms**

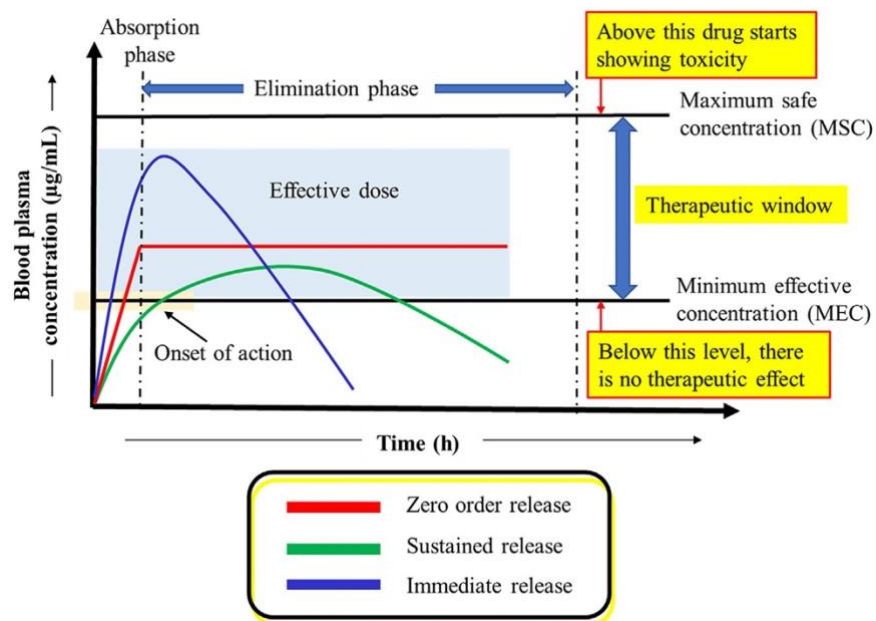
### **1.2.1 Release profile shape**

Controlled drug delivery offers advanced and improved drug release kinetics as well as therapeutic effectiveness. Thus, the level of drug in the bloodstream increases, followed by a constant range, which varies between the least and most effective level (Figure 9).<sup>[30]</sup> The release profile is usually used as a base for determining the release mechanism.<sup>[31]</sup> As drug delivery systems (DDSs) are different, the release profiles are correspondingly different (Figure 10). Ideal

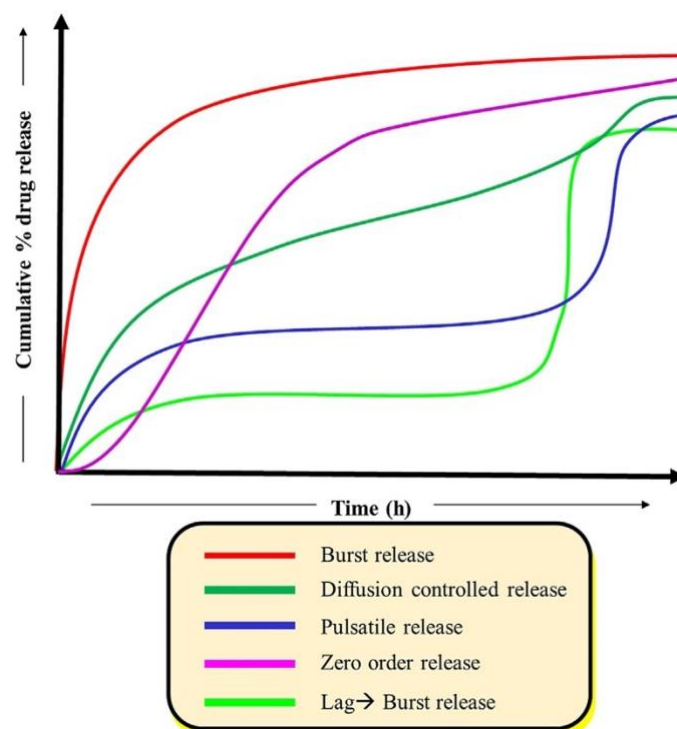


DDSs offer a zero-order release profile, however in many controlled release systems, a considerable amount of drug is released immediately after being placed in physiological medium. This phenomenon is termed burst release.<sup>[30]</sup> Burst release results in a higher amount of drug being released and decreases the efficient life-time of the system. Burst release is usually attributed to the unencapsulated drug particles on the surface or near the surface, which are readily accessible by hydration. Other possible reasons include the formation of cracks as well as disintegration of the particles.<sup>[31]</sup> In a diffusion-controlled release system, the dissolved drug diffuses through the rate-controlling carrier. In such systems, the rate controlling element is insoluble, non-erodible and non-degradable.

Diffusion is defined as the random movements of the molecules, which is driven by the chemical potential gradient.<sup>[31]</sup> Diffusion DDSs are categorized into four different types including constant drug reservoirs, non-constant drug reservoirs as well as monolithic dispersions and non-monolithic dispersions. Pulsatile DDSs represent a drug delivery system with a lag time, which is well-defined. A pulsatile release system is defined by a period of no release, which is referred to lag time, followed by a fast and complete release of drug. These systems are classified into site-specific and time-controlled devices. In a site-specific system, the drug is released at a favorable site within the intestinal tract and is governed by environmental factors such as pH and enzymes, whereas in a time-controlled system the drug is released after a well-defined period and the release is controlled by the system and not by the environment.<sup>[32]</sup>



**Figure 9.** Plasma drug concentration release profile of different delivery systems. <sup>[30]</sup>



**Figure 10.** Plasma profile from different delivery systems. <sup>[30]</sup>

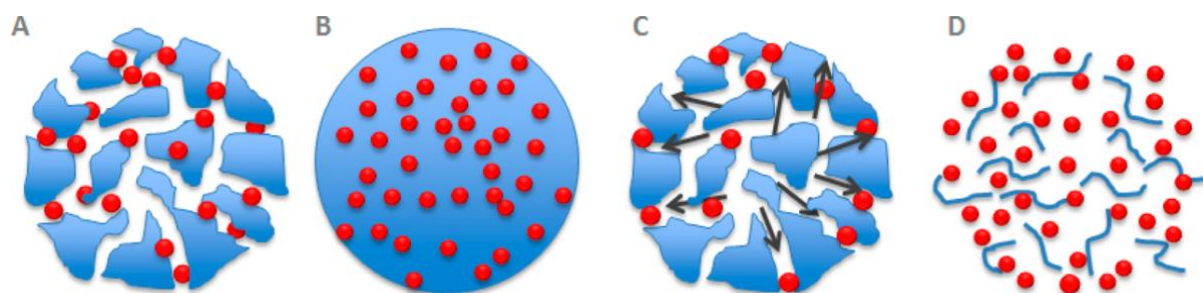
## 1.2.2 Drug release mechanisms

For polymer systems, the term “drug release” refers to the method by which the drug molecule is transported from a position inside the polymer matrix to the outer surface of the polymer matrix and ultimately its release into the surrounding moiety. Table 1 outlines the different release mechanisms. <sup>[31]</sup>

**Table 1.** Different release mechanisms or rate controlling processes in drug release.

Release mechanism	Reference
Drug dissolution (combined with diffusion)	[33]
Diffusion through water-filled pores	[34]
Diffusion through the polymer matrix	[35]
Hydrolysis	[36]
Erosion	[37]
Osmotic pumping	[38]
Water absorption/swelling	[39]
Polymer-drug interactions	[40]
Drug-drug interactions	[41]
Polymer relaxation	[42]
Pore closure	[43]
Heterogenous degradation	[44]
Formation of cracks or deformation	[45]
Collapse of the polymer structure	[46]

The main factors governing controlled-release mechanisms are (A) drug diffusion through water-filled pores, (B) diffusion through polymer matrix, (C) osmotic pumping and (D) erosion (Figure 11). <sup>[47]</sup> In the next parts, these mechanisms are explained in detail.



**Figure 11.** Drug release mechanisms from polymeric nanoparticles: (A) diffusion through water filled pores, (B) diffusion through the polymer matrix, (C) osmotic pumping, and (D) erosion. <sup>[47]</sup>

### 1.2.3 Drug diffusion through water filled pores

Water is absorbed by polymeric nanoparticles in a fast way compared to the drug release. The water that inhabits the polymer matrix causes the formation of water filled pores and the pore sizes enlarges, which leads to large amount of pores facilitating the drug release process. <sup>[47]</sup>

### 1.2.4 Drug diffusion through polymer matrix

Through this mechanism, drug molecules diffuse out of the polymer matrix. In case of nondegradable drug delivery systems, diffusion is the major factor for drug release with a constant release rate and is influenced by the polymeric membrane properties such as permeability and thickness and not by the concentration gradient. <sup>[47]</sup> The idea behind is that a solute diffuses from higher concentration regions to adjacent regions with lower concentrations. <sup>[48]</sup>

### **1.2.5 Osmotic pumping**

In a non- swelling system, the water influx is caused by osmotic pressure and consequently the drug transport is regarded as osmotic pumping. <sup>[47]</sup> This mechanism could be observed in drug delivery systems using polymers such as ethyl cellulose. <sup>[31]</sup>

### **1.2.6 Surface erosion**

Surface erosion happens when polymer degradation starts at the matrix surface, resulting in a slow reduction in the size of the matrix, beginning from the outside and continuing towards the inside and occurs in the case when the erosion rate is higher than the water penetration rate in the bulk polymer. <sup>[47]</sup>

### **1.2.7 Bulk erosion**

Bulk erosion takes place when water penetrates the polymer bulk, resulting in a homogeneous degradation of the whole matrix. In this case, the permeation rate of the water is higher than the erosion rate, hence the polymer within the bulk is liable to be hydrolyzed. Bulk erosion is less probable compared to surface erosion and does not consider the protection of drug from the environment. <sup>[47]</sup> Having knowledge about release mechanisms that have an impact on the release rate is crucial for developing the DDSs.

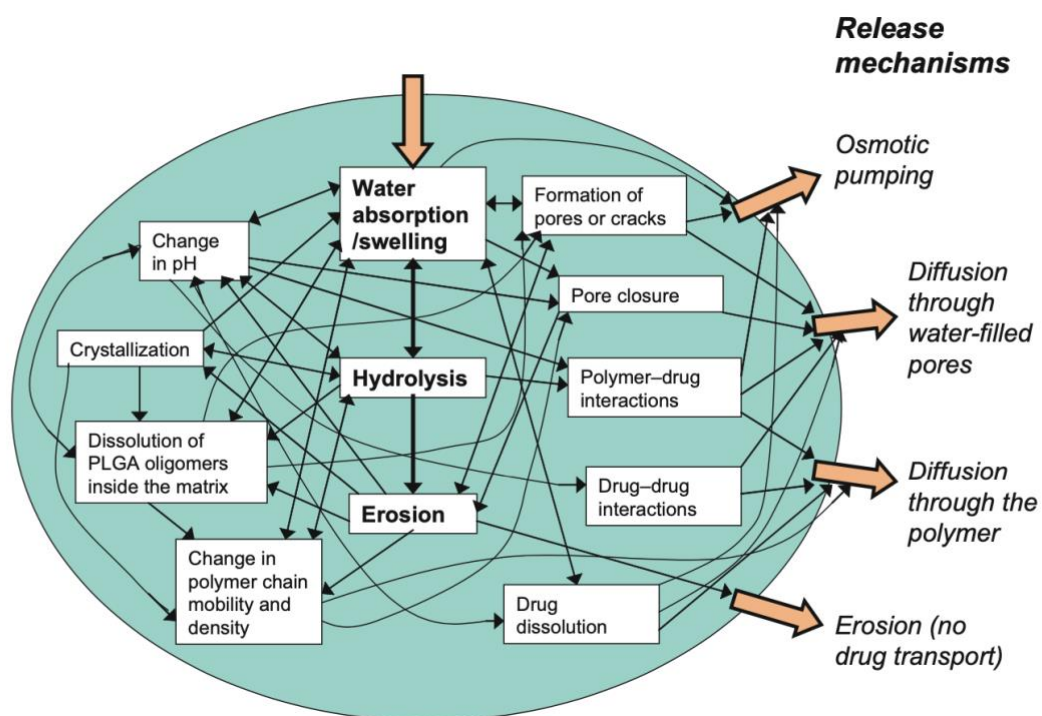
## **1.3 Factors influencing drug release from PLGA-based DDSs**

### **1.3.1 Physiochemical processes occurring in PLGA-based DDSs**

In PLGA-based DDSs, there are complex physiochemical processes occurring with PLGA matrices, contributing to the drug release (Figure 12). Generally, water is absorbed very fast by the polymer after immersion in water or being administered in-vivo. The rate at which water is absorbed is faster than the drug release.<sup>[49]</sup> The volume inhabited by water within the polymer matrix is called a pore. The so-called pores are too small for drug transport at the early stage, but as their number in polymer increases, a network of connected pores is formed, thereby making the drug release possible<sup>[31,39]</sup>. On the other hand, hydrolysis, the scission of ester bonds and the following decrease in molecular weight happens immediately after exposure to water. As a result of hydrolysis, acids are created, which catalyzes hydrolysis. As a result of this auto-catalytic phenomenon, a heterogeneous degradation inside PLGA matrices happens, which translates to a faster degradation rate at the center of the PLGA matrix than the surface<sup>[31]</sup>. Erosion, regarded as the mass loss of the polymer, happens as the dissolved polymer degradation products diffuse into the release medium. In the case of PLGA, bulk erosion usually happens rather than surface erosion, as PLGA is hydrated relatively fast.<sup>[50]</sup> The process of erosion and the dissolution of polymer degradation products generates pores. These pores created by water absorption or polymer erosion start to grow and causes hydrolysis. The produced acids catalyze degradation and leads to polymer dissolution within the pores, resulting in a subsequent erosion. In some cases, the pores can close, which can be attributed to the mobility of polymer chains. The mobility of the polymer chains is related to the glass transition temperature, which decreases with decreasing molecular weight.<sup>[51]</sup>

The degradation products influence the release system:

- These products are acids and they catalyze the hydrolysis process.
- They are plasticizing, which enhances the water absorption rate and reduces the transport resistance of the polymer.
- They are known to be able to crystallize. This crystallization hinders water absorption and further degradation. <sup>[31]</sup>



**Figure 12.** The complex schematic of physico-chemical processes occurring within PLGA matrices, resulting in drug release. The influence of processes on drug release and on other processes is represented by arrows. <sup>[31]</sup>

### 1.3.2 Factors influencing the physiochemical behavior of PLGA

A method of controlling the drug release is to choose PLGA with appropriate properties. The molecular weights of PLGA used for drug release are relatively low, less than 50 KDa. The L:G ratio, which is defined as the ratio of lactide to

glycolide, is varied from 50:50 to 100:0. The polymer end group may or may not be capped with a hydrophobic ester group such as a stearyl group. The combination of low molecular weight, a low L:G ratio and uncapped polymer end groups results in a less hydrophobic polymer with a higher water absorption rate, hydrolysis, and erosion. The encapsulated drug might also influence the drug release in different ways. These are as following:

- They result in enhanced or inhibited water absorption as well as hydrolysis owing to enhanced hydrophilicity/hydrophobicity or osmolality. <sup>[52]</sup>
- Increased or reduced amount of hydrolysis because of acid or base catalysis or acid neutralization. <sup>[53]</sup>
- Plasticization of the polymer. <sup>[49]</sup>

The amount of drug, which is encapsulated become meaningful, as the space being left free after drug release will form pores, thus facilitating the drug release. Additionally, the release behavior is also influenced by the location of the drug in the DDS, which is totally affected by physiochemical properties of the drug <sup>[31]</sup>. DDS characteristics such as porosity and polymer chain density play a major role, as larger DDSs contribute to an enhanced pH gradient and therefore the autocatalytic effect on degradation increases. Besides, the shape of DDS, i.e surface to volume ratio, influences the release of the drug and PLGA degradation products. Size of particles might affect the distribution of the drug within particles. The environmental conditions such as temperature gives rise to the mobility of the polymer, therefore the rate of pore closure. Additives such as salts, surfactants and plasticizing agents in the release medium affect the release as if they were encapsulated with an exception that the high osmolality in the release media reduces the rate of water absorption by DDS. <sup>[54]</sup>



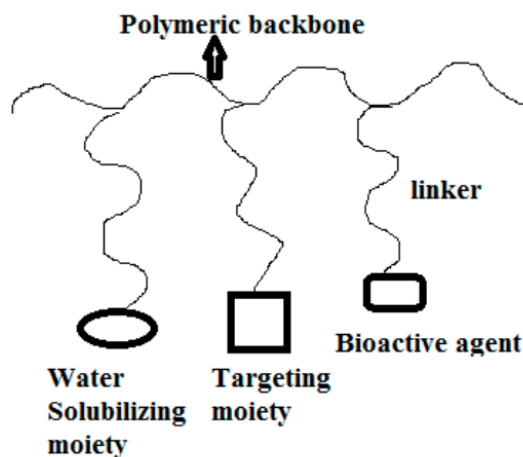
## **1.4 Development of different drug-loaded carriers**

Our concept was to develop drug-loaded carriers and subsequently encapsulate these particles into electrospun nanofibers. Encapsulation has played an influential role in nanomedicine modifying the pharmacology of drugs. The polymer itself must be biocompatible and biodegradable. Currently, there have been different drug delivery systems, in which drugs are encapsulated. These are as following: <sup>[55]</sup>

### **1.4.1 Polymer-drug conjugates**

Polymer-drug conjugates are polymeric therapeutics, consisting of a water soluble biodegradable polymeric carrier, a targeting moiety as well as a low-molecular weight biologically active molecule, incorporated into a polymer via covalent bond through a bioresponsive linker (Figure 13). <sup>[55]</sup> The polymer contribution is that it increases the solubility of the hydrophobic drug. Additionally, the polymer protects the drug from degradation. The linker plays a role not only in making a bond between the drug and polymer, but also it could be activated by stimulating the drug release under specific condition, like pH change or in the presence of enzymes. <sup>[31]</sup> In general, polymer-drug conjugates offer variety of advantages such as increased drug solubilization, prolonged circulation, controlled release as well as increased safety. <sup>[56]</sup> Cai et al. prepared polymer drug conjugates immobilized with paclitaxel as an anticancer drug. The drug was incorporated into polymer backbone through a tetrapeptide linker. The results showed the aforementioned conjugates considerably inhibited the proliferation of breast cancer cells and supported the degradation of the conjugate with high molecular weight to a much more low molecular weight product, which was further followed by the drug release in the cancer microenvironment. <sup>[57]</sup> In other work, Wang et al. reported that the

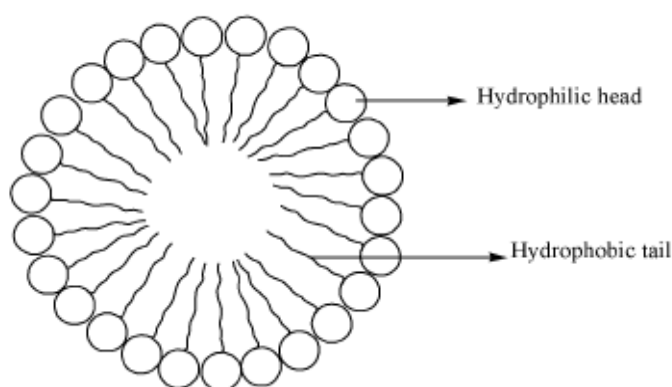
incorporation of dihydroxy artemisinin (DHA) into hydroxypropyl-cyclodextrin for oral administration resulted in enhanced solubility and stability of DHA. It was observed that no side effect was seen compared to free artemisinin. <sup>[58]</sup>



**Figure 13.** A schematic diagram of polymer-drug conjugate. <sup>[55]</sup>

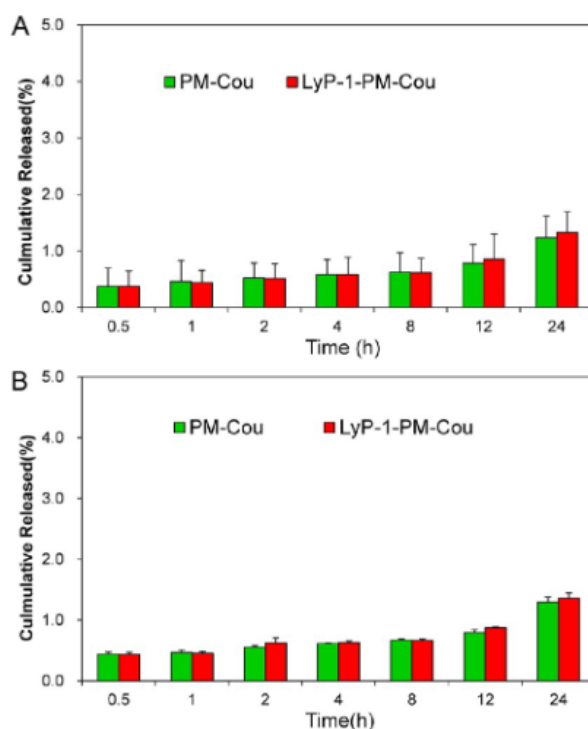
### 1.4.2 Micelles

Micelles are polymeric drug delivery systems used for the delivery of bioactive molecules. They are composed of amphiphilic copolymers, which form a hydrophobic core for the encapsulation of lipophilic drugs. <sup>[55]</sup> Figure 14 shows a schematic of a micelle.



**Figure 14.** Schematic of a micelle. <sup>[55]</sup>

Amphiphilic di-block or tri-block copolymers are mostly applied to prepare polymer micelles for drug delivery. The most conventional hydrophilic block which is used to create the hydrophilic shell are poly(ethylene glycol) (PEG) or poly(ethylene oxide) (PEO). Generally, when the drug is physically incorporated into the polymer micelles, the release rate is controlled by diffusion of the drug from the core of the micelle, its stability as well as polymer degradation rate. <sup>[59]</sup> Wang et al. incorporated artemisinin into PEG-PCL micelles to deliver to the highly metastatic tumor. This resulted in a high cellular uptake as well as inhibition impact on cancer cell lines. Figure 10 shows the release behavior of coumarin 6 from micelles. They observed that only 2 % of coumarin 6 was released after 24 h in both pH 5 (Figure 15A) and pH 7.4 (Figure 15B ) release medium. <sup>[60]</sup>

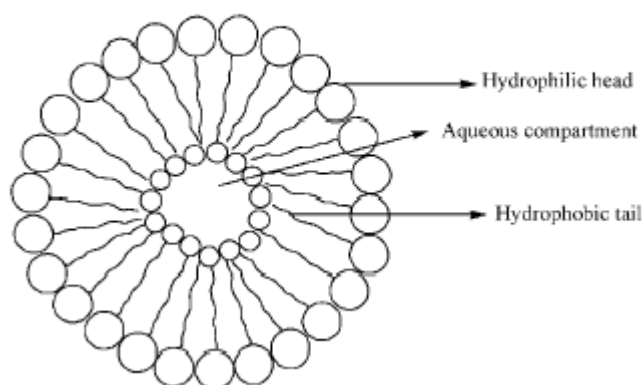


**Figure 15.** In vitro release of coumarin 6 from micelles (PM-Cou stands for polymeric micelles and LYP-1-PM-Cou stands for tumor lymphatics-homing peptide) (a) pH 5 and (b) pH 7.4. <sup>[60]</sup>

### 1.4.3 Liposome

Lipid-based drug delivery is a key factor for improving the potential of hydrophobic drugs. Liposomes are biodegradable and biocompatible and has amphiphilic molecules, which are comprised of an aqueous core that is suitable for carrying hydrophilic drugs and a lipid lamellar that is capable of entrapping hydrophobic drugs. <sup>[55,61]</sup> They improve therapeutic efficacy of drug by increasing drug absorption, prolonging half-life and decreasing drug toxicity. To achieve these goals, artemisinin and its derivatives have been successfully loaded into liposomes. Isacchi et al. fabricated artemisinin loaded PEG liposomes. The results proved that the liposomal formulation exhibited a much longer blood circulation, and the drug was still detectable even after 24 h of

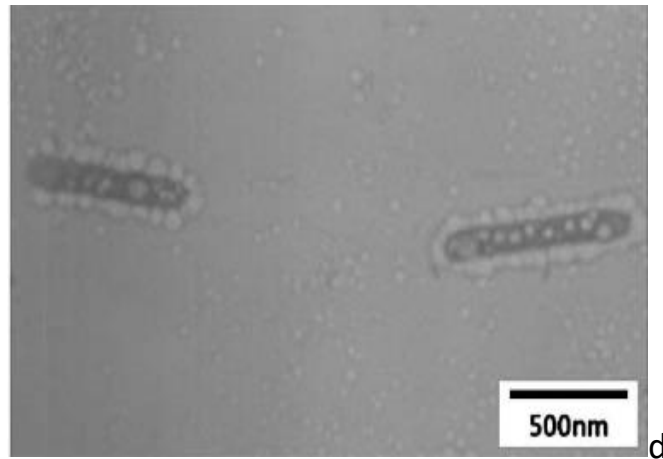
administration.<sup>[62]</sup> Liposomes characteristics can be tailored in order to attain slow or fast drug release, which is optimal for Artemisinin-based combination therapy (ACT), having various pharmacokinetic profiles.<sup>[61]</sup> Schematic of a liposome structure could be seen in Figure 16.



**Figure 16.** Schematic of liposomes.<sup>[55]</sup>

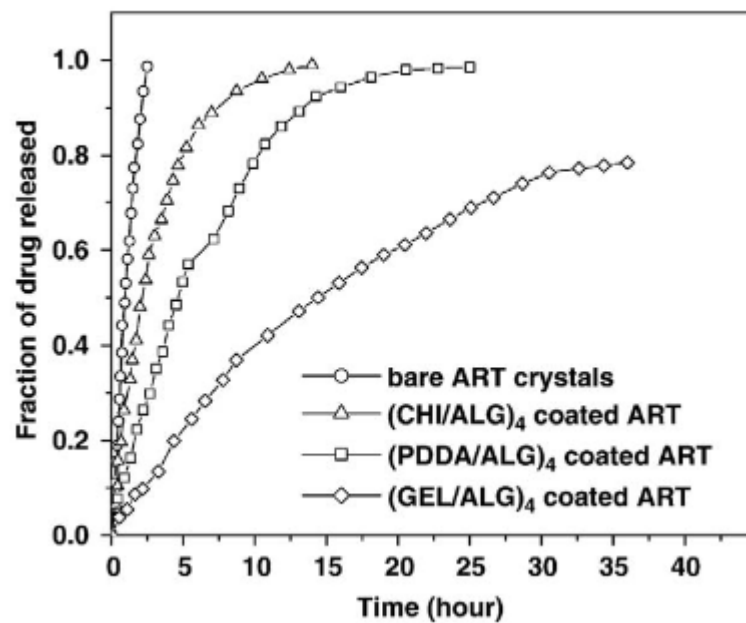
#### 1.4.4 Nanocapsules

Nanocapsules are categorized in a class of nanoparticles which has a core and a protective shell. They merit the advantages such as sustained drug release, improved drug bioavailability and reduced toxicity.<sup>[55]</sup> Chen et al. incorporated artemisinin into poly (dimethyldiallyl ammonium chloride) (PDDA), gelatin (GEL), chitosan (CHI) and alginate (ALG) nanocapsules, which resulted in a prolonged release behavior. TEM of the nanocapsules could be seen in Figure 17. The average nanocapsule size obtained was 766 nm.<sup>[63]</sup>



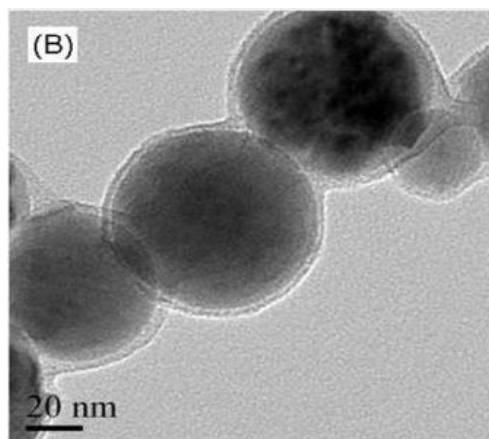
**Figure 17.** TEM micrograph of Artemisinin capsules coated with (CHI/ALG)<sub>6</sub> multilayers. <sup>[63]</sup>

On the other hand, release results from artemisinin itself and nanocapsules (Figure 18) showed the release behavior is highly related to the polyelectrolyte type, number of polyelectrolyte multilayers and composition. Regarding this, the most prolonged release was achieved up to 35 h by using (GEL/ALG)<sub>4</sub> coated ART. <sup>[63]</sup>



**Figure 18.** Release profiles of ART coated with different polyelectrolyte multilayers in PBS. <sup>[63]</sup>

Xiao et al. <sup>[64]</sup> encapsulated artesunate in nanocapsules using microcrystallization method (Figure 19). This resulted in an improved stability of drug as well as a prolonged drug release. The size of artesunate loaded nanocapsules was about 76 nm.



**Figure 19.** TEM micrograph of nanocapsules. <sup>[64]</sup>

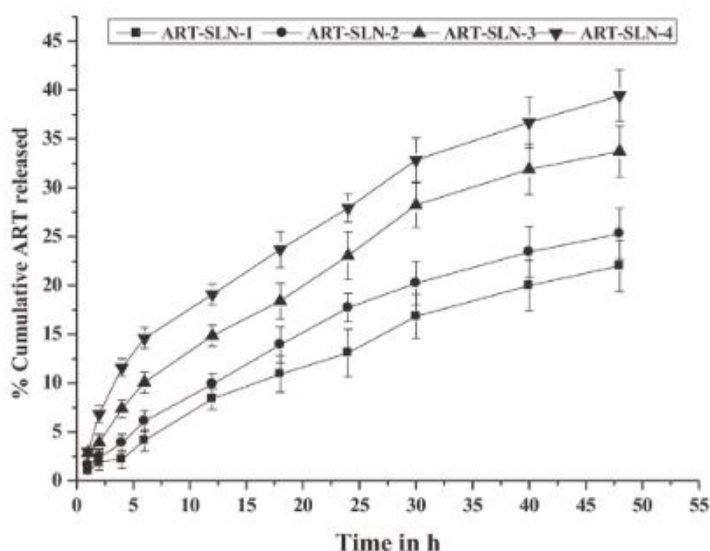
### 1.4.5 Nanoparticles

In the design of an appropriate drug delivery carrier, the controlled release of the active agent to the specific site of action at an optimal rate and dosage should be majorly taken into consideration. Recently there has been considerable interest in synthesizing biodegradable nanoparticles as efficient drug delivery carriers. These could find variety of applications from injectable drug carriers to non-parenteral delivery of drugs through pulmonary, nasal and oral routes. <sup>[65]</sup>

#### 1.4.5.1 Lipid-based nanoparticles

Lipid-based nanoparticles are potential candidates for the delivery of highly

hydrophobic drugs, but they provide an alternative drug delivery system for both hydrophilic and hydrophobic drugs. [61] Their size ranges between 50-1000 nm. However, their low stability and the need for certain storage condition hampers their application to be used for tropical diseases. [55] The system is comprised of nano-sized spherical solid lipid particles, which are dispersed either in water or in an aqueous solution containing surfactant. [66] As lipid-based nanoparticles have an amorphous structure, they would encounter less burst effect of drug. [55] Dwivedi et al. encapsulated artemether into solid lipid nanoparticles (SLN) for the treatment of cerebral malaria. They observed that using this method, the release of drug was slow (Figure 20) as well preserved the drug from being degraded in acidic pH of the stomach. [67]



**Figure 20.** In vitro release of ART from ART-SLN in phosphate buffer pH 7.4. [67]

#### 1.4.5.2 Polymer-based nanoparticles

Polymer based nanoparticles have been used for delivery of therapeutics due to their biodegradability, biocompatibility, controlled release and their significant bioavailability. [67] Different polymers have been used as vesicles for long term



sustained release including poly lactic acid (PLA), Poly-D,L-lactic-co-glycolic acid (PLGA) and polycaprolactone (PCL).<sup>[68,69]</sup> Among biodegradable polymers, PLGA has attracted lots of attention for long-term sustained release of drug,<sup>[68]</sup> since it is subjected to hydrolysis in the body and produces nontoxic natural byproducts like water and carbon dioxide, which could be simply removed.<sup>[47]</sup>

Researchers have reported the application of polymer-based nanoparticles for delivery of artemisinin and its derivatives due to their outstanding therapeutic effects.<sup>[55]</sup> Golenser et al. encapsulated ART into PCL-mPEG nanoparticles synthesized by solvent displacement method. Results showed a controlled sustained release of ART for the treatment of cerebral malaria, through which mice were cured or if they were treated late, a delay about a week was observed before their death.<sup>[70]</sup> Nguyen et al. loaded Artesunate into PLGA nanoparticles using solvent evaporation method. They evaluated the effect of different parameters on physiochemical properties of nanoparticles. The encapsulation of Artesunate into the core resulted in a sustained release up to 48 h. Additionally, they conducted cytotoxicity test, which represented strong artesunate activity against cancer cell lines.<sup>[71]</sup>

#### **1.4.5.3 Inorganic-based nanoparticles**

Recently, there has been progress in the fabrication of different inorganic nanoparticles as drug vesicles for drug delivery. These include gold nanoparticles (AuNPs), magnetic nanoparticles, semiconductor nanoparticles, carbon nanotubes (CNTs). They own the advantage of being easily prepared with a specific size. Besides, they offer multiple functions beneficial in medicine such as exothermic reactors and contrast agents. Magnetic nanoparticles with average diameter of 10 nm are of huge interest for cancer therapy.<sup>[72]</sup> Chen et al. incorporated artemisinin into iron nanoparticles. In vitro studies on HeLa cell

lines showed that drug-loaded iron nanoparticles showed inhibited growth of cells. <sup>[73]</sup>

Overall, nanocarrier based drug delivery systems are much preferable over ordinary drug delivery systems as the higher surface to volume ratio makes it possible for the drug to have a higher contact area with body, thereby makes the same drug dosage a more effective delivery of the drug. This decreased dosage will reduce the side effects of the drug as well its toxicity. Furthermore, nanocarriers possess tunable surface chemistry for different drugs and bioactive agents. This translates to a more sustained and prolonged release, which results in an improved bioavailability of drug. <sup>[74]</sup> Having the knowledge about release mechanisms is essential in developing drug delivery systems. Understanding the release mechanisms along with parameters affecting the drug release enable us to modify the drug release. <sup>[31]</sup>

## **1.5 Nanomedicines**

Different methods have been used to increase the solubility and bioavailability of poorly water-soluble drugs, including both modifications of the drug itself and the development of specific formulations. <sup>[75]</sup> Nanomedicines have created a significant impact on therapeutic handling of different diseases and rendered reduced toxicity, enhanced efficiency, prolonged drug release as well as an improved stability and bioavailability.

## **1.6 Methods for preparing drug-loaded nano and microparticles**

### **1.6.1 Solvent displacement method**

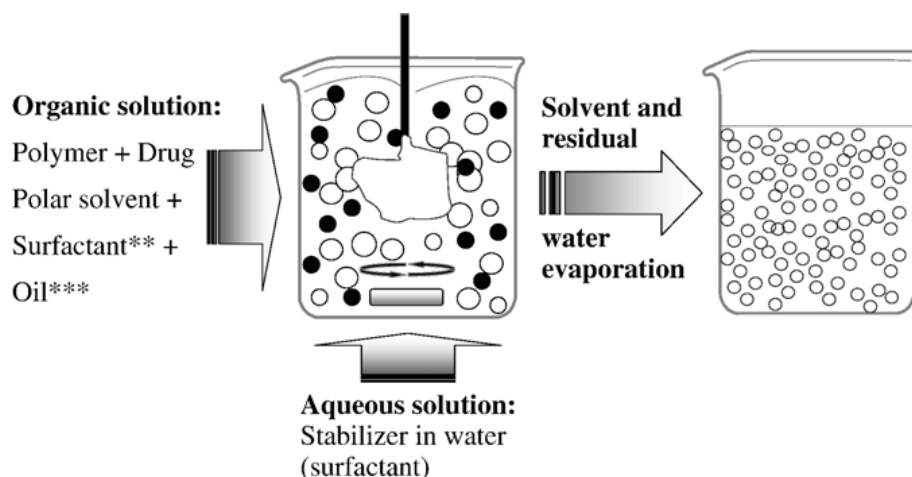
Nanoencapsulation or solvent displacement method was introduced and patented by Fessi et al. <sup>[76]</sup> and is considered in the pharmaceutical field to encapsulate hydrophobic or hydrophilic drug as well as natural compounds. <sup>[69]</sup>

Solvent displacement includes the precipitation of a polymer from an organic solution and subsequently the diffusion of the organic solvent into an aqueous medium in presence or absence of a surfactant. Conventionally, the polymer and the drug are dissolved in a water miscible solvent with an intermediate polarity, which results in the precipitation of nanospheres. In the next step, the organic phase is injected dropwise into an aqueous solution under stirring, which might or might not contain a stabilizer. The deposition of the polymer at the interface between organic solvent and water as a matter of the solvent diffusion, brings about the simultaneous formation of a suspension. Following this, the organic solvent is evaporated, resulting in the formation of drug-loaded nanoparticles. <sup>[47,77]</sup> The nanosphere suspension is concentrated under reduced pressure and subsequently purified using centrifugation or dialysis, whilst non-entrapped drug and excessive surfactant would be removed. <sup>[78]</sup> Figure 21 shows the schematic of the method. Briefly, this method is based on nucleation, growth and aggregation, through which polymeric particles are formed. <sup>[79]</sup>

This method benefits from several advantages including simplicity, easy scale-up, mild shear rates, reproducibility, acquiring submicron particle sizes with narrow size distribution and avoiding large amounts of toxic solvents. <sup>[69]</sup>

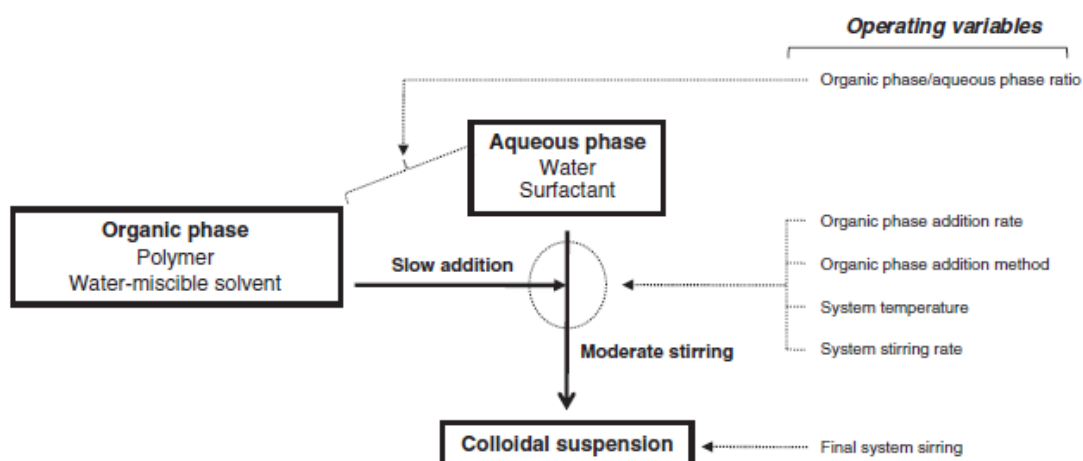
However, this method is not appropriate for the encapsulation of water-soluble drugs, due to significant drug leakage into the aqueous phase. Another limitation

of this method is that many drugs are not solubilized well in semipolar solvents like acetone or alcohols. To overcome this drawback and to improve the drug encapsulation, a mixture of acetone and dichloromethane could be used. [78]



**Figure 21.** Schematic representation of the solvent displacement technique. [77]

In the solvent displacement method, several processing parameters play a critical role in determining the final characteristics of nanoparticles and cause a decisive change in the physiochemical characteristics of the nanoparticles such as particle size, encapsulation efficiency and so on (Figure 22). [69]



**Figure 22.** Preparation of particles by solvent displacement method: schematic procedure and operating variables. [80]

### **1.6.1.1 Effect of different parameters on solvent displacement method**

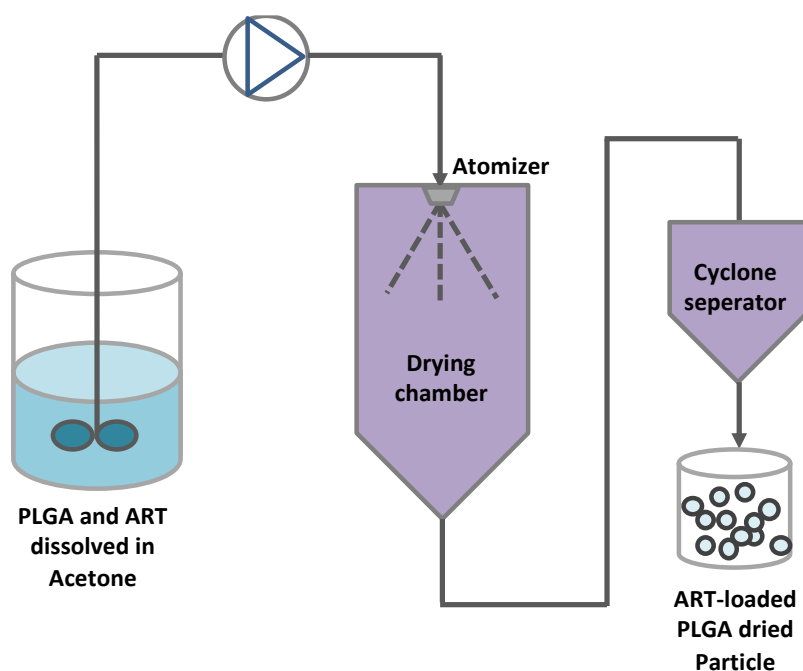
In general, process and formulation parameters in the solvent displacement method have major impacts on the final characteristics of nanoparticles. <sup>[69,79,80]</sup> The controlled release of a drug from nanoparticles is highly dependent on the nanoparticles' properties such as particle size, size distribution, drug content, surface morphology and encapsulation efficiency. <sup>[27–29]</sup> The most important parameters in the solvent displacement method include PLGA concentration, ART concentration, stirring rate, organic to aqueous ratio, organic phase injection rate and stabilizer concentration, which influence the particle size and encapsulation efficiency of the particles, thereby affecting the release behavior from nanoparticles. <sup>[69,79,81]</sup> The aim of polymeric nanoparticles in drug delivery applications is to provide a controlled drug release, to improve the stability of bioactive agent, to achieve higher intracellular uptake compared to free drug and to increase biocompatibility with cells and tissue. Regarding this, control of particle size and encapsulation efficiency is crucial to achieving these goals. The particle size should be big enough to prevent its rapid entrance into blood vessels, but on the other side small enough so that it would not be eliminated from the immune system. <sup>[84]</sup> There is a size limit related to the use of particles, as the diameter of the smallest capillaries in the body is 5-6  $\mu\text{m}$ . As a result, the size of particles must be notably less than 5  $\mu\text{m}$ , so that they don't form any aggregates, resulting in embolism. <sup>[83]</sup> The influential parameters and their influence on particle size and encapsulation efficiency are given in Table 2.

**Table 2.** Different parameters and their effect on particle size and encapsulation efficiency in solvent displacement process.

Parameter	Effect on particle size	Effect on encapsulation efficiency
<b>Polymer concentration</b>	(↑)	(↑)
(↑)	[79,81,84–86]	[69,81,87,88]
<b>Drug concentration</b>	(–)	(–)
(↑)	[88]	[88]
	(↑)	(↓)
	[81,89,90]	[87]
		(↑)
		[80]
<b>Organic to aqueous ratio</b>	(↑)	(↓)
(↑)	[40,81,91,92]	[81,88,93,94]
	(↓)	
	[87,93]	
	(–)	
	[88]	
<b>Stirrer rate</b>	(↓)	(↓)
(↑)	[79,95,96]	[81,97]

## 1.6.2 Spray drying

Spray drying is a simple, widely used technique in the pharmaceutical field, regarded as a way of transforming liquids (solution, emulsion, suspension, melts) into dried powder.<sup>[98]</sup> The specific favorable characteristic of this method is that it can be used for both heat resistant and heat sensitive drugs as well as both water soluble and insoluble drugs.<sup>[99]</sup> Additionally, the drying rate and the speed of the process are fast enough to provide drying of temperature sensitive materials without degradation.<sup>[98,100]</sup> Spray drying has been used to increase solubility and bioavailability of drugs along with modifying their release behavior.<sup>[101]</sup> The typical spray drying process comprises four steps including atomization of the liquid, its further drying through drying gas, particle formation and finally the separation and collection of the product.<sup>[101–104]</sup>



**Schematic 1.** Spray drying process.

Using the spray drying method, the particle size and physiochemical properties of the particles could be controlled by varying the operating conditions.<sup>[105]</sup> Recently, great attention has been drawn to improving the encapsulation

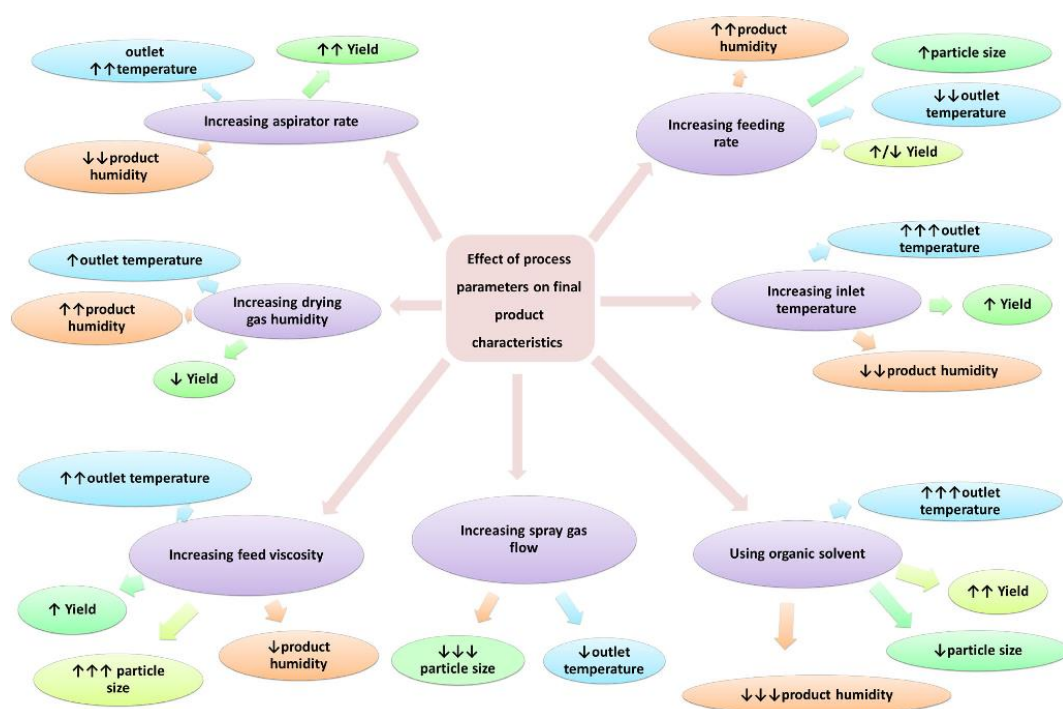
efficiency of the spray drying method, with the aim of reducing the amount of unencapsulated drug, which exists at the surface of the particles. Therefore, it is important to optimize the conditions to get the highest encapsulation efficiency.<sup>[102]</sup> However, the spray drying conditions also play a considerable role on the particle size and distribution.<sup>[101]</sup> Fatnassi et al.<sup>[106]</sup> concluded that optimization of the process conditions and formulation materials results in high encapsulation efficiencies, obtaining spherical morphology as well as appropriate particle size and particle size distribution.

Rattes et al.<sup>[103]</sup> evaluated the effect of spray drying conditions and encapsulating composition on the properties of the prepared sodium diclofenac microparticles. Round multi-sized microparticles were obtained and they concluded that physiochemical properties of the particles are dependent on spray drying parameters as well as their material composition. Additionally, statistical analysis showed that the feed flow rate was the most influential parameter, delaying the dissolution rate of the microparticles.

#### **1.6.2.1 Factors influencing properties of spray-dried particles**

The characteristics of the final spray-dried particles can be tuned by either process parameters (feed rate, inlet temperature, aspirator rate, spray gas flow or fluid feed properties (polymer and drug concentration)). Figure 23 shows the effect of process parameters on the characteristics of the final product.<sup>[100]</sup>





**Figure 23.** Effect of process parameters on the final product characteristics. ↑↑↑, high increasing influence; ↑↑, moderate increasing influence; ↑, minor increasing influence; ↓↓↓, high decreasing influence; ↓↓, moderate decreasing influence; ↓, minor decreasing influence. <sup>[100]</sup>

However, the results are controversial. It has been reported that increasing the polymer concentration contributes to larger particles, <sup>[104]</sup> whereas Rivera et al. reported that neither the polymer concentration nor polymer type has an effect on particle size or encapsulation efficiency. <sup>[107]</sup> Table 3 shows the impact of some the most influential parameters on particle size and encapsulation efficiency.

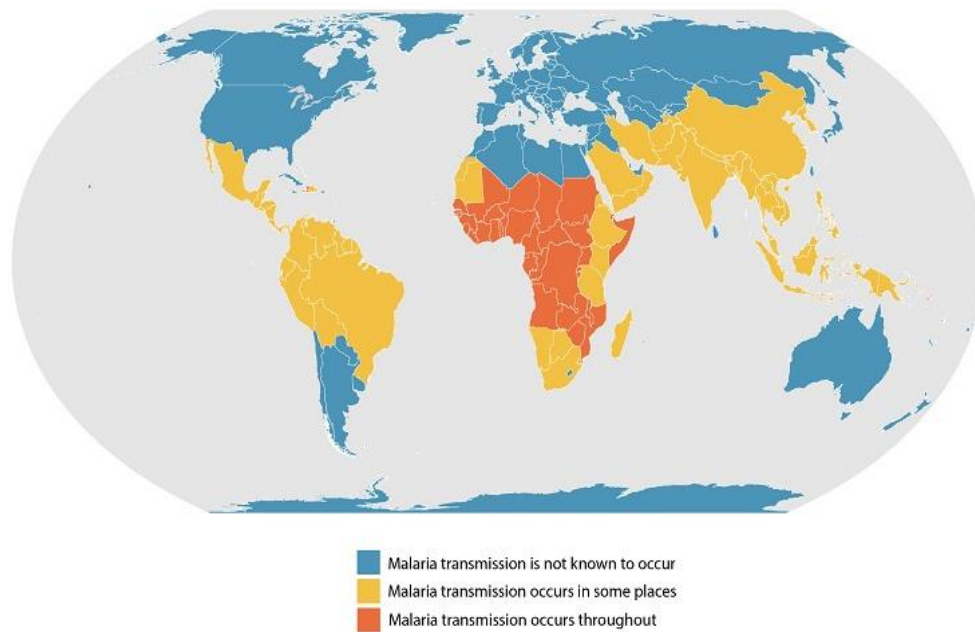
**Table 3.** Effect of different parameters on particle size and encapsulation efficiency of particles prepared by spray drying method.

Parameter	Effect on particle size	Effect on encapsulation efficiency
<b>Polymer concentration</b>	(↑)	(↑)
(↑)	[100,104,106,108]	[102,109]
<b>Drug concentration</b>	(↑)	(↓)
(↑)	[107]	[102,107,110]
<b>Flow rate</b>	(↑)	(↑)
(↑)	[100,103,111]	[103]
		(-) [111]
<b>Inlet temperature</b>	(↑)	(↓)
(↑)	[102,109,111]	[103,111]

## 1.7 Malaria

Malaria is considered as a dangerous infectious disease, caused by plasmodium parasites, <sup>[112,113]</sup> leading to the death of about 409 000 people (according to WHO 2019) mainly in tropical and subtropical regions <sup>[114,115]</sup> like Africa, South and Southeast Asia and Central and South America (Figure 24). <sup>[116]</sup> Despite all the advances in understanding the disease itself and the parasite mechanism, Malaria is still one of the major causes of mortality in endemic parts of the world.

The development of resistant parasite strains to most common drugs and inadequate improvement in developing new drugs resulted in slow progress in conducting specific measurements. However, in the recent ten years financing in research and development (R&D) for malaria and other tropical diseases has been increased considerably. <sup>[115]</sup>



**Figure 24.** Malaria map showing an approximation of the parts of the world, where malaria transmission mostly occurs. <sup>[117]</sup>

Malaria is transmitted to humans by female mosquitos of the genus anopheles (Figure 25). <sup>[113]</sup> When one is infected, there would appear series of symptoms including fever, shaking chills along with flulike illness. There are four different species, which infect humans including *Plasmodium falciparum*, *Plasmodium vivax*, *Plasmodium ovale* and *Plasmodium malariae*, among which *P.falciparum* is regarded as the most deadly one. <sup>[113,114]</sup>



**Figure 25.** Anopheles mosquito causing malaria. <sup>[118]</sup>

The most major challenge recently limiting the effectiveness of malaria treatment is the appearance of parasite resistance for the most of available antimalarial drugs. <sup>[119]</sup> Drug-resistant malaria happens with single or multiple point-mutations in genome resulting in parasites being insensitive to drugs. The arising of this phenomenon has completely influenced the treatment of malaria in endemic countries. Consequently, major measurements should be taken so that the effectiveness of the conventional antimalarial drug could be preserved. <sup>[113]</sup>

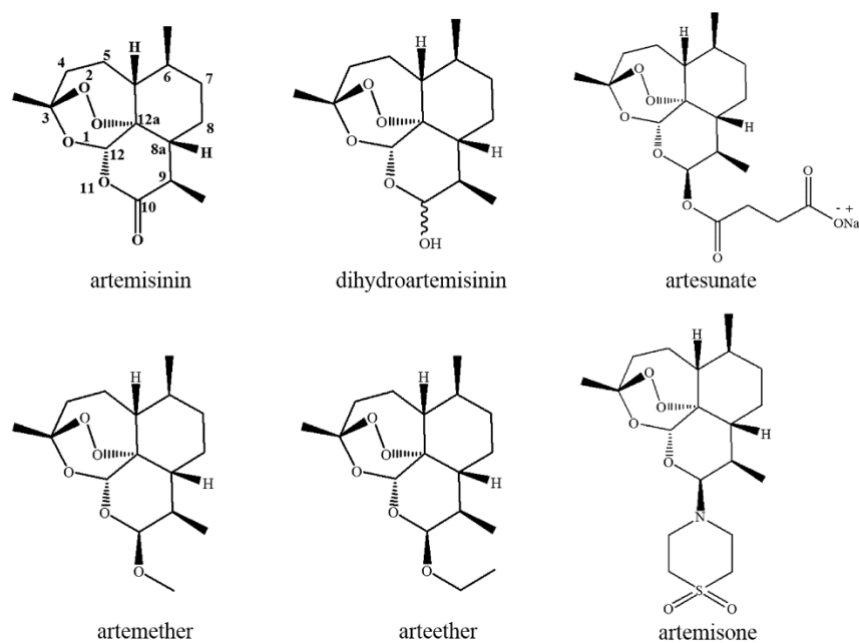
## **1.8 Available treatments for Malaria**

Artemisinins have opened up a new era in the treatment of malaria saving the lives of million people all around the world in the last 40 years. It was firstly discovered in China in early 1970s and is an extraction product of *Artemisia annua* L <sup>[120]</sup> (Figure 26) and belong to the most developed class of antimalarial drugs. <sup>[121]</sup> ACT was recommended by WHO at the beginning of the 21<sup>st</sup> century and is considered as the most effective, potent and rapidly acting antimalarial treatment, which shows higher treatment rates and faster parasite clearance <sup>[115]</sup> as well as optimal compatibility in their half-lives and their capability to obstruct

transmission of drug resistant strains.<sup>[61]</sup> Owing to their specific mechanism of action, fast impact on plasmodium and high in-vivo efficiency, artemisinins are regarded as a required part of malaria treatment.<sup>[119]</sup> Figure 27 shows artemisinin and its derivatives.



**Figure 26.** *Artemisia Annua*.<sup>[122]</sup>



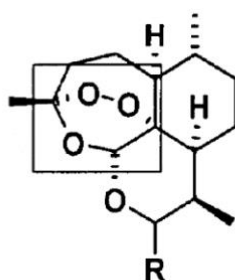
**Figure 27.** Artemisinin and its derivatives.<sup>[123]</sup>

Since the emersion of Artemisinin, different derivatives such as DHA, artesunate, arthemeter, arteether have been investigated.<sup>[115,123]</sup> However, their use have

been limited due to their poor bioavailability, short in-vivo half-life, poor water solubility <sup>[55]</sup> and low stability in aqueous medium. On the other hand, all artemisinins are metabolized into DHA, to which some parasite resistance was observed. Commonly it is believed that artemisinins mediate oxidative stress in the malaria parasite. <sup>[67,124]</sup>

## 1.9 Stability of Artemisinin and its derivatives

The most significant part in an artemisinin structure is the endoperoxide moiety, which is located in a heterocyclic ring called a 1,2,4-trioxane (Figure 28). In this structure, the peroxide bridge of two oxygen atoms is connected through a carbon to a third non-peroxidic oxygen atom. The peroxide group is considered as pharmacophore, which is crucial in antimalarial activity of the artemisinin compounds, <sup>[61]</sup> even though the presence of third non-peroxidic oxygen is essential to increase the activity. This peroxide group is chemically sensitive to reduction or electron transfer. <sup>[116]</sup>

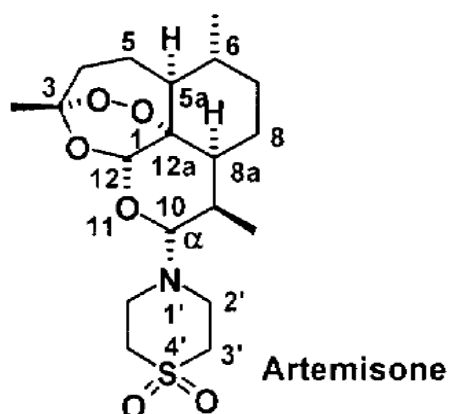


**Figure 28.** 1,2,4-trioxane pharmacophore of artemisinin molecules. <sup>[116]</sup>

## 1.10 Artemisone

Among artemisinin derivatives, ART is considered as a novel non neurotoxic

treatment for malaria <sup>[67]</sup> due to its longer half-life, higher anti-plasmodial activity, great therapeutic effect against cerebral malaria <sup>[125]</sup> and most important of all that it is not converted to DHA. <sup>[70]</sup> The structure of ART could be observed in Figure 29. ART is a second-generation derivative of artemisinin and is active against all stages of the malaria protozoan parasite, *Plasmodium falciparum*. <sup>[124]</sup> It has been reported that ART degradation happens by protonation at nitrogen atom following by elimination in acidic environment. <sup>[126]</sup> The physiochemical properties of ART is brought in Table 4.



**Figure 29.** Structure and name of ART. The chemical abstract name is 4-(3R,5aS,6R,8aS,9R,10R,12R,12aR)-decahydro-3,6,9-trimethyl-3,12-epoxy-12H-pyrano4,3-j-1,2-benzodioxepin-10-ylthiomorpholine 1,1-dioxide. <sup>[116]</sup>

**Table 4.** Physiochemical properties of ART. <sup>[116]</sup>

Artemisinin derivative	Crystal shape	m.p. (°C)	Aqueous solubility (mg/L)
Artemisone	needles	152.3-152.7	89 (23 °C, pH 7.4)

### **1.10.1 ART decomposition at different pHs**

When drugs are administered orally, they should pass firstly through the stomach and then into the intestine and finally into blood circulation. The pH in stomach is about 2 and, in the intestine, and blood is about 7. That's why, it is highly important to investigate if the drug is stable at different pH values. Lung et al. reported that ART is very stable at pH 7.24 and no degradation is detected at all, whereas at pH 2.24, ART is very unstable and is decomposed to DHA. <sup>[116]</sup>

### **1.10.2 Overcoming shortcomings of ART**

Recently, new drug delivery systems were developed which resulted in an increase in the use of number of drug molecules, which possess low water solubility, low aqueous stability and poor bioavailability. <sup>[75]</sup> Regarding this, it is important to mention that poor solubility of ART compound in water is liable for the toxic side effect. <sup>[55]</sup> Another issue regarding artemisinin derivatives is that they suffer from not being very stable and they easily decompose, mostly due to the opening of lactone ring, probably because of the peroxide group. <sup>[71]</sup> Furthermore, the artemisinin derivative, which is already formulated into tablets, capsules or other dose forms has to be transported, used and stored in climatically warm areas of the world, which significantly makes this process complicated. <sup>[116]</sup>

To overcome these concerns, it has been proved that the encapsulation of drug into various types of carriers brought about not only increased water solubility, improved their stability and thus enhanced bioavailability but also a more controlled release of drugs over a longer period of time and targeted delivery of drugs to a specific site of action, preserving drug against chemical and enzymatic degradation as well as exposing the parasites for a longer period of time to an



adequate high non-toxic drug concentration for eliminating the pathogens.<sup>[70,94,127]</sup> Additionally, encapsulation of therapeutic agent leads to lowering the dosing frequency and increasing patient compliancy as well as reduced drug side effect.<sup>[128]</sup>

## 1.11 Cellulose electrospinning

Bio-based raw material sources have attracted huge interest as a potential substitute for their fossil-based counterparts. Cellulose, which is the most abundant renewable polymer material in nature, offers huge valuable opportunity as a feasible alternative.<sup>[129]</sup> Furthermore, cellulose offers an advantage over other bio-based resources, since it does not compete with food or feed, and accounts for 35 – 50 % of the more than  $170 \times 10^9$  tons of lignocellulosic biomass produced every year.<sup>[130–132]</sup> Cellulose derivatives such as cellulose esters, cellulose ethers or cellulose carbonates, have found applications in different areas from optical films, textile, coating, cigarette filters, to non-woven fibers and drug release.<sup>[129,133–135]</sup>

A big challenge regarding elctrospinning of cellulose is the difficulty of solubilizing cellulose in a sustainable way. Owing to strong intra- and inter-molecular hydrogen bonds, it is difficult to solubilize cellulose in common solvents including water.<sup>[129]</sup> Therefore, specific solvents capable of breaking the intra-inter hydrogen bonds are needed to solubilize cellulose. These include N,N-dimethylacetamide-lithium chloride (DMAc-LiCl),<sup>[136]</sup> N-methylmorpholine N-oxide (NMMO),<sup>[137]</sup> dimethyl sulfoxide-tetramethyl ammonium fluoride (DMSO-TBAF), or trifluoroacetic acid (TFA).<sup>[138]</sup> These solvents impose some limitations including complicated recovery and toxicity and therefore they are not regarded as sustainable. However, these solvents have been investigated for direct electrospinning of cellulose. Ohkawa et al.<sup>[139]</sup> carried out the direct

electrospinning of cellulose in TFA, which resulted in the formation of nanocellulose fibers with average diameter of 40 nm. It is important to mention that using TFA in the solubilization of cellulose proceeds through a derivative step, where cellulose is modified to cellulose trifluoroacetate,<sup>[140]</sup> while the direct electrospinning of cellulose offers advantages such as avoiding any pre-derivatization step. The use of TFA gives rise to the environmental and safety problems. Similarly, DMAc-LiCl and NMMO/H<sub>2</sub>O were used by Kim et al.<sup>[141,142]</sup> for direct electrospinning of cellulose, which contributed to sub-micron fibers with diameters ranging from 150 - 750 nm.

Another class of solvents serving as a more sustainable alternative for direct solubilization of cellulose are ionic liquids. These solvents are generally described as molten salts with melting temperatures below 100 °C<sup>[143,144]</sup> and are categorized as “greener” solvents owing to their very low vapor pressures with recyclability and reusability potential, which are significant aspects for sustainability.<sup>[145]</sup> Coutinho et al. used a mixture of the ionic liquids 1-ethyl-3-methylimidazolium acetate and 1-decyl-3-methylimidazolium to electrospinn cellulose fibers. Results showed that they obtained nanofibers with an average diameter ranging between 165 and 185 nm.<sup>[146]</sup> The cellulose fibers were collected via coagulation in water and the ionic liquid is able to be recovered and reused. In a similar fashion, Linhard et al. reported the direct electrospinning of cellulose and cellulose-heparin in RTIL (room-temperature ionic liquids), using 1 N-butyl-3-methylimidazolium chloride and 1 N-ethyl-3-methylimidazolium benzoate).<sup>[147]</sup> In this case, the cellulose fibers were obtained by extraction of the RTIL using ethanol. However, larger micron-sized cellulose fibers were achieved and this phenomenon was ascribed to the non-volatility of the solvents. Finally, 1-allyl-3-methylimidazolium chloride (AMIMCl) in DMSO was used by Xu et al.<sup>[148]</sup> Although ionic liquids might be “greener” solvents compared to the traditional ones, they own their limitations and challenges.<sup>[149]</sup>

Among their limitations are toxicity <sup>[150]</sup> and non-inertness to cellulose, <sup>[149,151]</sup> which makes their recovery more difficult and costly compared to other solvents. To overcome the challenges in solubilizing cellulose, cellulose derivatives such as Cellulose acetate (CA), methyl cellulose (MC) and carboxymethylcellulose (CMC) have been employed, which could be more easily solubilized in common solvents for electrospinning. <sup>[152]</sup> However, it is noteworthy that a post-derivatization step is necessary to recover the native cellulose fibers. This additional step results in more wastes, thereby making the approach less sustainable. Son et al. <sup>[153]</sup> reported the electrospinning of CA in an acetone/water mixture containing between 10 and 15 wt. % water. CA fibers with average diameter of 2.3  $\mu\text{m}$  were obtained under acidic conditions, whereas thinner fibers with an average diameter of 460 nm were obtained under basic conditions. Frenot et al. reported the electrospinning of CMC, HPMC (hydroxy propyl methylcellulose), and MC. CMC was electrospun in a 1:1 ratio with PEO using water as a solvent. <sup>[154]</sup> Nanofibers with an average diameter between 200 and 250 nm were obtained. Nanofiber morphology was investigated using SEM and results showed that the morphology was independent of the molecular weight (MW) and degree of substitution (DS) but rather dependent on the substitution pattern. Additionally, extraction of PEO after the electrospinning process caused a change in fiber morphology and relied on the substitution pattern in the CMC.

To ensure more sustainable electrospinning of cellulose, the use of a more sustainable solvent system with a potential of recyclability will enable us to improve the sustainability of this process. A sustainable solvent system based on  $\text{CO}_2$  in the presence of an organic super-base was developed by Jessop et al. <sup>[155]</sup> This system allows the possibility to switch the polarity of a solvent simply by addition or removal of  $\text{CO}_2$ .

Recently, Onwukamike et al. reported a thorough optimization of the solvent system and proved the presence of a cellulose carbonate intermediate, which

demonstrated the solubility of cellulose in the DMSO solvent.<sup>[156]</sup> They achieved complete cellulose solubilization within 10 – 15 min at 30 °C under very low CO<sub>2</sub> pressure (2 – 5 bar). Such mild solubilization conditions enable the exploration of the switchable solvent system, which exhibits a more sustainable succinylation of cellulose<sup>[157]</sup> as well as transesterification of cellulose using plant oils directly.<sup>[158]</sup>

## **1.12 Aim and concept**

Based on the previously described knowledge, I successfully developed the hypothesis that the release of therapeutic agents could be retarded from electrospun nanofibers, if they are further encapsulated in particles within the fibers. This would open up a wide field for the modulation of release of different therapeutic agents and could extend the release of drug from electrospun nanofibers. Consequently, the aim of my thesis was to encapsulate different drug-loaded particles in electrospun nanofibers to merit both from reducing the amount of burst release as well as obtaining a more sustained release over time. To achieve these goals, different electrospinning techniques including co-electrospinning, suspension electrospinning and core-shell electrospinning were employed to encapsulate the drug-loaded particles in electrospun nanofibers. In order to verify the hypothesis and to attain the goal, I developed the concept to systematically investigate the release of a highly relevant drug incorporated in different micro- and nanoparticles as drug carriers, incorporated in electrospun nanofibers. ART was selected as the hydrophobic drug for the investigation, accordingly. The relevance of ART for Malaria treatment and its inherent instability in physiological medium was another motivation for me to evaluate this system, as I am convinced that the results of my thesis will make an

important contribution, which is described in detail in the following results and discussion.

# **Chapter 2**

## Results and discussion

## **2 Results and discussion**

### **2.1 Synthesis of ART-loaded PLGA nanoparticles using solvent displacement method**

We synthesized ART-loaded PLGA nanoparticles using solvent displacement method. We were aiming at achieving stable nanoparticles dispersion with high encapsulation efficiencies and homogeneous particle size. Design expert software was used as a tool to optimize the conditions to obtain a homogeneous particle size as well as encapsulation efficiency and to find out, which parameter has the most prominent parameter. Response surface methodology (RSM) was used on the basis of a three level, four parameter Box-Benken design (BBD). Among different design of experiment methods (DOE), BBD is of great interest, as it take into account the interactions of different parameters, while providing less experiments. <sup>[159]</sup> It is important to mention that some preliminary experiments were done in order to not only choose between the outmost influencing parameters, but also to set the range of parameters. In case of solvent displacement method, temperature and organic phase addition rate were selected at the beginning. Based on the preliminary test, it was observed that these parameters do not play an important role on particle size and encapsulation efficiency. Ultimately, four major parameters including PLGA concentration, ART concentration, organic to aqueous ratio and stirrer rate were found out as the most influential parameters. The range of PLGA concentration was set between 30 and 40 mg. A higher amount of PLGA than 40 mg resulted in a precipitation of the PLGA polymer (Figure 30).



**Figure 30.** Precipitation of PLGA during solvent displacement method (containing 40 mg PLGA).

On the other hand, higher amounts of ART (20 wt. %) resulted in the formation of drug crystals in the dispersion (Figure 31), which could be due to crystallization of the drug after the evaporation of the solvent, as ART forms a crystalline structure. This phenomenon was also observed in the work done by Bagheri et al. <sup>[125]</sup>



**Figure 31.** Formation of ART crystals after solvent evaporation (containing 20 wt. % ART).

Table 5 shows the parameters, their range as well as the result of the parameters on particle size and encapsulation efficiency of the nanoparticles prepared by solvent displacement method.



**Table 5.** Different parameters and their effect on particle size and encapsulation efficiency for solvent displacement method.

Run	PLGA concentration (mg)	ART concentration (wt. %)	Organic to aqueous ratio (-)	Stirrer rate (rpm)	Particle size (nm)	Encapsulation efficiency (%)
1	35	15	1:4	500	175	61
2	30	15	1:4	750	170	53
3	35	15	1:5	750	180	62
4	30	15	1:5	500	165	62
5	35	15	1:4	500	176	63
6	35	20	1:3	500	172	56
7	35	10	1:5	500	178	59
8	40	15	1:5	500	191	72
9	35	15	1:3	750	163	53
10	35	15	1:4	500	180	65
11	35	20	1:5	500	187	62
12	35	10	1:4	750	166	50
13	30	10	1:4	500	149	50
14	35	15	1:5	250	197	70
15	35	15	1:4	500	182	62
16	35	20	1:4	750	168	54
17	35	15	1:3	250	176	62
18	40	20	1:4	500	182	65
19	40	15	1:4	750	186	64
20	30	15	1:3	500	150	53
21	30	20	1:4	500	151	54
22	40	15	1:4	250	218	71
23	35	15	1:4	500	185	60
24	35	20	1:4	250	184	62
25	40	15	1:3	500	177	64
26	40	10	1:4	500	178	61
27	35	10	1:4	250	180	58
28	30	15	1:4	250	187	61
29	35	10	1:3	500	170	50

Figure 32 Show the results of the effect of different parameters including PLGA concentration, ART concentration, organic to aqueous ratio and stirrer rate on particle size and encapsulation efficiency of nanoparticles prepared by solvent displacement method. Polymer concentration is considered as a crucial factor which controls the particle size that is pivotal for drug delivery applications.<sup>[78,80]</sup> Likewise, it was seen in this work that PLGA concentration plays an important role in the obtained drug encapsulation efficiency and size of nanoparticle (Figure 32a). Our results is in agreement with the literature.<sup>[79,81,84]</sup> By increasing the PLGA concentration, a significant increase in particle size was acquired from 160 nm to 190 nm. This is in agreement with the literature.<sup>[83]</sup> Generally, the higher polymer–polymer interaction hinders the diffusion of solvent into aqueous phase, thus producing larger nanoparticles.<sup>[71]</sup> Beside this, the encapsulation efficiency rises from 58 % to 70 % as the PLGA concentration increases. This could be due to an increase in the particle size. An enhancement in the diameter of the particles causes a decrease in surface to volume ratio, thereby reducing the possibility that the drug leaks through diffusional routes to the aqueous medium and therefore resulting in higher encapsulation efficiencies,<sup>[159]</sup> as it is shown in Scheme 1.

Diameter	Surface to volume ratio	Drug leakage	Encapsulation efficiency
↑	↓	↓	↑

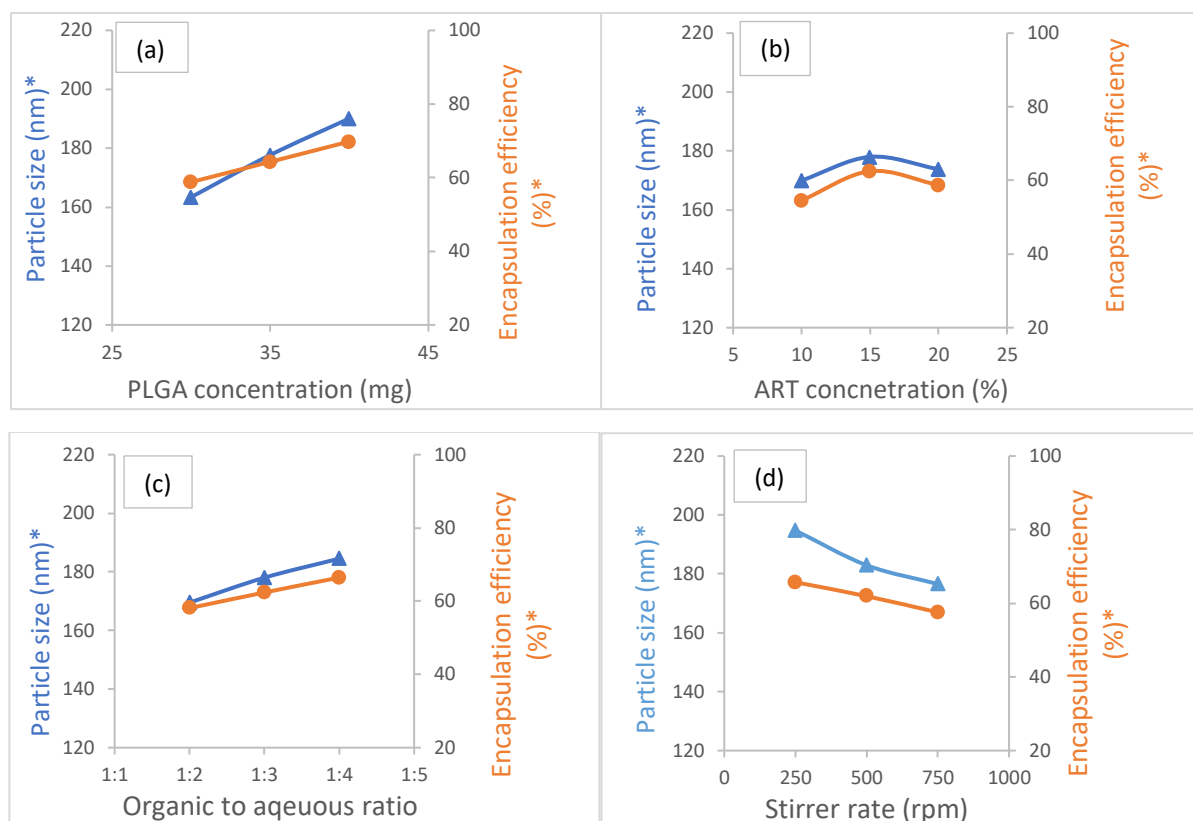
**Scheme 1.** The relationship between different parameters affecting encapsulation efficiency.

When the ART concentration increases, a slight increase in nanoparticle size was observed (from 170 nm to 178 nm) as well as encapsulation efficiency (from 55 % to 61 %) followed by a decrease to 174 nm and 59 %, respectively (Figure 32b). This is in agreement with the results of Budhian et al. : “an increase in the drug

amount increases the resistance to solvent diffusion into aqueous phase, resulting in higher particle sizes".<sup>[81]</sup> Concerning encapsulation efficiency, it has been proven that the drug loss happens by further increasing the drug concentration, due to the tendency of drug molecules in the polymer matrix to move toward the drug molecules in the aqueous medium, creating crystals in the aqueous phase. This proves that the highest encapsulation and loading efficiency of the nanoparticles is reached and a further addition of ART does not increase encapsulation efficiencies.<sup>[81]</sup>

Figure 32c shows the impact of organic/aqueous phase ratio on particle size and encapsulation efficiency. An increment in encapsulation efficiency from 58 % to 66 % as well as particle size from 170 nm to 184 nm was observed, when organic to aqueous phase ratio decreases. Increasing the amount of organic to water ratio enables the diffusion of the solvent into the aqueous phase, hence decreasing the particle size and enhancing the surface area. This results in better partitioning of the drug in the aqueous phase, and eventually decreasing the encapsulation efficiency.<sup>[40,94]</sup>

An enhancement in the stirring rate (Figure 32d) caused a decrease in the particle size from 195 nm to 175 nm. This is in agreement with the literature.<sup>[84,160]</sup> As previously described, the formation of particle is largely dependent on the diffusion of organic phase into aqueous phase. As a result, particle formation is time-dependent because of solvent diffusion. As soon as the stirring rate is low, the possibility that the organic phase would quickly diffuse into the aqueous phase is reduced.<sup>[95,160]</sup> As the stirring rate increases, which reduces the time it takes for the ART to diffuse, a diffusion hindrance might take place, causing a decrease in the amount of drug, which is encapsulated in nanoparticles (from 65 % to 57 %).<sup>[81]</sup>



**Figure 32.** Effect of different parameters on particle size ( —▲— ) and drug encapsulation efficiency ( —●— ) of ART-loaded PLGA nanoparticles prepared by solvent displacement method obtained by RSM (particle size was measured by SEM and encapsulation efficiency by HPLC). \*P-values for particle size: PLGA concentration (0.0001), ART concentration (0.4091), organic to aqueous ratio (0.005), Stirrer rate (0.0012). \*P-values for encapsulation efficiency: PLGA concentration (<0.0001), ART concentration (<0.0001), organic to aqueous ratio (<0.0001), Stirrer rate (<0.0001).

The data obtained from SEM and HPLC for particle size and encapsulation efficiency, was given in RSM was used to assess and optimize the effect of different parameters. Based on the RSM results for particle size, PLGA concentration, organic to aqueous ratio and stirrer rate are the most governing parameters ( $P < 0.05$ ). For encapsulation efficiency, all four parameters including PLGA concentration, ART concentration, organic to aqueous ratio and stirrer rate are significant ( $P < 0.05$ ). Moreover, as it could be concluded from Figure 32, among all parameters, PLGA concentration has the most influence on the particle size and encapsulation efficiency.

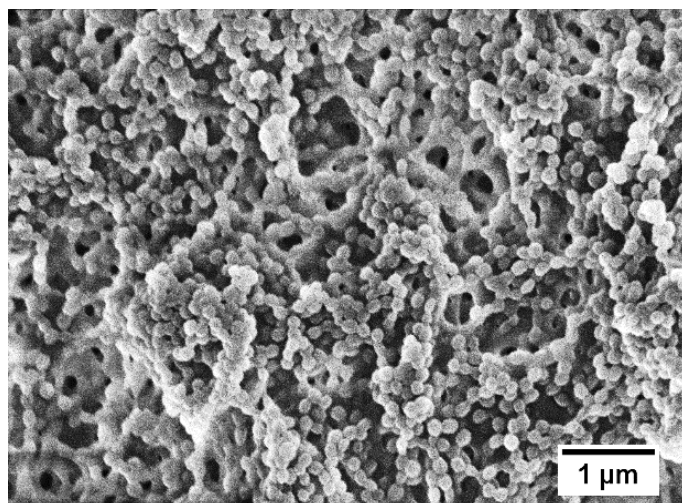
On the other hand, results exhibited for solvent displacement method that both particle size and encapsulation efficiency perform dependently. This means that the same trend was observed for particle size and encapsulation efficiency with an increase in value of each parameter.

The optimized conditions, in which the highest encapsulation efficiency is achieved, were chosen based on RSM to prepare nanoparticles for further use for release tests. These optimized conditions are presented in Table 6.

**Table 6.** Optimized conditions for nanoparticles synthesized by solvent displacement method.

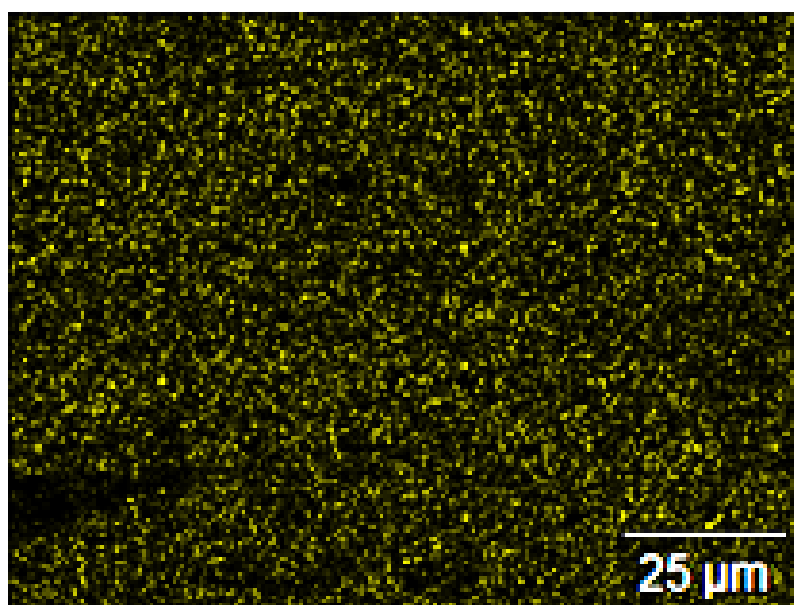
<b>PLGA concentration</b>	<b>ART concentration</b>	<b>Organic to aqueous</b>	<b>Stirrer</b>
<b>(mg)</b>	<b>(wt. %)</b>	<b>ratio</b>	<b>rate (rpm)</b>
40	20	1:4	250

Under optimized condition, the highest encapsulation efficiency achieved was 71 % and an average particle diameter of  $173 \pm 15$  nm determined by SEM. The AFFF results show a particle diameter of  $171 \pm 10$  nm, which is in agreement with both the DLS and SEM results. SEM micrographs demonstrated round particles homogenous in size (average particle size:  $160 \pm 18$  nm). A slightly higher particle size for DLS and AFFF is obtained probably due to the reason that for these two analyses the particles were performed in an aqueous medium, resulting in a difference compared to SEM results, where particles are measured in a dried condition (Figure 33).



**Figure 33.** SEM micrographs of ART-loaded nanoparticles by solvent-displacement method under optimized condition.

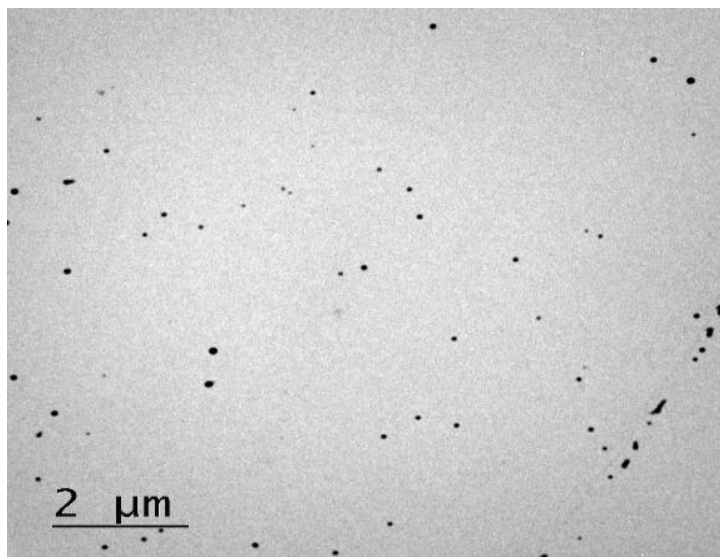
Energy-dispersive X-ray (EDX) was used to evaluate the distribution of ART in the nanoparticles by tracking its characteristic element sulfur. Figure 34 proves the presence of sulfur and that it is distributed evenly.



**Figure 34.** Representative EDX image of ART-loaded PLGA nanoparticles under optimized condition.

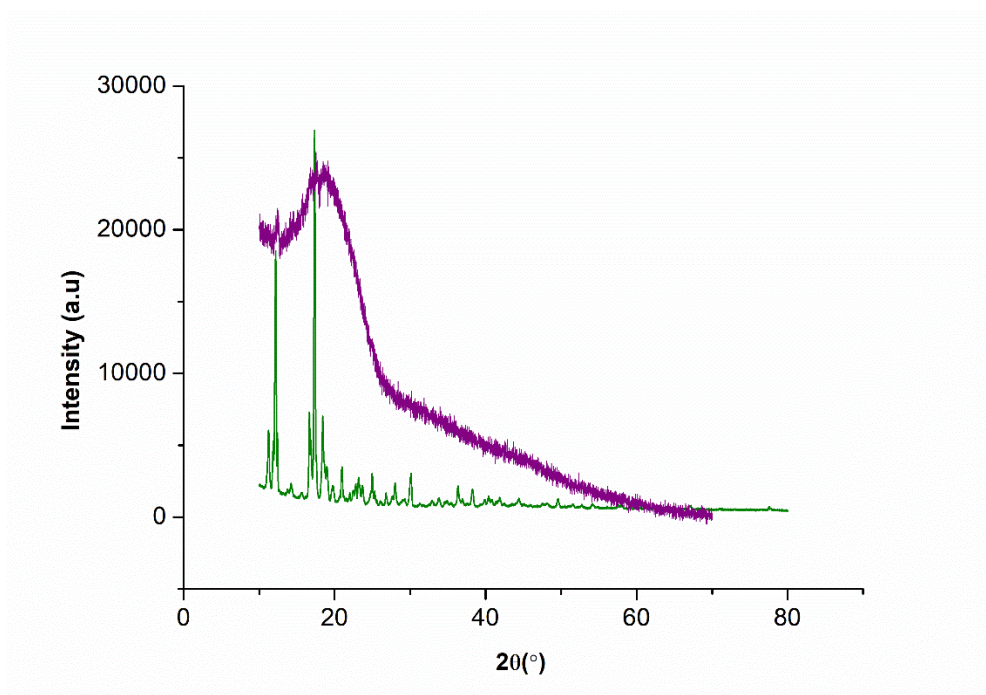
TEM micrographs of ART-loaded nanoparticles (Figure 35) prove the spherical shape of nanoparticles as well as their homogeneous size distribution. Moreover, it is also visible that the particles are not adhered to each other,

representing their good dispersion and stability in water without use of any surfactant. Additionally, the average particle size obtained by TEM is in good agreement with those of SEM, DLS and AFFF measurements.



**Figure 35.** TEM micrographs of ART-loaded PLGA nanoparticle dispersion under optimized condition.

ART alone was found to be completely crystalline, showing diffraction peaks at 11.25 °, 12.18 °, 16.66 °, 17.34 °, 18.43 ° and 25.34 ° respectively.<sup>[161]</sup> XRD analysis shows that ART-loaded nanoparticles reveal two characteristic peaks with low intensity at 11.25 ° and 17.34 °, which could be attributed to the characteristic crystalline peaks of the ART.<sup>[161]</sup> Based on XRD results (Figure 36), it could be inferred that the drug has retained its crystalline structure, and that justifies the results obtained by HPLC that the ART is not completely encapsulated into PLGA particles resulting in lower encapsulation efficiencies. Our results are in agreement with the literature.<sup>[162]</sup>



**Figure 36.** XRD pattern of ART and ART-loaded PLGA nanoparticles produced by solvent displacement. ( — ) shows ART and ( — ) ART-loaded PLGA nanoparticles under optimized condition.

## 2.2 Preparation of ART-loaded PLGA microparticles by spray drying method

Spray drying method was used in order to fabricate ART-loaded microparticles. Design expert was employed to optimize the parameters and to achieve high loading and encapsulation efficiencies. Table 7 shows the parameters, their range and the effect of the parameters on particle size and encapsulation efficiency of the microparticles prepared by spray drying method.



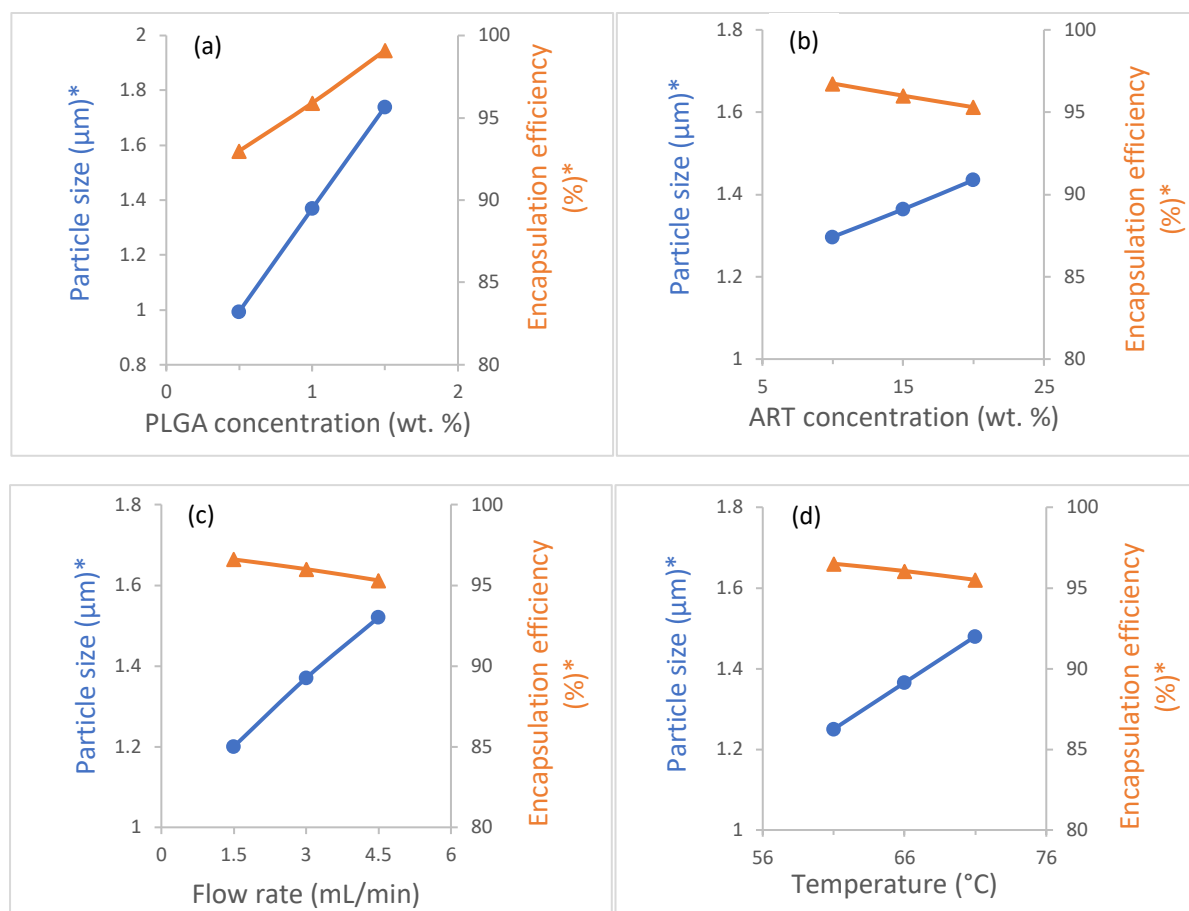
**Table 7.** Different parameters and their effect on particle size and encapsulation efficiency for spray drying.

Run	PLGA concentration (wt. %)	ART concentration (wt. %)	Flow rate (mL/h)	Inlet temperature (° C)	Particle size (nm)	Encapsulation efficiency (%)
1	1	15	4.5	71	1,439	95.0
2	1.5	15	3	61	1,530	99.7
3	1	20	1.5	66	1,195	95.0
4	1	15	3	66	1,590	96.0
5	1	15	3	66	1,480	96.6
6	0.5	20	3	66	0,987	91.5
7	0.5	10	3	66	0,817	95.5
8	1	15	4.5	61	1,270	96.3
9	1	10	3	71	1,579	96.3
10	1	15	3	66	1,578	96.8
11	1	20	3	61	1,480	96.5
12	0.5	15	3	61	0,886	93.4
13	1	20	3	71	1,610	95.4
14	0.5	15	1.5	66	0,875	94.6
15	0.5	15	4.5	66	1,300	91.2
16	1	15	1.5	71	1,154	96.5
17	1	10	3	61	1,370	97.5
18	1.5	15	4.5	66	1,954	98.8
19	1	15	3	66	1,535	96.5
20	1	15	1.5	61	0,915	97.0
21	1	20	4.5	66	1,395	94.0
22	1.5	20	3	66	1,799	99.6
23	1	15	3	66	1,430	95.0
24	1	10	4.5	66	1,270	95.0
25	1	10	1.5	66	0,945	96.0
26	1.5	10	3	66	1,659	99.5
27	1.5	15	1.5	66	1,599	98.9
28	1.5	15	3	71	1,899	97.5
29	0.5	15	3	71	1,095	92.2

Figure 37 exhibits the effect of different parameters on particle size and encapsulation efficiency of the ART-loaded particles prepared by spray drying method based on the data from RSM methodology. According to Figure 37a, higher PLGA concentrations resulted in significant increase in the particle size from 1  $\mu\text{m}$  to 1.7  $\mu\text{m}$ . These data are in agreement with the literature.<sup>[101]</sup> As a result, a higher amount of ART is encapsulated into particles from 92 % to 99 % for the higher PLGA concentration. Noticeably, an increase in the PLGA amount of each droplet, results in bigger particle diameters and encapsulation efficiency. Additionally, with an increase in the PLGA concentration, the chances that the drug would be exposed to the particle surface decreases and thus the encapsulation efficiency is enhanced.<sup>[98]</sup>

By keeping the PLGA concentration in a constant level, an increase in the ART concentration contributes to a minimal increase in particle size from 1.3  $\mu\text{m}$  to 1.45  $\mu\text{m}$  (Figure 37b). This could be originated from the higher amount of solution which is sprayed through the nozzle.<sup>[100]</sup> It was seen that the drug encapsulation efficiency was slightly reduced from 96.5 % to 95 %, possibly, because some amount of ART might not be encapsulated into the PLGA polymer matrix, owing to the lack of optimal ratio of ART to PLGA.<sup>[104]</sup> Alternatively, it could be due to high osmotic pressure of the loaded droplets, which results in the formation of pores and the loss of the ART.<sup>[107,163]</sup> Nevertheless, there is still high loadings of ART in particles, which has 20 wt. % ART. With an increase in the flow rate, an increase in droplet size was observed because of larger droplets are formed during the spray drying process, as more liquid is sprayed thorough the nozzle.<sup>[103]</sup> As a result, particle size was increased as well from 1.2  $\mu\text{m}$  to 1.5  $\mu\text{m}$ , (Figure 37c). Despite that, as there would not be enough time for the ART to be encapsulated into particles as a result of higher flow rate, a slight decrease in encapsulation efficiency was observed from 96.5 % to 95 %.

As the inlet temperature increases (Figure 37d), a slight increase from 1.25  $\mu\text{m}$  to 1.45  $\mu\text{m}$  in particle size was obtained. Increasing the inlet temperature could contribute to a much faster formation of particle structure, thus preventing the particles from being shrank during the drying process and thereby producing higher particle diameter, accordingly. <sup>[102,164]</sup> On the other hand, the reduce in the encapsulation efficiency from 96.5 % to 95.5 % could be associated to a rise in the temperature causing the solvent to be evaporated faster and consequently there would not be enough time for the ART to be encapsulated into polymer matrix, resulting in a partial encapsulation of the drug. <sup>[165]</sup>



**Figure 37.** Effect of different parameters namely (a) PLGA concentration (b) ART concentration (c) Flow rate (d) Temperature on particle size (—●—) and drug encapsulation efficiency (—▲—) of ART-loaded PLGA microparticles prepared by spray drying method obtained by RSM (particle size was measured by SEM and encapsulation efficiency by HPLC).

\*P-values for particle size: PLGA concentration (0.0001), ART concentration (0.1124), flow rate (0.0013), temperature (0.0118). \*P-values for encapsulation efficiency: PLGA concentration (<0.0001), ART concentration (0.0097), flow rate (0.0105), temperature (0.0118).

RSM results showed that for particle size, PLGA concentration, flow rate and inlet temperature are meaningful parameters. For encapsulation efficiency, all four parameters including PLGA concentration, ART concentration, flow rate and inlet temperature are considered significant ( $P < 0.05$ ). It could be also deduced from the ANOVA results that among the different parameters, PLGA concentration has the most influential effect on both particle size and encapsulation efficiency of the microparticles. In spray drying method, only in case of PLGA

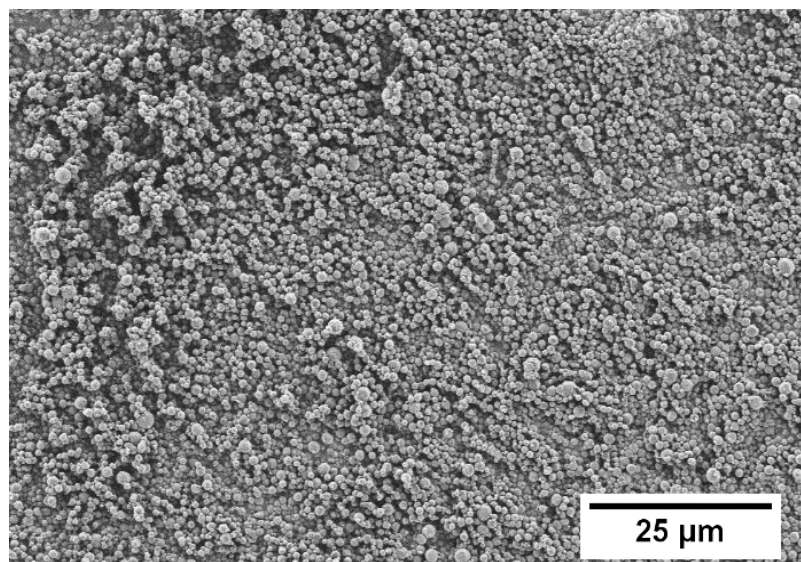
concentration, the same trend was seen in particle size and encapsulation efficiency. This means an increase in the PLGA concentration, resulted in an increase in both particle size and encapsulation efficiency. Whereas for other parameters, a rise in the value of that parameters resulted in a converse effect in both particle size and encapsulation efficiency.

The optimal conditions given by RSM, where the highest encapsulation efficiency is achieved, were chosen to prepare nanoparticles for further analyses (Table 8).

**Table 8.** Optimized conditions of ART-loaded PLGA microparticles fabricated by spray drying method.

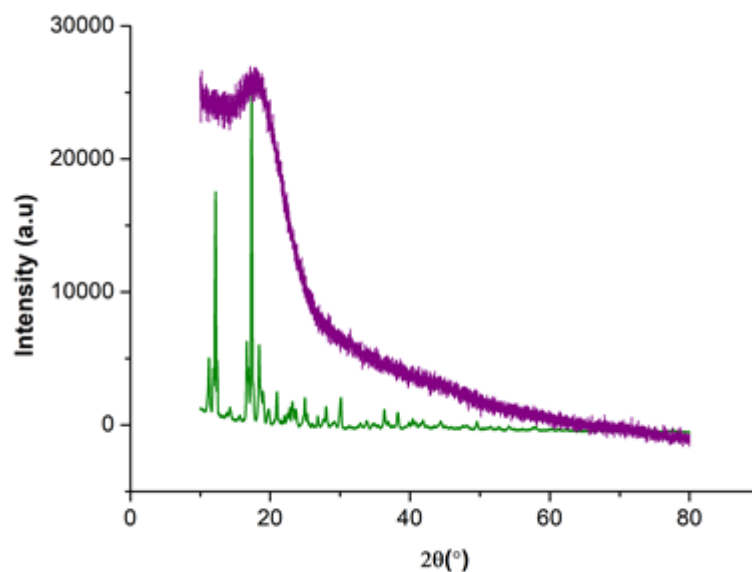
PLGA concentration	ART concentration	Flow Rate	Temperature
(wt. %)	(wt. %)	(mL/h)	(°C)
1.5	15	4.5	61

Figure 38 shows the SEM micrographs of optimized spray-dried particles. Particles with very high encapsulation efficiencies of 97 % and average particle diameter of  $1400 \pm 550$  nm were obtained with this method. For analysis by AFFF, microparticles were redispersed in Tween 80. The average size obtained by AFFF was  $1270 \pm 30$  nm.



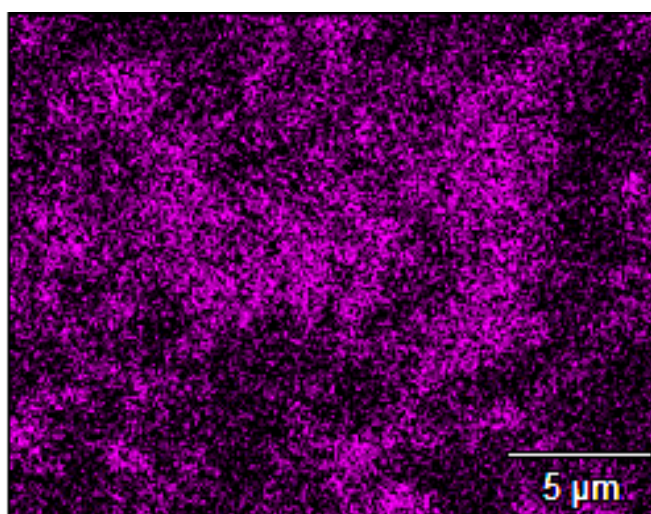
**Figure 38.** SEM micrograph of ART-loaded PLGA microparticles prepared by spray-dried method under optimized condition.

Figure 39 exhibits the XRD pattern of ART. According to the Figure 41, no crystalline peak was found in ART-loaded PLGA microparticles. This could be due to the complete encapsulation of the crystalline drug in the PLGA matrix, an amorphous polymer, which resulted in obtaining particles with an amorphous structure. This justifies the fact that the drug is entirely encapsulated in polymeric nanoparticles,<sup>[101]</sup> producing high encapsulation efficiencies of more than 97 %, which is also in agreement with Raman results.



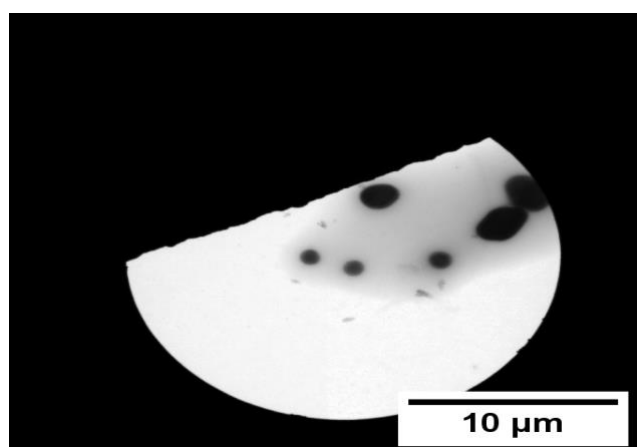
**Figure 39.** XRD pattern of ART and ART-loaded PLGA microparticles produced by spray drying. ( — ) shows ART and ( — ) ART-loaded PLGA microparticles under optimized condition.

EDX was performed to trace ART in ART-loaded microparticles (Figure 40). The EDX results proves the presence of the element sulphur, which is the distinguishable element in the structure of ART and illustrates the homogenous distribution of ART in the microparticles.



**Figure 40.** Representative EDX spectrum of spray-dried ART-loaded PLGA microparticles under optimized condition.

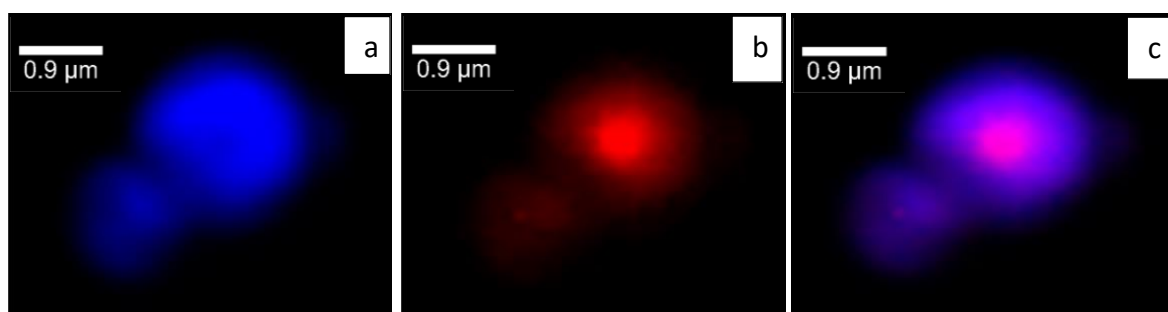
Figure 41 indicates the TEM micrograph of ART-loaded spray-dried particles. The drug-loaded particles are redispersed in water homogenously with Tween 80 as a stabilizing surfactant, and the particles mostly kept their round structure. The average particle size was  $1700 \pm 500$  nm, which is slightly more than that of SEM. This could be ascribed to the presence of Tween 80, which adheres to the surface of the particles. Other surfactants, including SDS and PVA were used, but did not form a stable dispersion and the particles were precipitated after a while.



**Figure 41.** TEM micrographs of ART-loaded PLGA spray-dried micro and nanoparticles in water containing 1 wt. % Tween 80.

Raman spectroscopy was carried out to investigate further, whether the drug is completely encapsulated into the particles or only located on the surface. Figure 42 represents the distribution of PLGA and ART along with the combined distribution of both components. It could be observed that the drug is completely encapsulated inside the polymer matrix. These results are in great agreement with the XRD results.

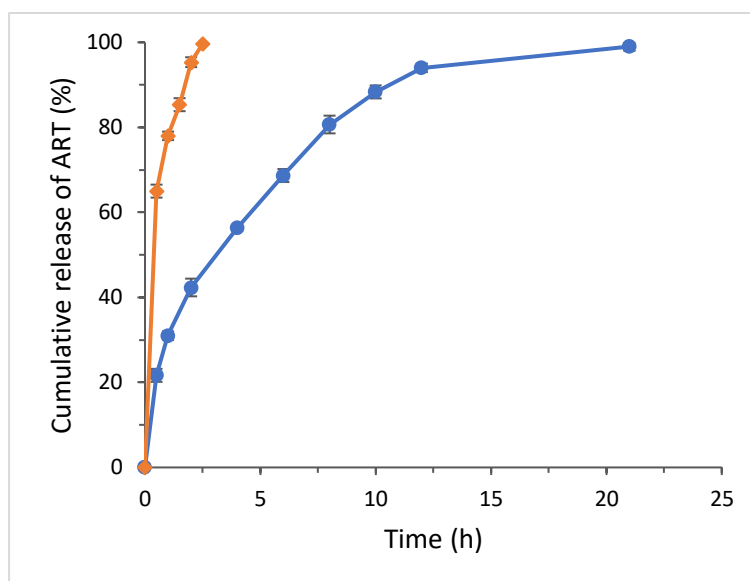




**Figure 42.** Raman image of (a) PLGA distribution, (b) ART distribution, (c), combined distribution of PLGA and ART.

## 2.3 Drug release from ART-loaded micro- and nanoparticles

Controlled release of drug from drug-loaded micro and nanoparticles is regarded greatly important owing to the feasible effect on the final application of the resultant product, as these systems merit the diminishing of systemic side effects of drug as well as increasing the patient compliancy.<sup>[165–167]</sup> Figure 43 shows time dependence drug release of micro- and nanoparticles containing 14 wt. % ART. In case of nanoparticles, a burst release of about 60 % was observed within 30 min and the whole drug release was accomplished after 2.5 h. On the contrary, for ART-loaded microparticles within 30 min only 20 % of the drug was released, followed by a slower release in a time period up to 22 h. These results could be attributed to the longer diffusion path of the drug within microparticles compared to the nanoparticles. However, based on XRD, the drug is not completely encapsulated in nanoparticles, meaning that there are some fractions of drug available on the surface of nanoparticle. In the case of spray-dried microparticles it was proved not only through XRD, but also by using Raman technique that the whole drug is encapsulated within microparticles and not located on the surface, consequently resulting in a much more sustained release.



**Figure 43.** ART release from ART-loaded PLGA micro (—●—) and nanoparticle (—◆—).

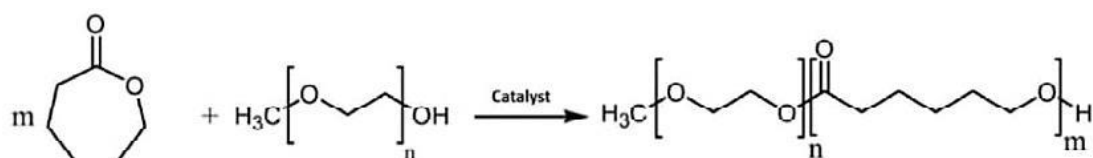
## 2.4 Synthesis of PCL-mPEG as a biocompatible biodegradable polymer

PCL-mPEG polymer was synthesized by ring opening polymerization  $\epsilon$ -caprolactone catalyzed by stannous octoate in the presence of  $\alpha$ -methoxy- $\omega$ -hydroxy-poly (ethylene glycol) (mPEG) as a macroinitiator according to Figure 44. In order to purify the polymer after precipitation in n-pentane, the polymer was extracted in water to remove the water-soluble parts of the product, such as the oligo PCL-b-mPEG and unreacted mPEG. Different parameters used for the synthesis are indicated in Table 9.

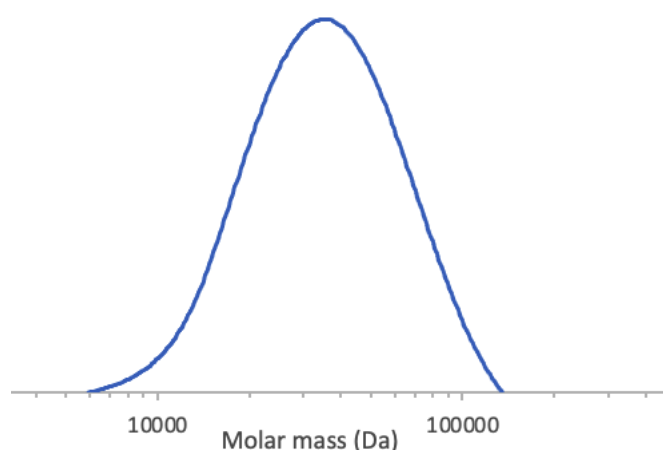
**Table 9.** Different parameters used for the synthesis of PCL-mPEG.

Caprolactone	mPEG	Catalyst	Temperature	Time
(g)	(g)	( $\mu$ L)	( $^{\circ}$ C)	(h)
13.95	4.65	30	130	2.5

In order to purify the polymer after precipitation in n-pentane, the polymer was extracted in water to remove the water-soluble parts of the product, such as the oligo PCL-b-mPEG and unreacted mPEG. The synthesized block copolymer showed a monomodal GPC curve (Figure 45). The x-axis represents molar mass and y-axis intensity.



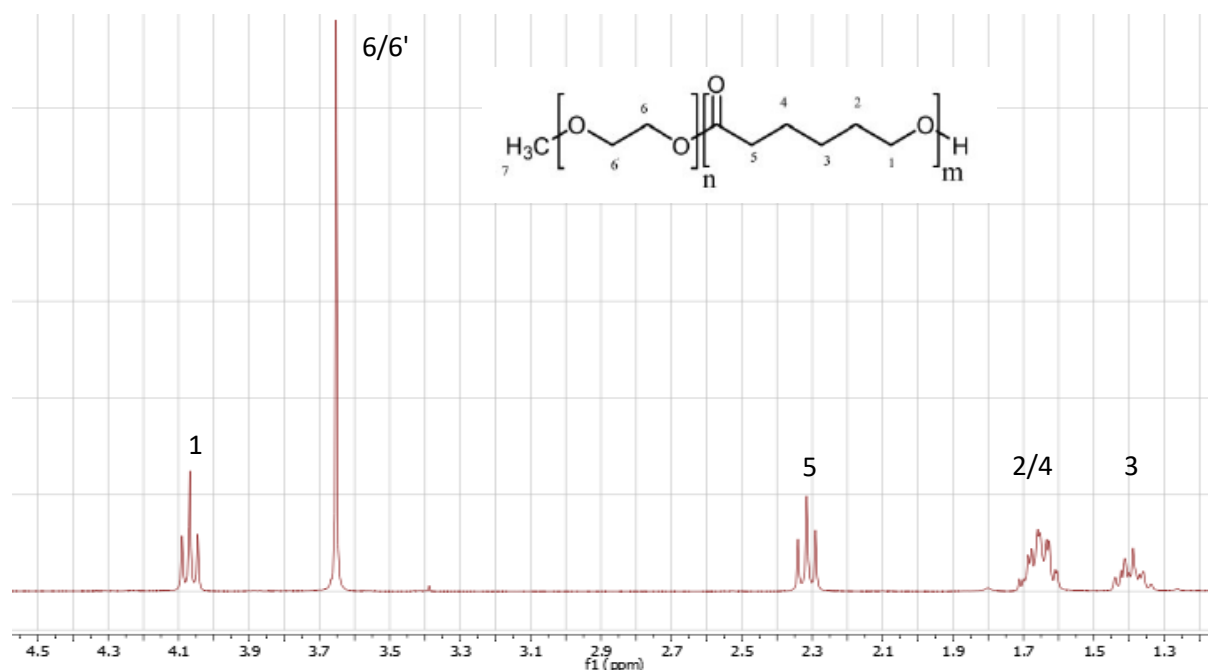
**Figure 44.** Formation of block copolymers of polycaprolactone (PCL) and methoxy terminated polyethylene glycol (mPEG).



**Figure 45.** GPC curve of synthesized PCL<sub>15000</sub>-mPEG<sub>5000</sub>

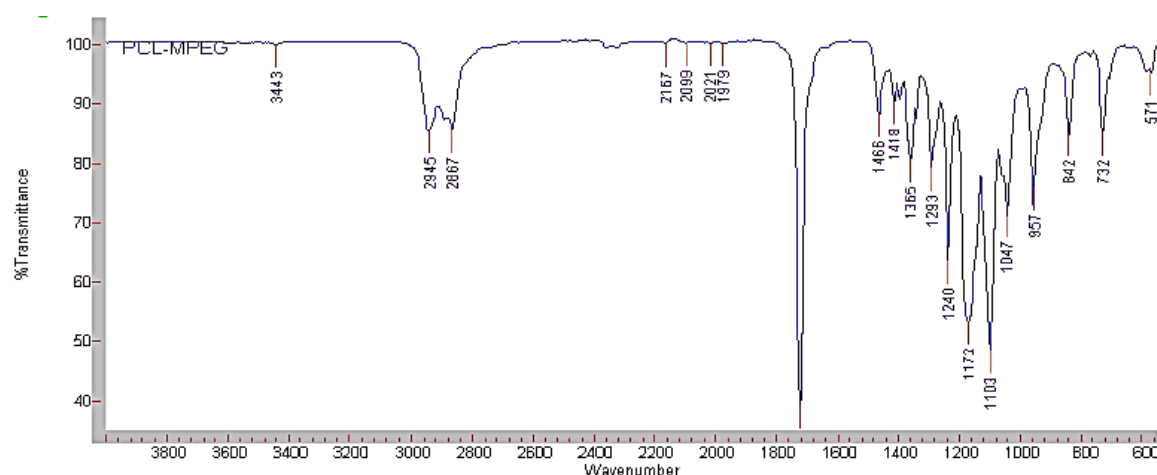
NMR analysis (Figure 46) ascertained the formation of the PCL and the presence of mPEG block copolymer by showing both characteristic peaks of PCL and mPEG.  $-OCH_2-$  of mPEG and PCL were found at 3.6 (s) ppm. Protons of PCL were also observed at 2.27 (t), 1.56–1.67 (t), 1.29–1.40 (t) ppm, which are attributed to the  $[CH_2CH_2C(O)O-]$ , 5,  $[-OCH_2CH_2CH_2CH_2-]$ , 2;  $-C(O)CH_2CH_2CH_2-$ , 4,  $[C(O)CH_2CH_2CH_2CH_2CH_2O-]$ , 3 and  $-OCH_2-$ . The ultimate yields from different

synthesis attempts were in range of 92 - 94%. The results of the NMR together with monomodal distribution affirms the formation of a block copolymer.



**Figure 46.** H-NMR spectra of PCL<sub>15000</sub>-mPEG<sub>5000</sub>.

FTIR spectra (Figure 47) proved that the sharp and intensive peak observed at 1725 and 1103 cm<sup>-1</sup> could be attributed to the presence of C=O carboxylic ester and C-O ether, respectively. This affirms that the formation of polymer was successful. Typical peaks of C-H stretching in PCL segment could be observed at 2867 – 2945 cm<sup>-1</sup>. Lastly, a specific peak at 1110.8 – 1180.2 cm<sup>-1</sup> indicated C-O-C stretching in PEG segment. Table 10 summarizes the characteristics of the synthesized PCL-mPEG polymer obtained by GPC, DSC and TGA Analyses.



**Figure 47.** FTIR spectra of PCL-mPEG.

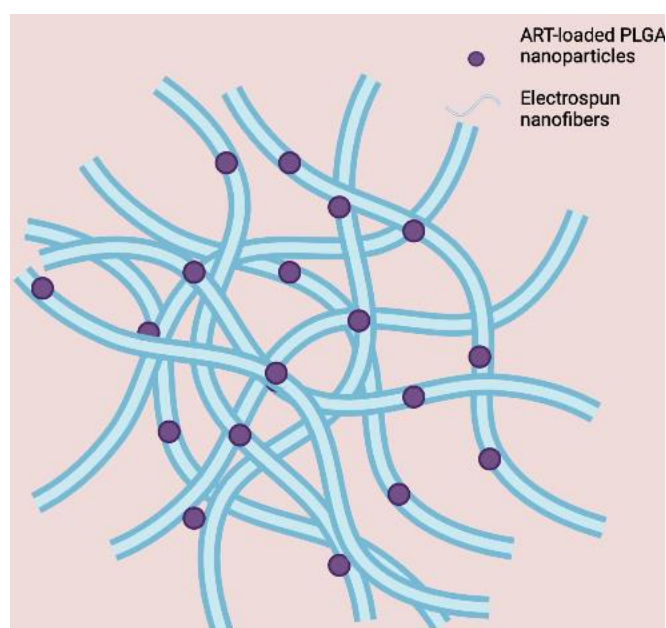
**Table 10.** Characteristics of the synthesized PCL-mPEG polymer.

Polymer	M <sub>n</sub> (expected)	M <sub>n</sub> (NMR)	M <sub>n</sub> (GPC)	PDI	T <sub>g</sub> (°C)	T <sub>m</sub> (°C)
PCL-mPEG	20000	18500	19470	1.49	-56 to -58	60-62

## 2.5 Immobilization of ART-loaded PLGA nanoparticles prepared by solvent displacement into PCL-mPEG electrospun nanofibers

ART-loaded PLGA nanoparticle, which were previously prepared by solvent displacement method were immobilized to nanofibers. The polymer used for electrospinning is the PCL-mPEG, which is well known from literature, <sup>[125]</sup> and was synthesized from  $\epsilon$ -caprolactone in the presence of  $\alpha$ -methoxy- $\omega$ -hydroxy-poly (ethylene glycol) (mPEG) as a macroinitiator (see section 4.4). For this purpose, nanoparticles dispersion with 15 wt. % ART, which was optimized by Design Expert, for the highest loading and encapsulation efficiency, were selected for the experiment. Firstly, the idea of this work was to evaluate, whether the encapsulation of ART into nanoparticles and then immobilization of

these particles into electrospun nanofiber leads to a more sustained release compared to both particles and nanofibers (schematic 2). Secondly, we investigated the effect of different parameters including ART amount per nanoparticle, nanoparticle amount per nanofiber as well as nanofiber diameter on the release behavior of the nanofiber.

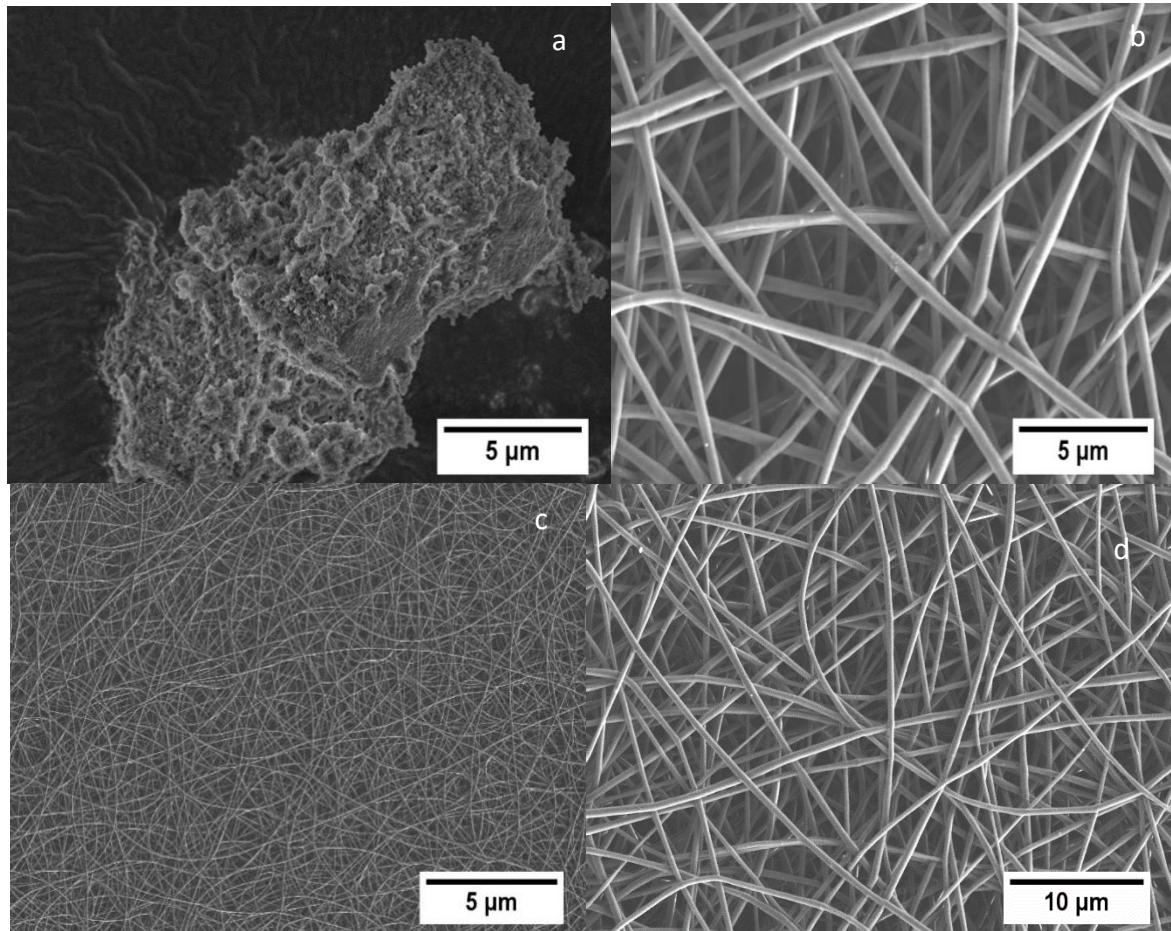


**Schematic 2.** The concept of this work of immobilization of ART-loaded nanoparticles in electrospun PCL-mPEG nanofibers.

### **2.5.1 Characterizations of electrospun nanofibers immobilized with ART-loaded nanoparticles**

SEM analysis was done in order to assess the morphology of ART-loaded nanoparticles (Figure 48a), ART-loaded electrospun PCL-mPEG nanofibers (Figure 48b), along with PCL-mPEG electrospun nanofibers, which are immobilized with ART-loaded nanoparticles (Figure 48c and 48d). As it could be seen, smooth bead-free fibers were produced. The average diameter of the nanofibers immobilized with ART-loaded nanoparticles was about  $220 \text{ nm} \pm 29$ .

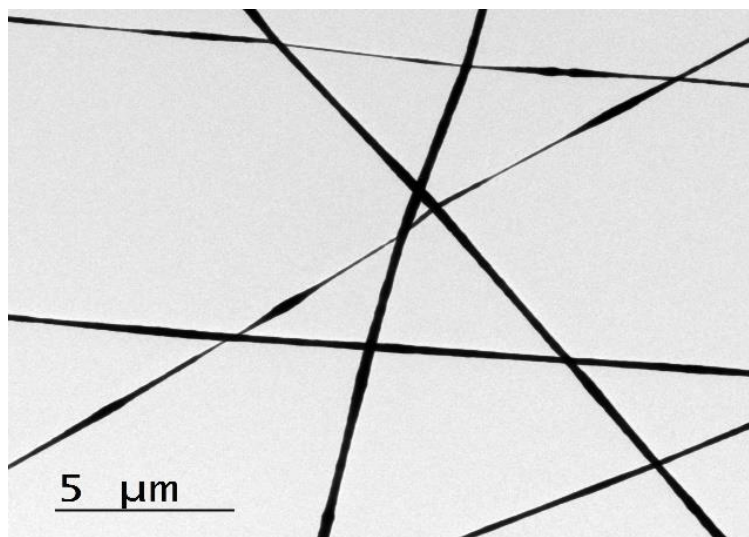
The average diameter of ART-loaded measured using 100 different random measurements.



**Figure 48.** SEM micrograph of (a) ART-loaded nanoparticles, (b) ART-loaded PCL-mPEG electrospun nanofibers, (c) and (d) PCL-mPEG nanofibers immobilized with ART-loaded PLGA nanoparticles.

TEM characterization of electrospun PCL-mPEG nanofibers immobilized with ART-loaded nanoparticles was conducted (Figure 49). As the nanoparticles have a smaller average diameter compared to nanofibers, nanoparticles could not be obviously characterized in the structure of nanofibers. Still, at some points, where nanofibers have a smaller diameter, bulges show the presence of nanoparticles inside the nanofibers.

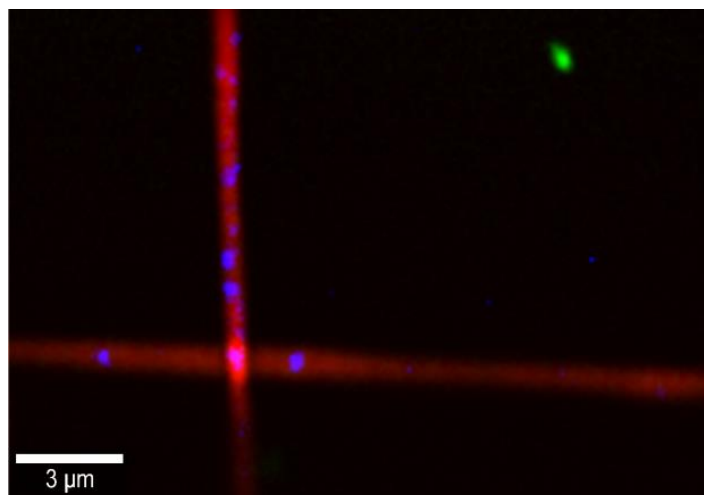




**Figure 49.** TEM micrograph of PCL-mPEG nanofibers with immobilized ART-loaded nanoparticles.

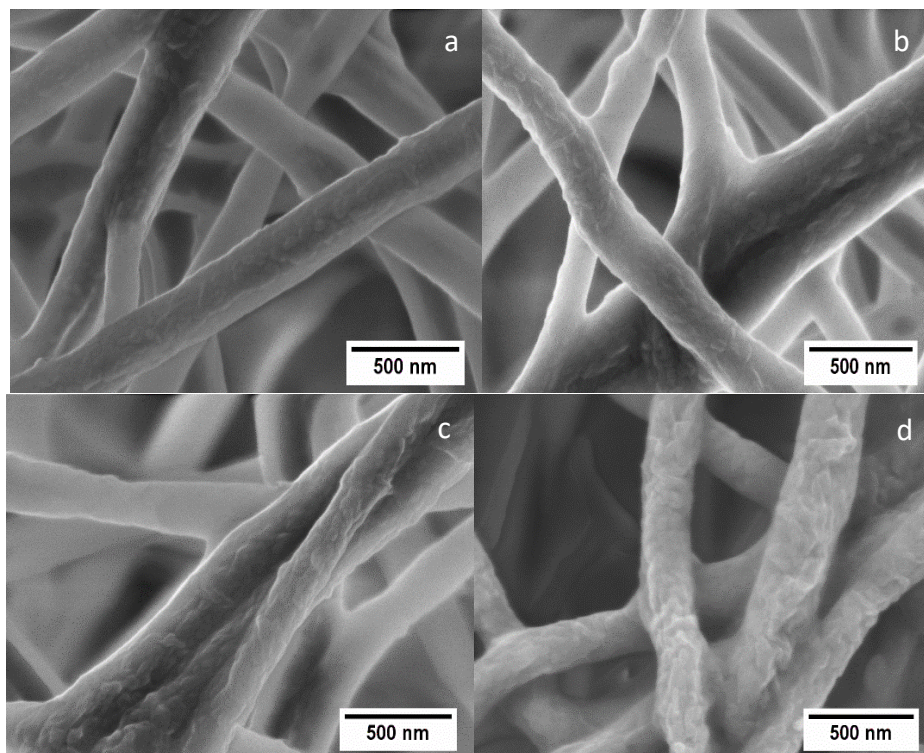
To characterize how particles are distributed within the structure of nanofibers, Raman spectroscopy was carried out. The Raman spectroscopy (Figure 50) successfully confirms the presence of nanoparticles within the nanofibers. The red signal is attributed to the presence of PCL-mPEG and the blue signal to the presence of ART. Evidently, most particles are incorporated in the inner part of nanofibers rather than on the surface, which could provide the nanofibers with a much more sustained release, which plays a significant role in drug delivery applications.





**Figure 50.** Raman spectroscopy of electrospun PCL-mPEG nanofibers immobilized with ART-loaded nanoparticles.

In drug delivery and tissue engineering applications, it is important for nanofibers to maintain their morphology and structural integrity resulting in a great impact on cell adhesion, proliferation and differentiation as well as on the release rate of the drug. <sup>[168]</sup> As it could be seen in Figure 51, mild swelling was observed, yet fiber retained their structural integrity even after being located for 8 h in a release medium for different time intervals, which is an indication of long-term degradation rate and that the drug release is mostly based on diffusion from the fibers and not on the degradation.



**Figure 51.** SEM micrographs of electrospun nanofibers in PBS containing tween 80 after after (a) 2, (b) 4, (c) 8 and (d) 10 h.

### **2.5.2 Determination of drug content in nanoparticles and in electrospun nanofibers by HPLC**

HPLC was used to determine the amount of ART in nanoparticles as well as nanofibers. For this purpose, three different batches of nanoparticles and nanofiber samples, with immobilized ART-loaded nanoparticles were dissolved in the mobile phase and analyzed at 200 nm with a flow rate of 0.8 mL/min. The values were obtained by comparing the data from the samples and the standard solution. The assay amounts were obtained by comparing the data achieved from ART-loaded electrospun nanofibers and the standard solutions (Figure 52). Each experiment was repeated three times.

Table 11 and 12 represents the experimental amount of ART which was detected in nanoparticles as well as nanofibers loaded with ART-loaded PLGA

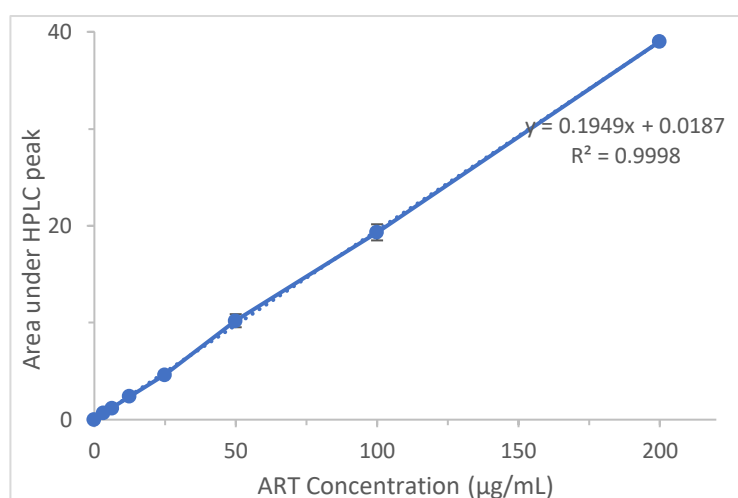
nanoparticles by HPLC. The results prove that for the electrospun nanofibers, which were immobilized with ART-loaded nanoparticles, the drug is completely loaded into nanofibers.

**Table 11.** Determination of the amount of ART in nanoparticle using HPLC.

Sample	Theoretical amount of ART (wt. %) in nanoparticle	Experimental amount of ART (wt. %) in nanoparticle	Assay (%)
1	5	3.35	67 ± 2
2	10	7	70 ± 1
3	15	10.7	71 ± 1

**Table 12.** Determination of the amount of ART in nanofiber using HPLC.

Sample	Theoretical amount of ART (wt. %) in nanofiber	Experimental amount of ART (wt. %) in nanofiber	Assay (%)
1	5	4.95	99 ± 0.5
2	10	9.93	99.3 ± 0.3
3	15	14.89	99.27 ± 0.6

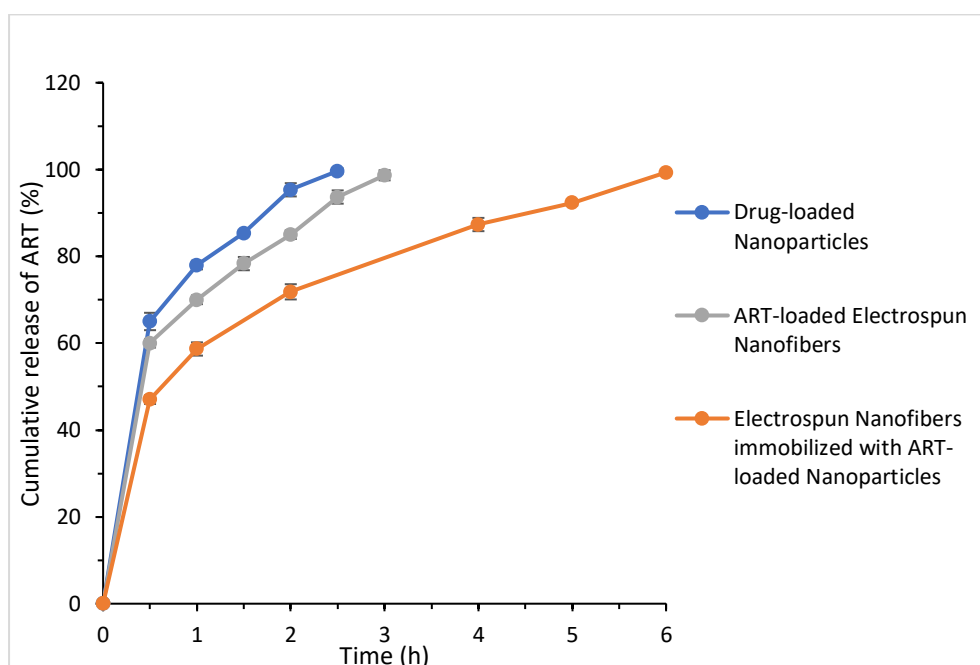


**Figure 52.** Calibration curve of ART in PBS containing 1 wt. % Tween 80.

### **2.5.3 Studies on drug release behaviors of ART from nanoparticles and electrospun nanofibers**

Finding an appropriate release medium is essential for conducting release tests, which provides the desirable sink condition for the drug over a specific timespan.<sup>[18]</sup> As ART is a hydrophobic drug, we employed a biocompatible surfactant, tween 80, which is regarded as a suitable solubilizer for increasing the solubility of the hydrophobic drug in an aqueous medium. In this section, the release behavior from ART-loaded PLGA nanoparticles, electrospun nanofibers with immobilized ART-loaded PLGA nanoparticles as well as electrospun nanofibers loaded with ART is comprehensively investigated (Figure 53). Based on literature,<sup>[9]</sup> the two main mechanisms, involved in drug delivery systems based on PLGA are diffusion and degradation. However, degradation is largely predominant in the later phases of the release experiments. It was seen in Figure 53 that 65 % of the whole drug was released after 30 min and the release was accomplished after 2 h for ART-loaded nanoparticles, whereas for nanofibers loaded with ART, a burst release around 60 % was detected, followed by a slower release which was completed after 2.5 h. On the other hand, for electrospun nanofibers with immobilized ART-loaded PLGA nanoparticles, the burst release was decreased to 43 % and the release was completed after 6 h. The burst release could be attributed to the drug, which is located around or on the surface of nanoparticles and is released out of nanoparticles before the experiment.<sup>[169]</sup> It could be concluded that the nanofiber, which are immobilized with ART-loaded nanoparticles showed a more sustained release in comparison to nanoparticles and ART-loaded nanofibers itself. This could be due to a longer diffusion path which takes for the drug to diffuse from nanoparticles which is followed by a further diffusion from electrospun nanofibers.

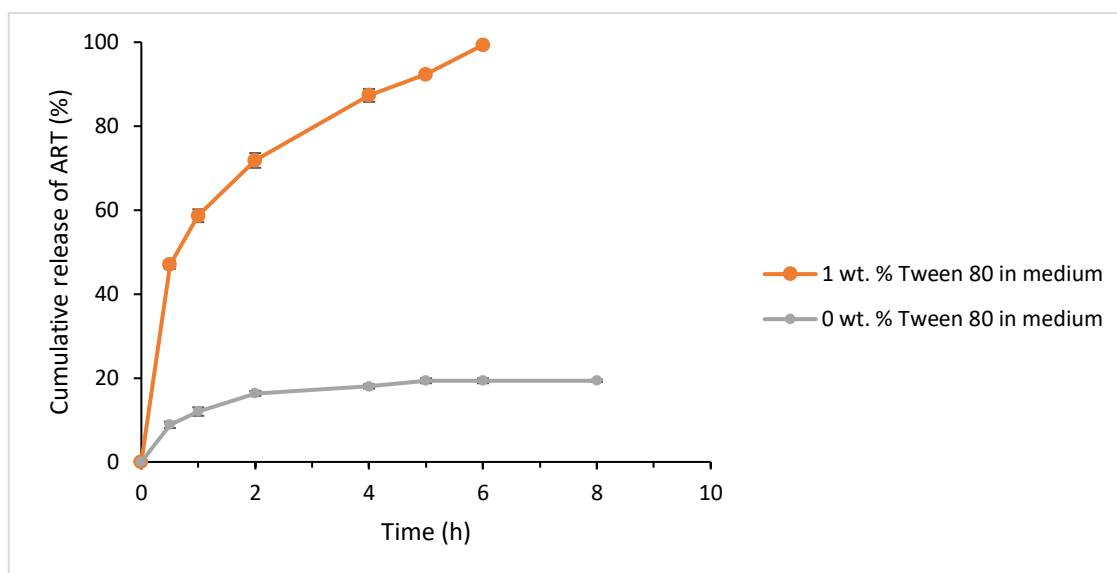
For the ART-loaded PCL-mPEG nanofibers, a higher amount of drug was released at the same time in comparison to electrospun nanofibers incorporated with ART-loaded PLGA nanoparticles. This could consequently occur due to possible following reasons: on the one hand, water can penetrate into nanofiber from all different directions. On the other hand, in case of particle loaded nanofibers, the presence of PLGA slows down the water penetrating into nanofibers. Additionally, it increases the diffusion path for the drug to be released from the inner site of nanoparticles to the medium, as a result, a reduced burst release as well as a more prolonged release of the drug could be obtained.



**Figure 53.** In vitro cumulative release of ART from ART-loaded nanoparticles, ART-loaded electrospun nanofibers and electrospun nanofibers with immobilized drug-loaded nanoparticles in an aqueous solution containing 1 wt. % Tween 80 (5 wt. % particle in nanofiber and 5 wt. % ART in nanoparticle).

The electrospun nanofibers with immobilized ART-loaded PLGA nanoparticles were selected for further studies. Release tests were conducted with 1 wt. % tween 80 in PBS and without Tween 80 (Figure 54) and the effect of tween 80 concentration on release behavior from electrospun nanofibers, with

encapsulated ART-loaded PLGA nanoparticles was evaluated. In the absence of Tween 80, only about 20 % of the drug was released after 5 h and then the release rate remained constant, whereas 1 wt. % Tween 80 resulted in complete release of ART after 6 h, which proves the higher solubility of ART in aqueous medium, contributing to higher dissolution and release rates.



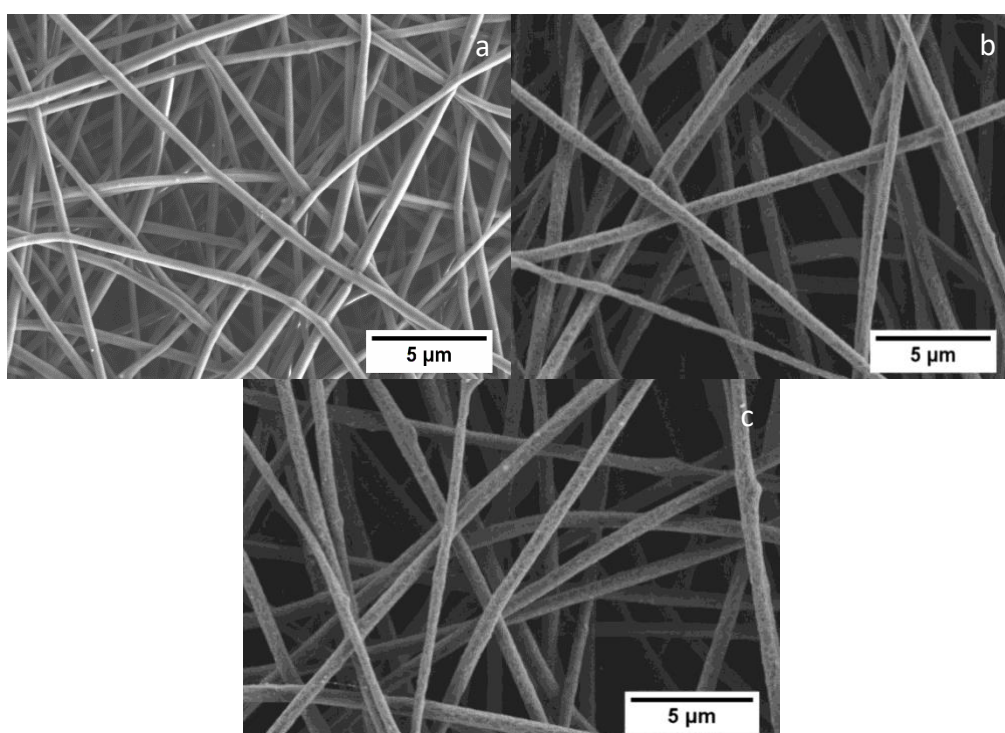
**Figure 54.** Effect of tween 80 concentration on release behavior from electrospun nanofibers immobilized with ART-loaded PLGA nanoparticles.

In this work, we tried to comprehensively assess the effect of different parameters affecting the release behavior of drug from electrospun nanofibers namely the ART loading in nanoparticles, particle loading in nanofibers and fiber diameter. In the following section, the results of the effect of these parameters indicated.

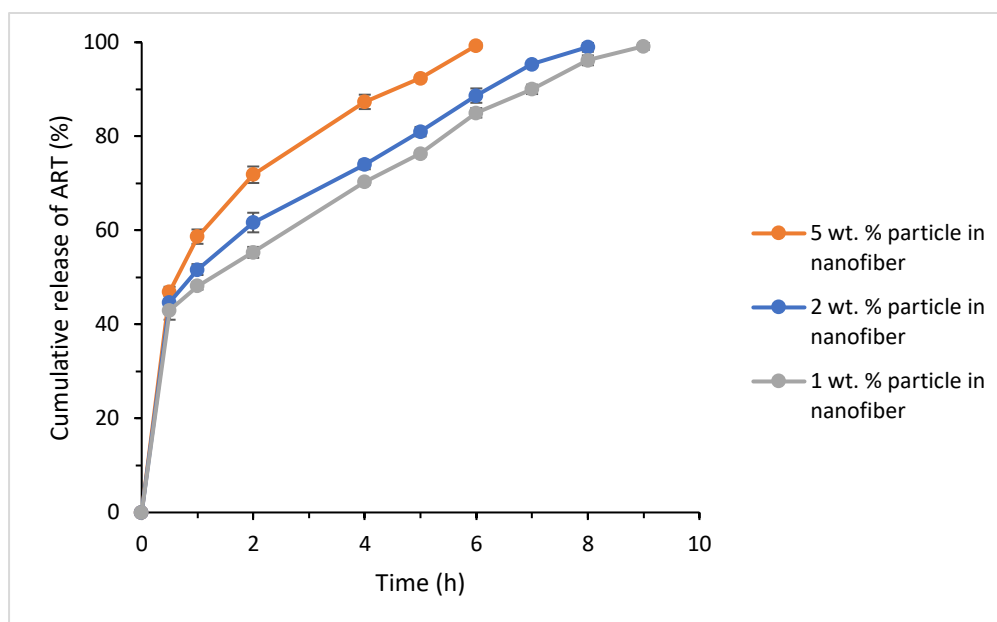
### 2.5.3.1 Effect of particle loading in nanofibers on release behavior from electrospun nanofibers

Different amounts of particles (1, 2 and 5 wt. %) were immobilized into electrospun nanofiber to evaluate how the drug release could be affected, which resulted in diameters  $370 \pm 25$ ,  $385 \pm 30$  and  $375 \pm 30$  nm, respectively. It is

noteworthy to mention that it was tried to keep the nanofiber diameter of the three different types of fibers in the same size range. SEM micrographs of the fibers could be observed in Figure 55. Figure 56 represents the release behavior from these nanofibers. The results prove a more sustained release of ART from nanofibers at lower nanoparticle loading. This phenomenon could be related to the fact that the amount of particle exposed to the surface of nanofibers would be more in case of nanofiber with higher loading of particles, thereby increasing the release rate. <sup>[170]</sup>



**Figure 55.** SEM micrograph of electrospun nanofibers immobilized with ART-loaded PLGA nanoparticles with different particle loadings including (a) 1, (b) 2 and (c) 5 wt. %.

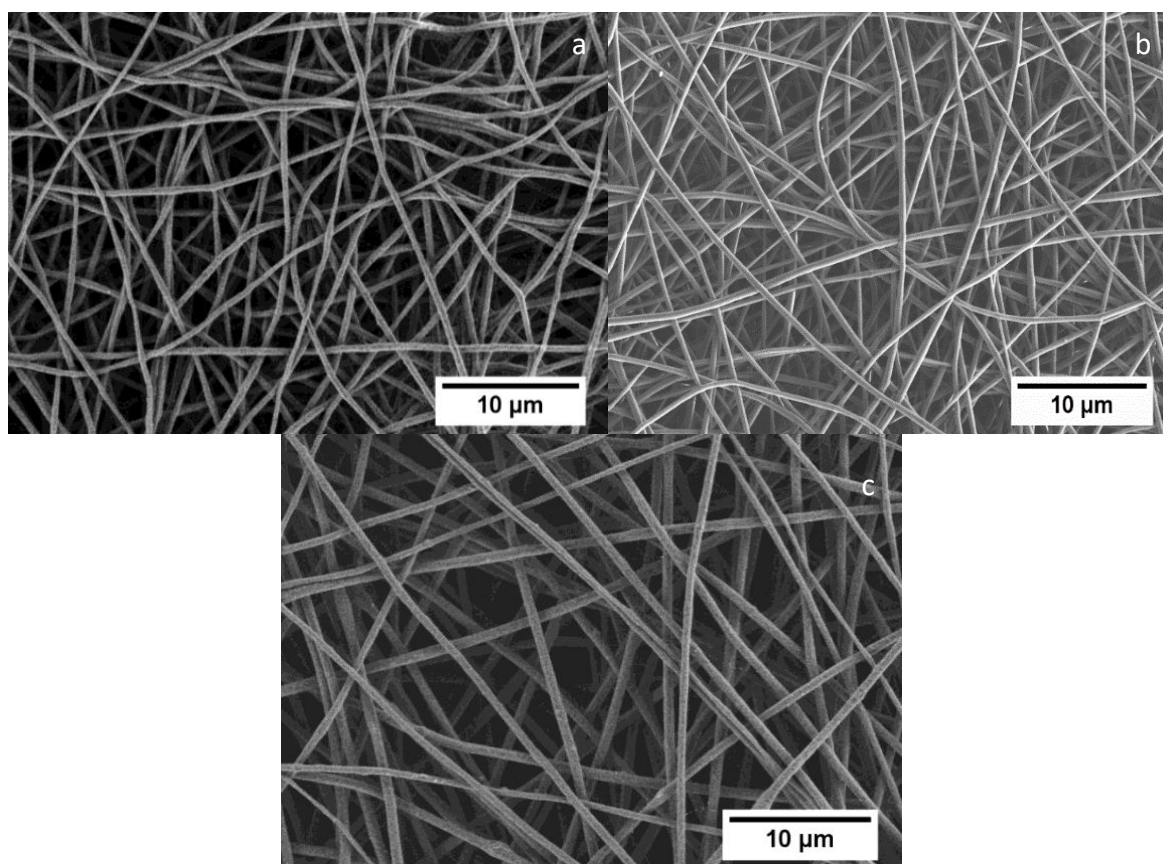


**Figure 56.** Effect of particle loading in nanofibers on release behavior from electrospun nanofibers immobilized with ART-loaded PLGA nanoparticles.

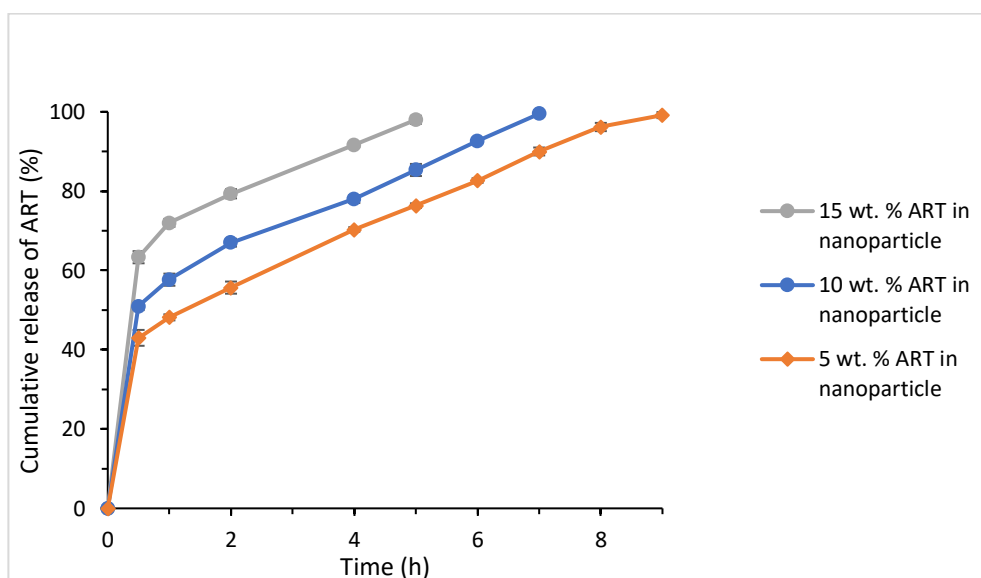
### 2.5.3.2 Effect of drug loading in nanoparticles on release behavior from electrospun nanofibers

Nanofibers of different drug loadings (5, 10 and 15 wt. %) were produced to investigate how drug loading in nanoparticles affects the drug release (Figure 57). The obtained nanofiber diameters are  $360 \pm 25$  nm,  $370 \pm 19$  nm and  $375 \pm 25$  nm. As it could be seen in Figure 58, increasing the loading of drug into nanoparticles contributes to a faster drug release. This could be ascribed to the higher amounts of drug which might be available at the surface of the particles, resulting in a faster release.





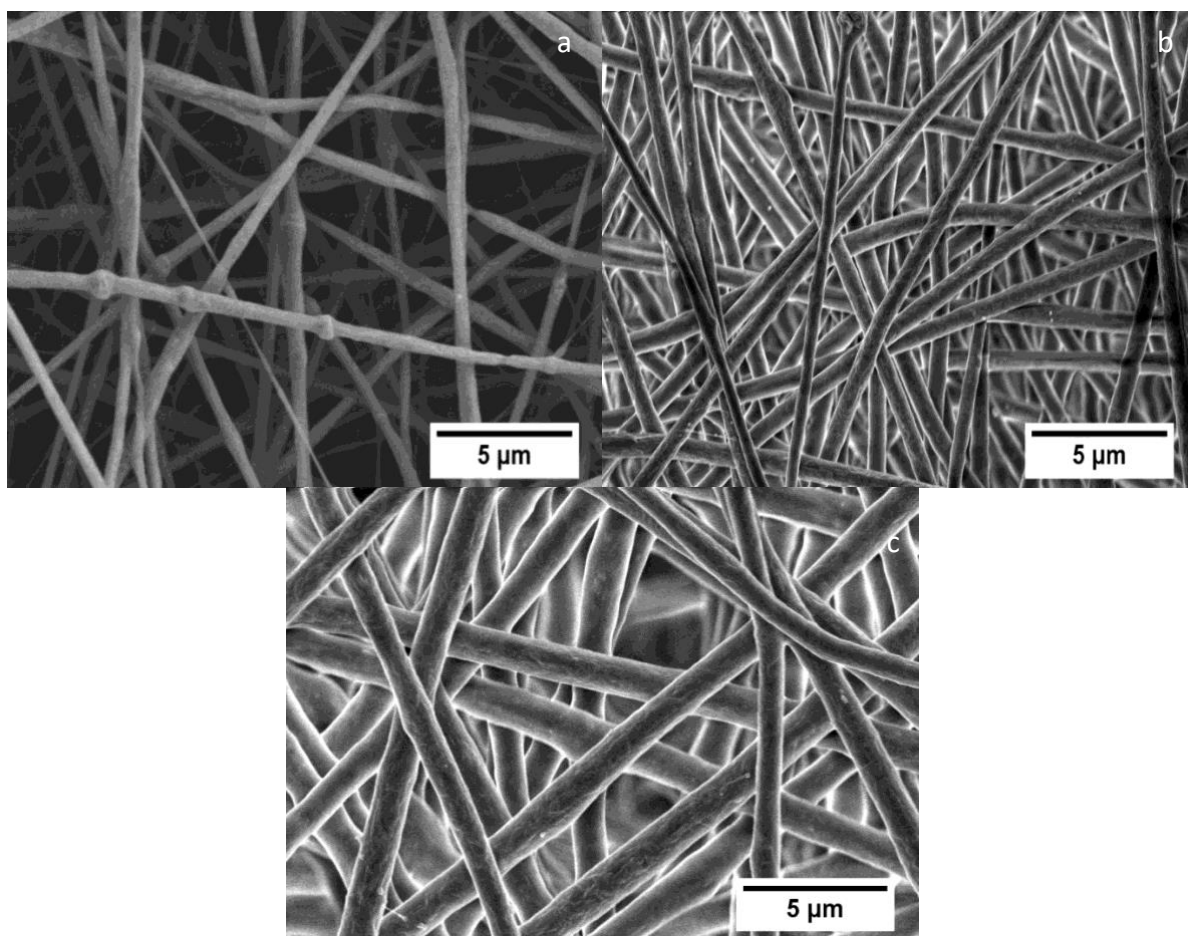
**Figure 57.** SEM micrographs of electrospun nanofibers immobilized with ART-loaded PLGA nanoparticles with different particle loadings including (a) 5, (b) 10 and (c) 15 wt. %.



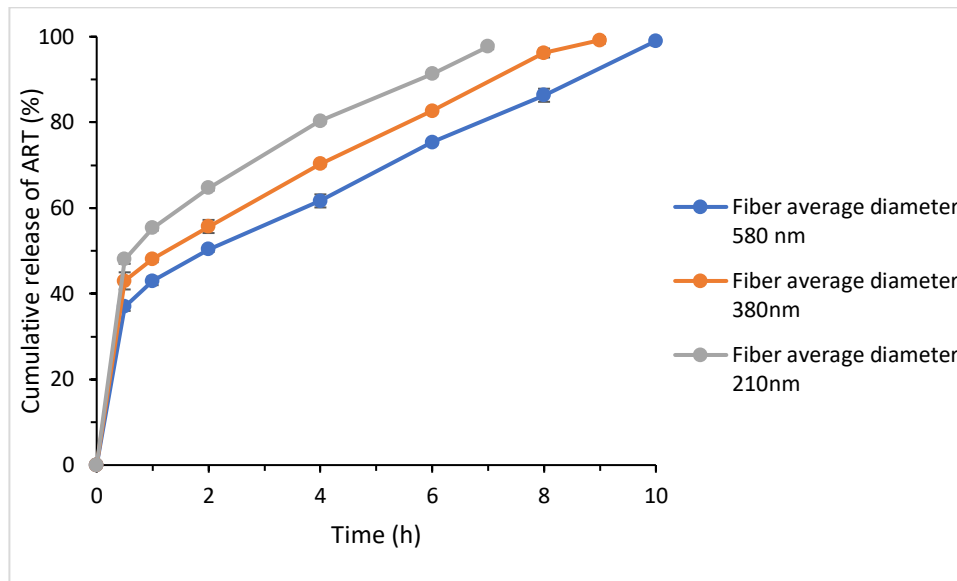
**Figure 58.** Effect of ART loading in nanoparticles on release behavior from electrospun nanofibers immobilized with ART-loaded PLGA nanoparticles.

### 2.5.3.3 Effect of nanofiber diameter on release behavior from electrospun nanofibers

In order to investigate how differences in nanofiber diameter affects the release of ART from nanofibers, three different fibrous diameters namely  $220 \pm 50\text{nm}$ ,  $380 \pm 42\text{nm}$  and  $580 \pm 25\text{nm}$  were prepared (Figure 59). The results of drug release showed that a larger diameter of the nanofiber is, results in a more prolonged drug release time (Figure 60). This is due to the longer diffusion path of the drug to diffuse out of the nanofibers. On the other hand, the release behavior is dependent on surface to volume ratio, which means, the thinner the fiber are, the faster would be the release from electrospun nanofibers. The result is in agreement with other literatures. <sup>[171]</sup>



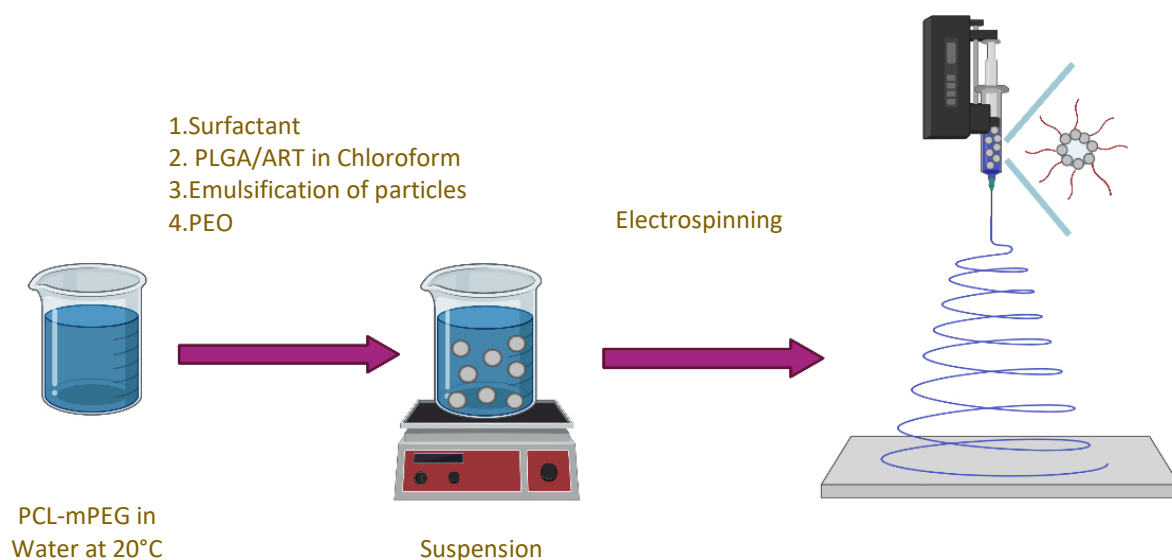
**Figure 59.** SEM micrographs of electrospun nanofibers with different nanofiber diameter (a)  $220 \pm 50$ , (b)  $380 \pm 42$  and (c)  $580 \pm 25$  nm.



**Figure 60.** Effect of electrospun nanofibrous diameter on release behavior from electrospun nanofibers immobilized with ART-loaded PLGA nanoparticles ART-loading (5 wt. %) and particle loading (1 wt. %) were kept constant.

## 2.6 Immobilization of ART-loaded PLGA micro and nanoparticles into PCL-mPEG electrospun nanofibers by suspension electrospinning

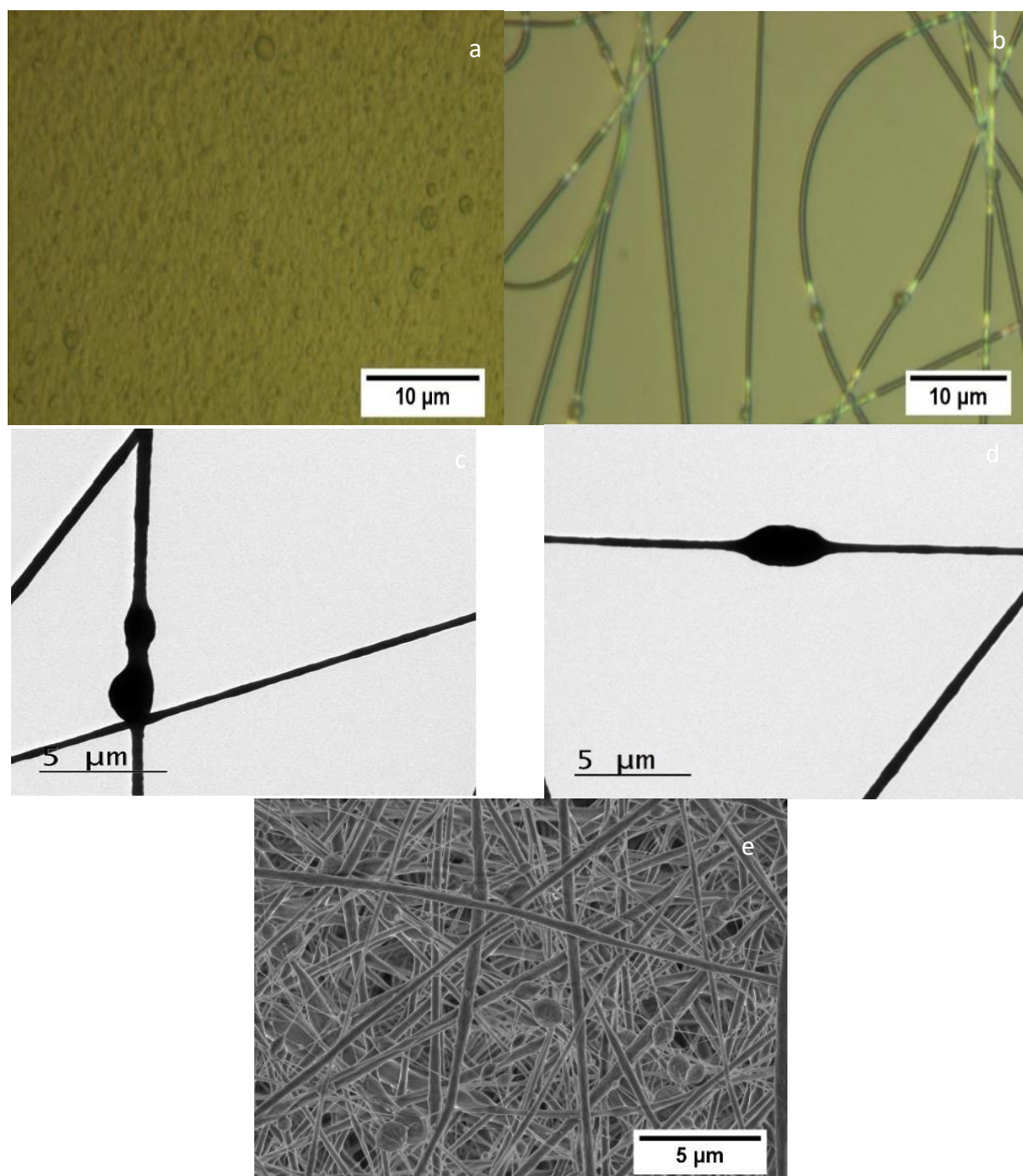
In this thesis, we were aiming at different methods of encapsulating ART into electrospun PCL-mPEG nanofibers. In this regard, suspension electrospinning was used to encapsulate ART-loaded micro- and nanoparticles in PCL-mPEG electrospun nanofibers. Two methods were used including ultrasonic and ultrasonifier to emulsify the particles in electrospun nanofibers, which resulted in the formation of ART-loaded micro and nanoparticles in nanofibers. To prepare the suspension. Schematic 3 show the suspension electrospinning process.



**Schematic 3.** Schematic preparation of the suspension electrospinning process.

### 2.6.1 Characterization of electrospun nanofibers immobilized with ART-loaded PLGA micro and nanoparticles by suspension electrospinning

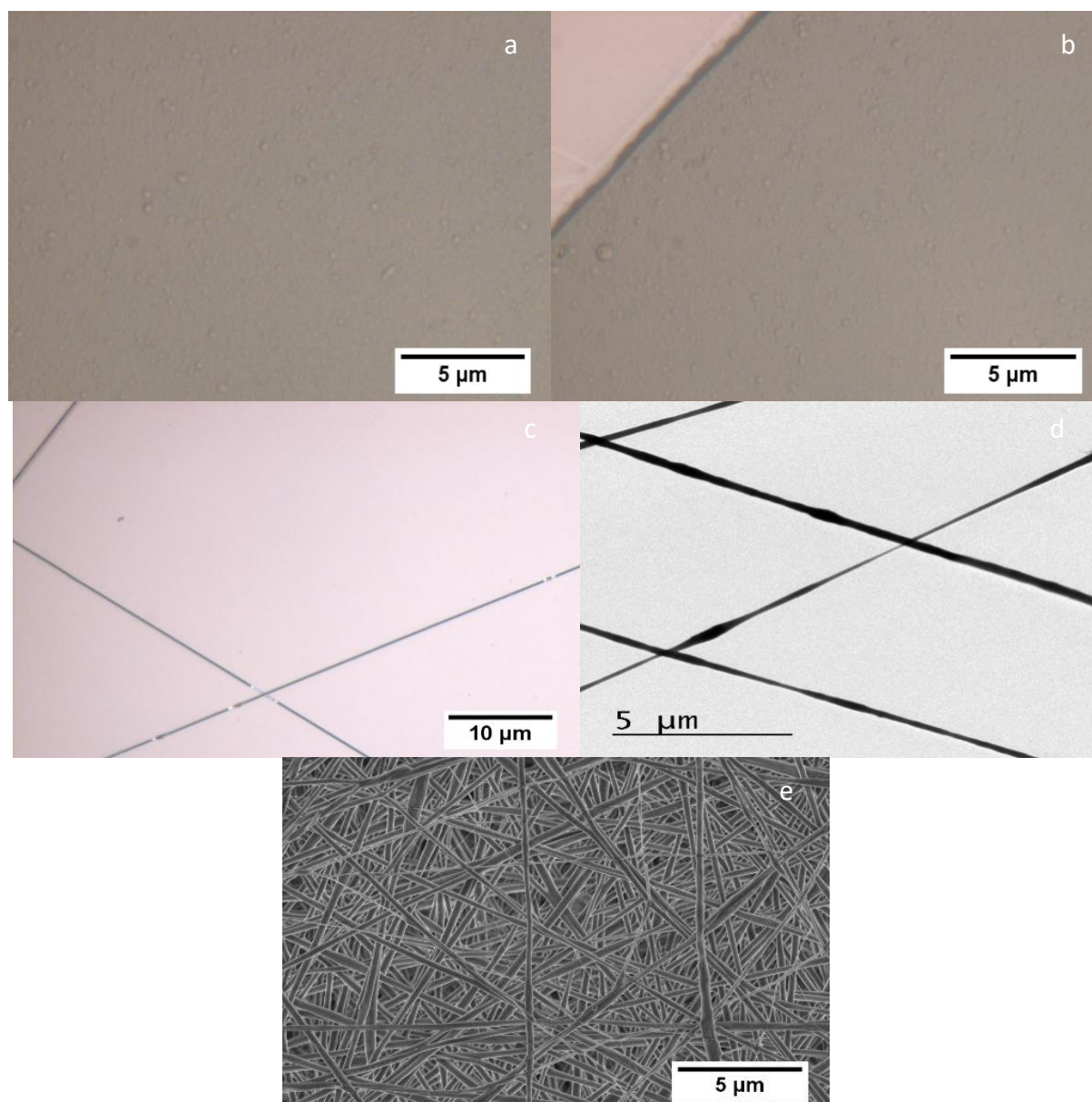
Figure 61 exhibits the optical microscopy of formed particles as well as SEM and TEM of nanofibers loaded with ART-loaded PLGA microparticles. Using ultrasonic for emulsification of particles into nanofibers, homogeneous particles in size with an average particle size of  $1.1 \pm 0.4 \mu\text{m}$  were obtained, whereas the average nanofiber diameter was  $530 \pm 45 \text{ nm}$ . From the optical microscopy, SEM and TEM micrographs, the presence of ART-loaded PLGA nanoparticles in electrospun nanofibers could be readily recognized.



**Figure 61.** Emulsification using ultrasonic. (a) Formed PLGA/ART microparticles before electrospinning. (b) ART-loaded PLGA microparticles in PCL-mPEG nanofibers. (c) and (d) TEM micrographs of ART-loaded PLGA microparticles in PCL-mPEG nanofibers, (e) SEM micrographs of ART-loaded PLGA microparticles in PCL-mPEG nanofibers.

Using an ultrasonifier to emulsify particles for nanofiber preparation, smaller particle sizes were acquired. The average particle size was  $545 \pm 97$  nm, while the electrospun nanofibers loaded with drug-loaded particles have an average diameter of  $560 \pm 34$  nm, which resulted in the formation of nanoparticles into nanofibers, which are nearly in the same size range. Yet, some bulges are observable in nanofibers (Figure 62), which could be attributed to the existence of nanoparticles in nanofibers.



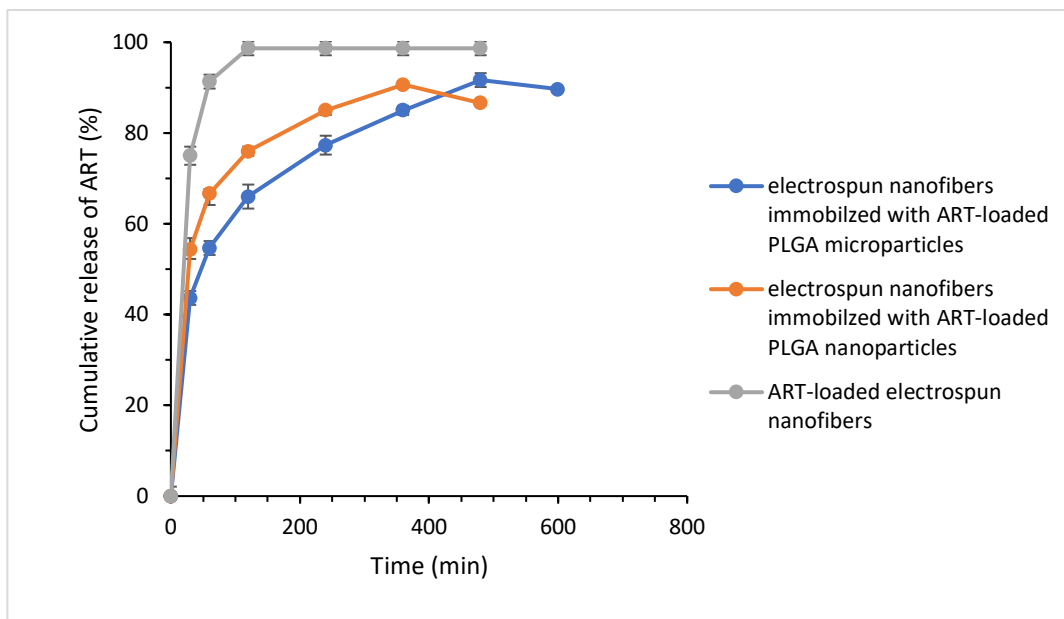


**Figure 62.** Emulsification using an ultrasonifier. (a) and (b) Optical microscopy of formed PLGA/ART nanoparticles before electrospinning. (c) Optical microscopy of nanofibers with immobilized ART-loaded nanoparticles, (d) TEM and (e) SEM of ART-loaded PLGA nanoparticles in PCL-mPEG nanofibers.

### **2.6.2 Release behavior of electrospun nanofibers immobilized with ART-loaded PLGA micro and nanoparticles by suspension electrospinning**

To investigate, how the release behavior is influenced by encapsulation of ART-loaded PLGA micro and nanoparticles into nanofibers and whether the encapsulation of particles into nanofibers serves in favor of a more sustained release compared to nanofibers, in which only the drug is loaded, ART-loaded nanofibers were fabricated in the same way. Figure 63 shows the release profiles of electrospun nanofibers with immobilized ART-loaded PLGA microparticles, electrospun nanofibers with immobilized ART-loaded PLGA nanoparticles as well as ART-loaded electrospun nanofibers. As it can be seen from Figure 63, for ART-loaded electrospun nanofibers the highest burst release of around 75 % was observed after 30 min, whereas in case of fibers loaded with nanoparticles this was noticeably reduced to 55 %. The least burst release was observed for nanofibers loaded with microparticles (42 %). For ART-loaded nanofibers the complete release was accomplished after 1.5 h, while for nanofibers loaded with microparticles this happened after 6 h and for fibers loaded with microparticles the most prolonged release among all was observed and the drug was completely released after 8 h. It is noteworthy to mention that for both micro- and nanoparticles the amount of drug released started to decrease, which could be related to the application of ultrasonic, which might result in the degradation of ART.





**Figure 63.** ART release from electrospun nanofibers with immobilized ART-loaded PLGA nanoparticles, electrospun nanofibers with immobilized ART-loaded PLGA microparticles and ART-loaded electrospun nanofibers in physiological medium containing 1 wt. % Tween 80.

## 2.7 Immobilization of ART into PCL-mPEG electrospun nanofibers by coaxial electrospinning

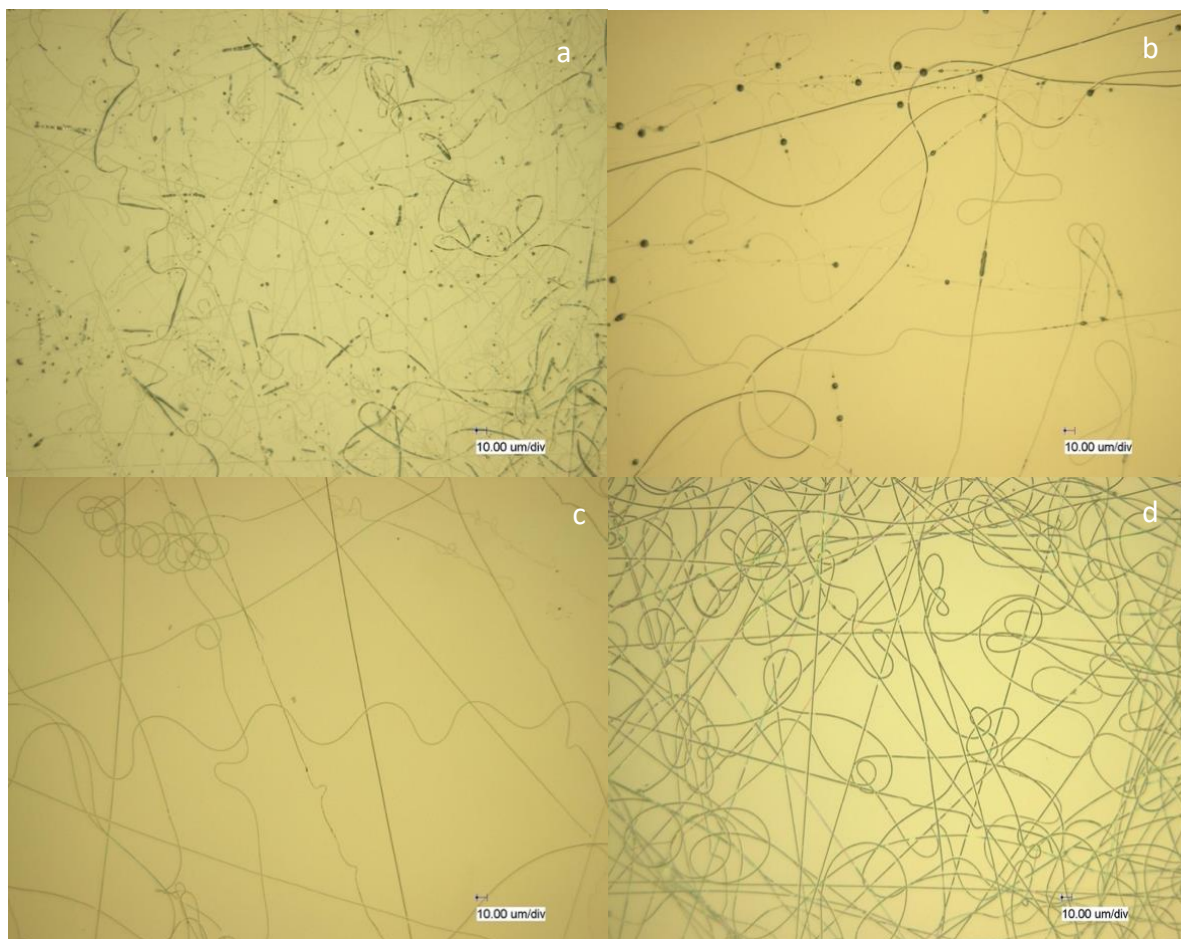
A coaxial electrospinning setup was used to conduct core-shell electrospinning, which could be seen in Figure 64. The polymer solution is injected through the outer spinneret, and the drug solution is injected through the inner one.



**Figure 64.** Core-shell apparatus used in this work.

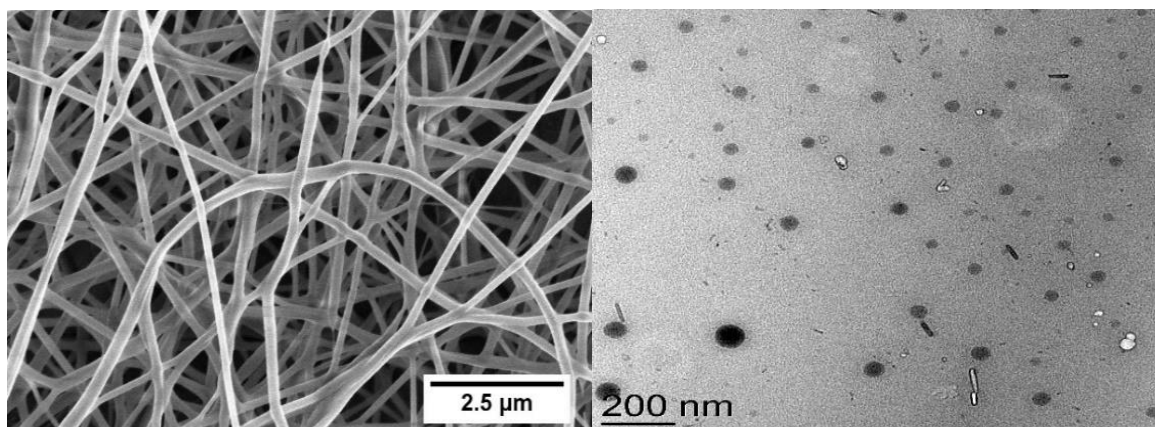
### **2.7.1 Preparation and characterization of core-shell nanofibers**

For dissolving both polymer and drug, dichloromethane was chosen as a solvent. To achieve this goal, different concentrations of PCL-mPEG in DCM were prepared, namely 10, 12.5, and 15 wt. %. For the sample containing 10 wt. % ART, 2.5 wt. % Pyridin Format (PF) 1:1 (mol:mol) was added to the PCL-mPEG solution to reduce the beads content (Figure 65a). Without using the pyridine format, there were so many beads and a combination of thin and thicker fibers in the nanofiber structure. Although in the presence of pyridine format and even increasing the concentration of the solution to 15 wt. %, there were still beads and droplets in the fiber structure (Figure 65b), which could be attributed to the low spinnability of the core solution. To tackle this problem, PEG Mw : 20000 was added to the core solution to enhance its spinnability. As observed in Figures 65c and 65d, adding PEG into the core solution led to the smooth bead-free electrospun nanofibers.



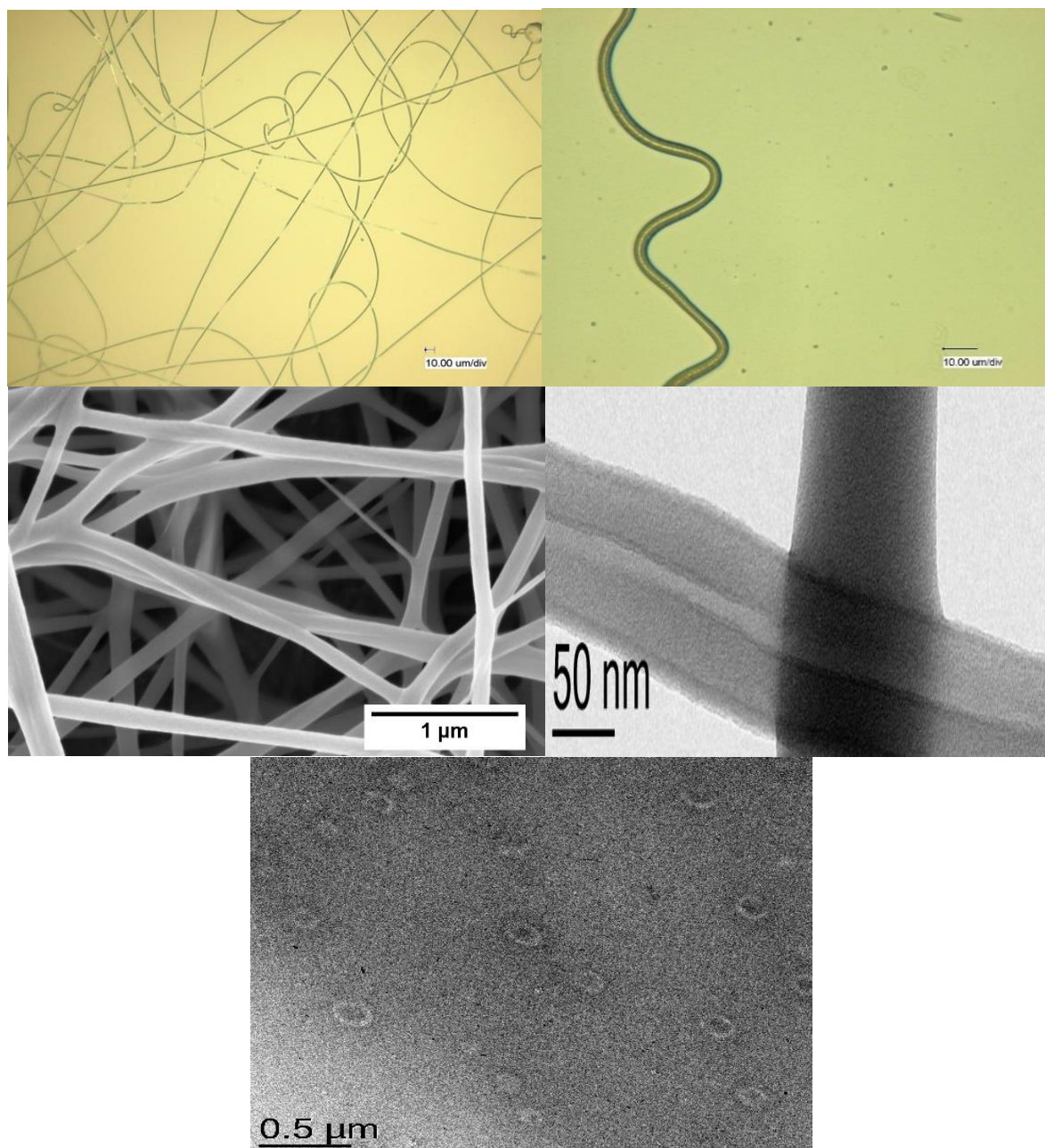
**Figure 65.** Optical microscopy of (a) electrospun ART-PCL-mPEG core-shell nanofibers (10 wt. % PCL-mPEG), (b) electrospun ART-PCL-mPEG core-shell nanofibers with pyridine format (12.5 wt. % PCL-mPEG), (c) and (d) electrospun ART/PEG-PCL-mPEG core-shell nanofibers (15 wt. % PCL-mPEG).

Nanofibers with 15 wt. % PCL-mPEG and 10 wt. % ART were chosen for further characterizations. SEM and TEM characterizations were done to analyze the morphology of nanofibers and to investigate whether the core-shell structure has been obtained (Figure 66). For TEM, the core was dyed with Rhodamine B, and then the TEM was performed on the cross-section of nanofibers. TEM results showed that the core-shell structure has not formed; instead, a hollow structure was observed, which could be due to the selection of the solvent system.



**Figure 66.** SEM and TEM cross-section micrographs of ART/PEG-PCL-mPEG core-shell Nanofiber in DCM (15 wt. % PCL-mPEG and 10 wt. % ART).

The interaction between both inner and outer solvents specifies the miscibility of both solutions. The solvent selection should be done appropriately to suppress each of the solvents to precipitate the other one. <sup>[19,21]</sup> In this regard, immiscible solutions could be easily electrospun into the core-shell structure due to phase separation during electrospinning. To prevent the phenomenon mentioned above and increase the possibility of forming a core-shell structure, PCL-mPEG was electrospun in water and ART/PEG in DCM. Figure 67 shows the optical microscopy, SEM, and TEM micrographs of these nanofibers. The results proved that the core-shell structure is obtained.



**Figure 67.** (a), (b) Optical Microscopy of ART/PEG-PCL-mPEG core-shell nanofiber, (c) SEM micrograph of ART/PEG-PCL-mPEG core-shell nanofiber, (d) TEM micrograph of ART/PEG-PCL-mPEG core-shell nanofiber, (e) TEM micrograph of cross section of ART/PEG-PCL-mPEG core-shell nanofiber (All fibers contain 15 wt. % PCL-mPEG and 10 wt. % ART).

### 2.7.2 Determination of the amount of ART in core-shell nanofibers

HPLC was done to characterize the amount of ART in core-shell nanofiber. For fibers prepared in DCM/water, a high loading efficiency of 99.3 % was obtained (Table 13), whereas a lower loading efficiency was observed for the fibers

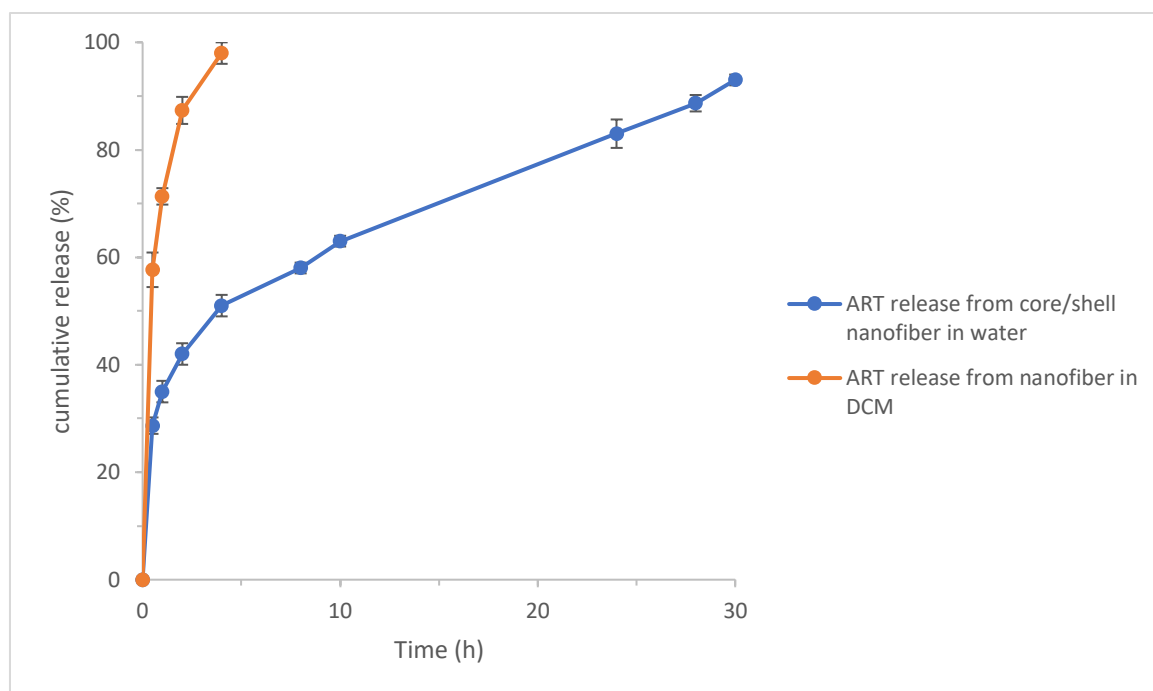
prepared in DCM. The obtained result could be related to the unsuccessful encapsulation of the ART in the core, evidenced by depositing in the form of droplets on the aluminum foil during the electrospinning.

**Table 13.** Determination of the amount of ART in ART-loaded core-shell nanofibers.

Sample	Theoretical content (wt. %)	Experimental content (wt. %)	Loading efficiency (%)
ART/PEG-PCL-mPEG (DCM/water)	10	9.93	99.3
ART/PEG-PCL-mPEG (DCM)	10	9.57	95.7

### 2.7.3 Release behavior from core-shell nanofibers

Figure 68 compares the release behavior from nanofibers fabricated in different solvent systems, namely in DCM and water. The 60 % burst release and releasing the rest of the drug within 3.5 h demonstrated the DCM solvent system does not result in a core-shell structure. This agrees with the TEM results and proves that most probably the core-shell structure has not formed. On the contrary, ART/PEG-PCL-mPEG core-shell nanofibers with PCL-mPEG being electrospun in water exhibited a lower burst release only 30 % after 30 min, and the whole drug was released after 28 h, showing a sustained release compared to the previous one.



**Figure 68.** ART release from ART/PEG-PCL-MPEG nanofibers (ART, PCL-mPEG and PEG in DCM) and ART/PEG-PCL-mPEG (ART/PEG in DCM and PCL-mPEG in water) core-shell nanofibers in physiological medium containing 1 wt. % Tween 80.

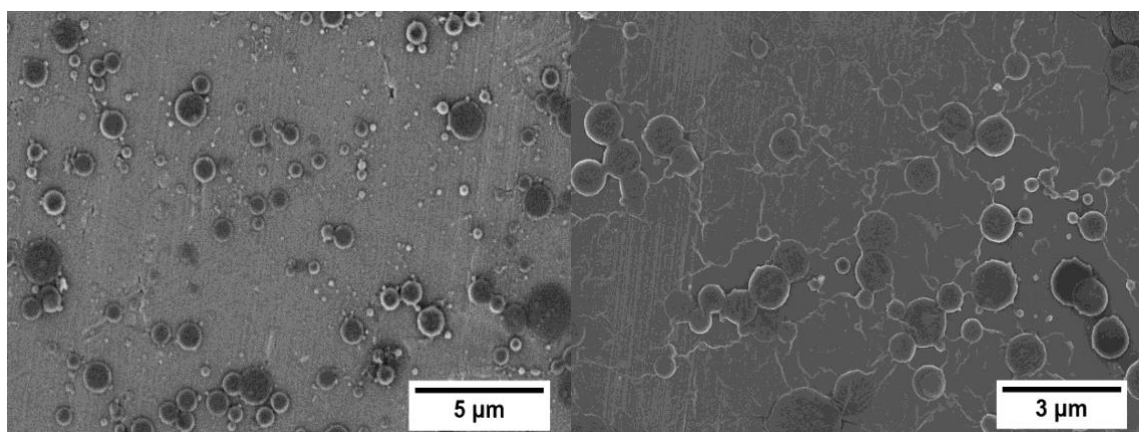
## 2.8 Cellulose electrospinning using DBU-CO<sub>2</sub> switchable solvent system

The polymer molecular weight and the ultimate viscosity of the electrospinning solution are other factors that could impact the electrospinning process. Among others, these parameters determine whether fibers (electrospinning) or particles (electrospraying) are fabricated. To find insight regarding this issue, two different cellulose types with obviously different molecular weights were used. In this case, the crystallinity of the cellulose type is less critical, as it is mostly lost in a solubilized state, as shown in previous works.<sup>[158,172]</sup> It is expected that the difference in their molecular weight plays a significant role in the electrospinning/electrospraying process.



### 2.8.1 Investigation on microcrystalline cellulose (MCC)

Preliminary experiments were done using MCC. In the first set of experiments, the cellulose concentration was changed between 1 and 10 wt %. It was observed that using all these concentrations, only particles with different size range between 600 nm and 1.30  $\mu\text{m}$  were obtained, and changing the electrospinning parameters (voltage, feed rate, electrospinning distance) did not make any difference, still resulting in particles. However, as expected, larger particle sizes were gained using higher cellulose concentrations. It is noteworthy to point that using 5 wt. % MCC, the electrospinning process was more stable, contributing to homogenous round-shaped particles with an average diameter of about 1.2  $\mu\text{m}$  (Figure 69). The resultant particles are smaller in diameter than the previous report by Kyung et al., where slightly larger particles with average particle diameter between 5-10  $\mu\text{m}$  were obtained by electrospinning of ionic liquids. [173] Although we mainly aimed to prepare cellulose fibers in this work, such homogenous and well defined cellulose microparticles could also find applications in different fields, including the food industry, electronic and pharmaceuticals, as reported by Chin et al. [174]



**Figure 69.** SEM image showing particles ( $1.3 \pm 0.5 \mu\text{m}$ ) produced from electrospinning of cellulose at 5 wt. % in DBU- $\text{CO}_2$  switchable solvent system (E-spraying conditions: 22 kV-15 cm-0.12 mL/h). [175]



The previous works on electrospinning showed that enhancing the viscosity of a solution is a way to transition from a particle to a fiber.<sup>[14]</sup> Therefore, we used higher concentrations of MCC. Nevertheless, using concentrations higher than 10 wt. % MCC, the solution became much more unstable after solubilization, making it impractical to be used for electrospinning. Sun et al. reported that using additives such as PVA or PEO improves the spinnability of a solution and facilitates particle removal during the electrospinning process.<sup>[17]</sup> These polymer additives can be removed after the fiber formation, as observed in Frenot and co-worker's report.<sup>[154]</sup> As 5 wt. % MCC provided a stable solution, this concentration was used for the subsequent trials with PVA and PEO as additive polymers.

**Table 14.** Electrospinning/Electrospraying using MCC solubilized in DBU-CO<sub>2</sub> solvent system at various PVA concentration and ratio.

Expt. No.	MCC conc. (wt. %)	PVA conc. (wt. %)	Ratio (%) MCC/PVA	Solution conc. (wt. %)	Voltage (kV)/distance (cm)/rate (mL/h)	Observation
1a	5	-	100/0	5.00	22-15-0.12	Particles
1b	-	5	0/100	5.00	8-20-0.12	Particles
1c	5	5	45/55	5.00	11-15-0.12	Particles
1d	5	5	50/50	5.00	12-20-0.12	Particles
1e	-	10	0/100	10.0	25-20-0.12	Particles & fibers
1f	5	10	50/50	7.50	13-20-0.12	Fibers with particles
1g	5	10	45/55	7.75	8-20-0.12	Beaded fibers
1h	-	15	0/100	15.00	20-20-0.24	Fibers
1i	5	15	90/10	6.00	20-20-0.12	Particles
1j	5	15	77/23	7.30	15-20-0.12	Fibers, particles and droplets
1k	5	15	70/30	8.00	20-20-0.12	Fibers, particles and droplets
1l	5	15	50/50	10.00	20-20-0.12	Beaded fibers
1m	3	15	45/55	9.60	15-20-0.12	Fibers/bead
1n	-	20	0/100	20.00	20-20-0.12	Fibers only
1o	5	20	60/40	11.00	6-20-0.12	Beaded fibres





### 2.8.1.1 Use of additives for MCC electrospinning

PVA was used as an additive. The required PVA concentration was prepared in DMSO, allowing easier miscibility when added to the solubilized cellulose in the

DBU/CO<sub>2</sub>/DMSO system. For this purpose, a 5 wt. % MCC solution was prepared as previously described. <sup>[176]</sup> In the next step, the PVA solution was added and allowed to become homogenous under mild stirring. At this stage, we did the addition as fast as possible to avoid the escape of CO<sub>2</sub>, which will otherwise lead to precipitation. Different ratios of MCC and PVA were used as shown in Table 14, and the corresponding optical images are shown in Table 15. For the first experiment set, 5 wt. % PVA was used as a reference, and electrospraying of neat 5 wt. % PVA caused only the formation of particles. Only particles were achieved by mixing this PVA concentration with 5 wt. % MCC at a 50/50 ratio. Likewise, particles were obtained by changing the ratio to 45:55 (MCC: PVA). To get fibers, the subsequent experiments (1f & 1g) were carried out using 10 wt. % PVA with the ratio of 5 wt. % MCC and 10 wt. % PVA being kept at 50/50, resulting in a mixture of particles and fibers.

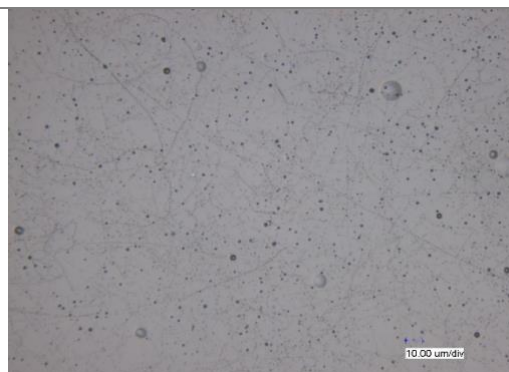
Interestingly, with a slight modification of this ratio to 45 % MCC & 55 % PVA, a stable electrospinning process was obtained, resulting in a specific type of beaded fibers (Figure 70), with the bead distributed evenly in the structure of nanofibers unlike the common beads in the structure of nanofibers obtained in different studies. <sup>[177,178]</sup> SEM was used to investigate the morphology of the obtained fibers. SEM results exhibited well distributed and homogenous beaded fibers with an average fiber diameter below 100 nm. It is worth mentioning that changing the electrospinning conditions did not affect the formation of this specific and uncommon structure.

**Table 15.** Different electrospinning conditions of MCC and PVA.

Expt. No.	Electrospinning condition	Optical microscopy
<b>1a</b>	22 kv-15 cm-0.12 mL/h	
<b>1b</b>	8 kV-20 cm-0.12 mL/h	
<b>1c</b>	11 kV-15 cm-0.12 mL/h	
<b>1d</b>	12 kV-20 cm-0.12 mL/h	

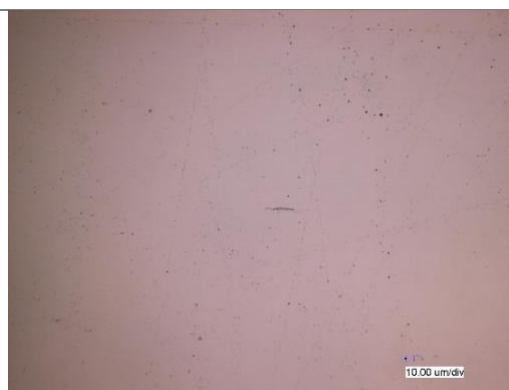
**1e**

25 kV-20 cm-0.12mL/h



**1f**

13 kV-20 cm-0.12 mL/h



**1g**

8 kV-20 cm-0.12 mL/h



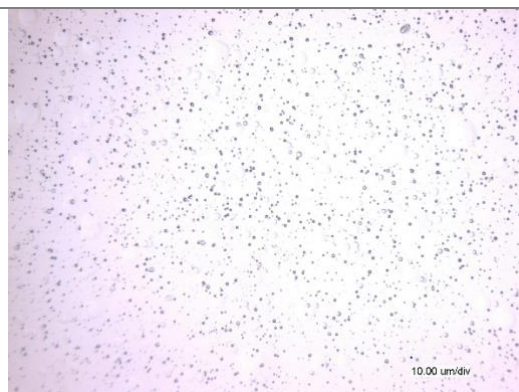
**1h**

20 kV-20 cm-0.24 mL/h



**1i**

20 kV-20 cm-0.12mL/h



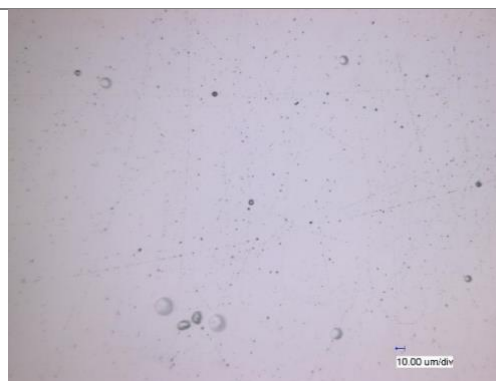
**1j**

15 kV-20 cm-0.12mL/h



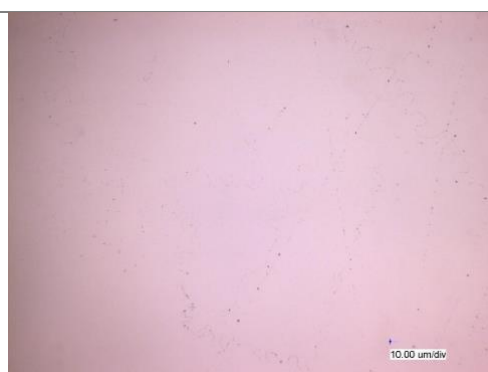
**1k**

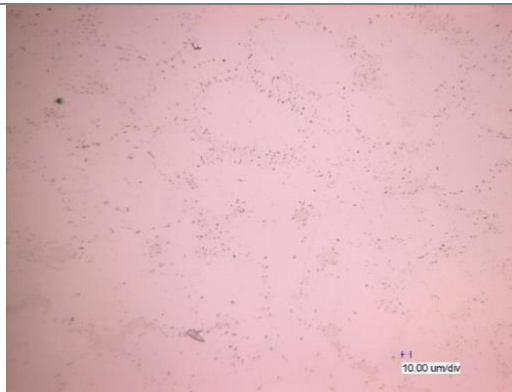

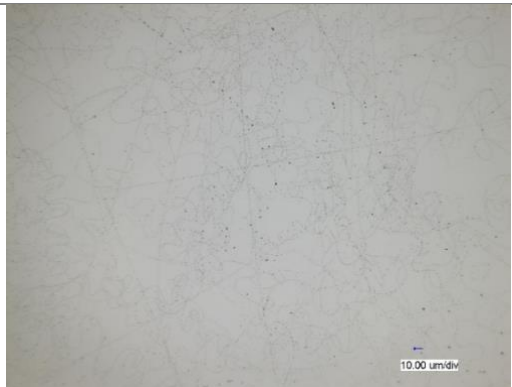
20 kV-20 cm-0.12 mL/h

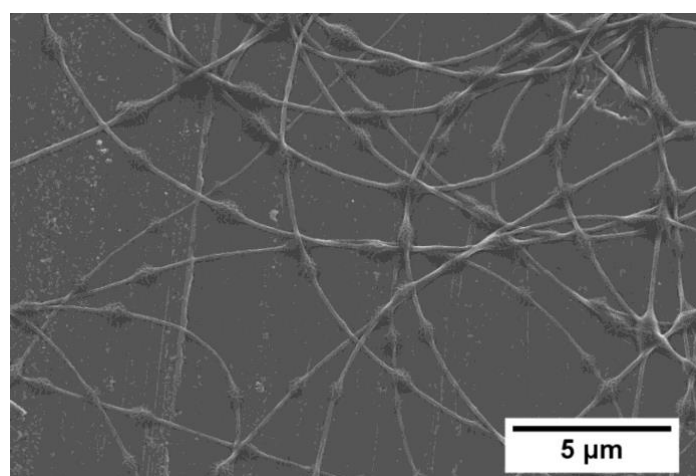


**1l**

20 kV-20 cm-0.12 mL/h

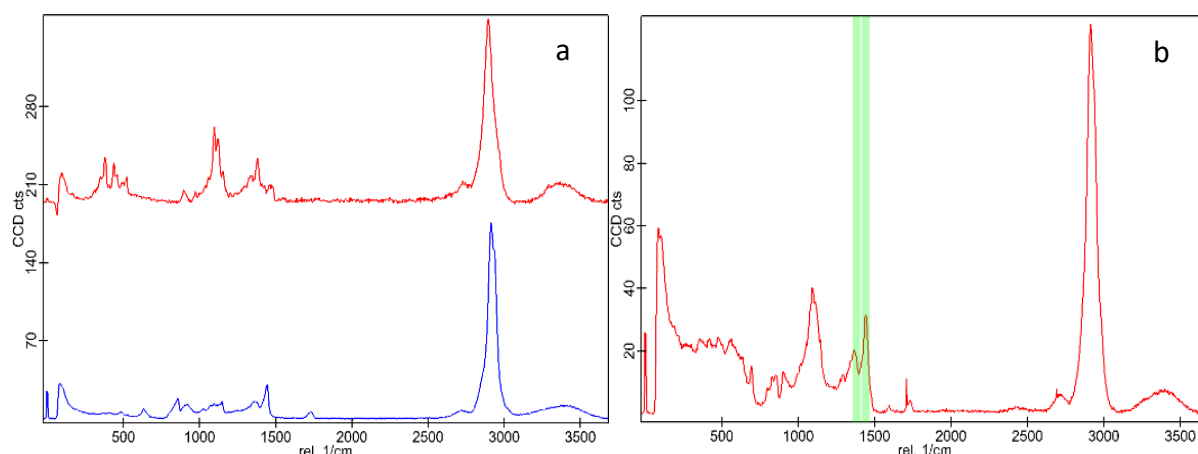


<b>1m</b>	15 kV-20 cm-0.12 mL/h	
<b>1n</b>	20 kV-20 cm-0.12 mL/h	
<b>1o</b>	6 kV-20 cm-0.12 mL/h	



**Figure 70.** SEM image showing beaded fibers (<100 nm) produced from electrospinning of 5 wt. % MCC and 10 wt. % PVA in a ratio 45/55 respectively in DBU-CO<sub>2</sub> switchable solvent system (E-spinning conditions: 7 kV-20 cm-0.12 mL/h).

The first hypothesis to explain the obtained result was potential phase separation between the MCC and PVA contributing to the formation of the beads. If this was the case, we would expect to observe either MCC or PVA in the beads. The appearance of symmetric bending mode of the CH<sub>2</sub> group of PVA and O-H bending of MCC at 1440 cm<sup>-1</sup> and 1380 cm<sup>-1</sup> on Raman spectroscopy of the mixture proved the presence of both MCC and PVA within the structure of the beads (Figure 71). Also, at this stage, the potential influence of CO<sub>2</sub>, which is trapped within the solvent system, should be considered. Zuo et al have investigated the origin of beads during electrospinning of poly(hydroxybutyrate-co-valerate).<sup>[179]</sup> They concluded that beads formation originates from the instability of the electrospinning solution (axisymmetric instability) and is affected by the viscosity, feed rate, applied voltage and surface tension. Although they investigated the general mechanism of bead-in-fiber formation during electrospinning, they did not observe the unique beads obtained in our work. So far, no other literature has reported a similar phenomenon.



**Figure 71.** Raman spectroscopy of (a) blue (PVA), red (MCC), (b) combined spectra in MCC/PVA nanofibers.

Based on the obtained result from 10 wt. % PVA, the higher PVA concentrations, including 15 and 20 wt. %, were also used. This was done to have higher viscosity at a lower addition ratio to obtain fibers at a higher MCC ratio. Using 15 wt. %



PVA, only particles were obtained, keeping the ratio with MCC at 90:10. Our results showed that a mixture of fibers and particles was obtained by increasing the PVA ratio up to 23 %, which is the highest concentration we could achieve to attain a homogenous solution. However, the electrospinning process was very unstable, leading to the formation of large droplets during electrospinning.

With increasing the PVA concentration to 20 wt. %, it was possible to achieve a stable electrospinning solution at the higher MCC ratio of 60 %. However, the most optimized electrospinning condition was attained using 10 wt. % PVA at 45:55 ratio of MCC and PVA.

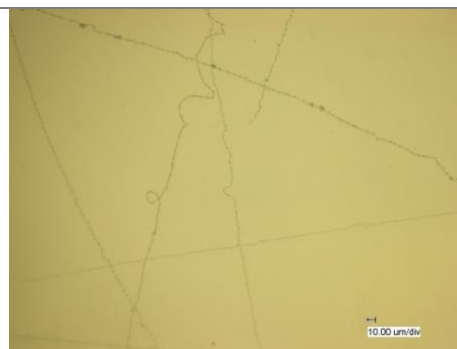
Besides using PVA as an additive to improve the spinnability of cellulose, we employed the use of high molecular weight polyethylene oxide (PEO). The different studied conditions are summarized in Table 16. As a reference, electrospinning of neat 2 wt. % PEO was carried out, which resulted in a mixture of fibers and beads (Table 17). In the subsequent experiments, the ratio of 5 wt. % MCC was increased from 45 to 90 %. It was interesting to note that, irrespective of the incorporated MCC ratio, beaded fibers were similar to those obtained with 10 wt. % PVA as an additive at 45 % MCC incorporation (Table 16). These results are interesting in that we could achieve a high MCC loading ratio while still maintaining a stable electrospinning process. One possible reason for still achieving such beaded fibers at a relatively low PEO ratio could be attributed to this polymer's very high molecular weight ( $9 \times 10^5$  g/mol). In an attempt to further increase the viscosity of these systems to eliminate these beads, a higher weight concentration solution of PEO was prepared (4.6 wt. %). With this much higher viscous solution, we could only achieve a stable electrospinning dope at a maximum MCC loading ratio of 45 %, which still resulted in beaded-fibers (Table 16, 2e).

**Table 16.** Different electrospinning conditions of MCC and PEO.

Expt. No.	Electrospinning condition	Optical microscopy
<b>2a</b>	25 kV-20 cm-0.36 mL/h	
<b>2b</b>	15 kV-20 cm-0.12 mL/h	
<b>2c</b>	15 kV-20 cm-0.12 mL/h	
<b>2d</b>	15 kV-20 cm-0.12 mL/h	

**2e**

15 kV-20 cm-0.12 mL/h



**Table 17.** Electrospinning using MCC solubilized in DBU-CO<sub>2</sub> solvent system at various PEO concentration and ratio.

Expt . No.	MCC conc. (wt. %)	PEO conc. (wt. %)	Ratio (%) MCC/PVA	Solution conc.	Voltage (kV)/distance (cm)/rate (mL/h)	Observation
<b>2a</b>	5	2	0/100	2.00	25-20-0.36	Fibers/beads
<b>2b</b>	5	2	45/55	3.35	15-20-0.12	Beaded fibers
<b>2c</b>	5	2	70/30	4.10	15-20-0.12	Beaded fibers
<b>2d</b>	5	2	90/10	4.70	15-20-0.12	Beaded fibers
<b>2e</b>	5	4.6	45/55	4.78	15-20-0.12	Beaded fibers

### 2.8.2 Investigation on using cellulose pulp (CP)

Cellulose pulp (CP) was solubilized in the DBU-CO<sub>2</sub> solvent system in the presence of DMSO as previously described. As the molecular weight of a polymer is a determining key factor in the viscosity of the electrospinning solution and due to the promising results obtained using MCC, we decided to employ a higher molecular weight cellulose type, i.e., CP. We hypothesized that by using CP, we could probably get rid of the beads in the beaded fibers obtained in the previous experiments with MCC. In the first set of experiments, the concentration of CP was varied between 1 to 5 wt. %. These experiments and resulting observations are summarized in Table 18.

**Table 18.** Electrospinning using CP solubilized in DBU-CO<sub>2</sub> solvent system at 5 wt.% PVA concentration and various ratios.

Expt No.	CP conc. (wt. %)	PVA conc. (wt. %)	Ratio (%) CP/PVA	Solution Conc.	Voltage (kV)/ distance (cm)/ rate (mL/h)	Observation
3a	1	-	100/0	1.00	17-15-0.12	Only Particles
3b	2	-	100/0	2.00	25-25-0.24	Mixture of particles and standing fibers
3c	2.5	-	100/0	2.50	17-15-0.12	Mixture of particles and standing fibers
3d	3	-	100/0	3.00	29-15-0.12	Standing fibers with particles
3e	4	-	100/0	4.00	29-20-0.12	Only standing fibers
3f	5	-	100/0	5.00	29-20-0.12	Only standing fibers
3g	3	5	56/44	3.80	8-20-0.12	Beaded fibres
3h	3	5	67/33	3.66	7-20-0.12	Beaded fibres
3i	5	5	67/33	5.00	8.5-20-0.12	beaded fibres

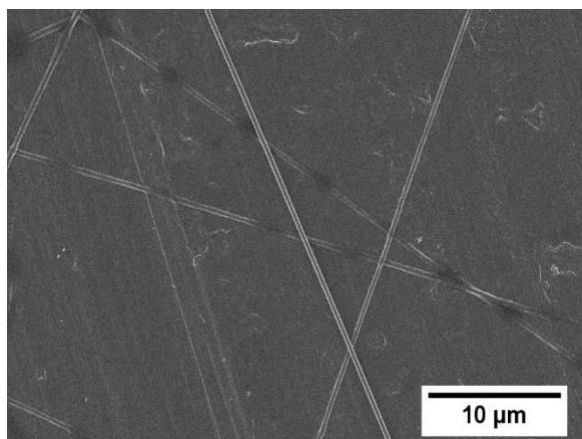
It was discovered that most particles were obtained with small amount of fibers when 1 wt. % CP was used (Table 18). As the CP concentration increased to 2 wt. % (3b), a mixture of particles and standing fibers were obtained. The standing fibers have been previously reported by Frenot et al. from a direct electrospinning of cellulose from a DMAC/LiCl solution as well, <sup>[154]</sup> which could be attributed to the high conductivity (high charges present) of the electrospinning solution, resulting in a stronger electrostatic attraction towards the opposite charged collector plate. Hence, it was not surprising for us to

consider that we employed an equally ionically charged solvent system  $[\text{Cellulose-OCO}_2]^- [\text{HDBU}]^+$ .<sup>[176]</sup> Similarly, standing fibers with fewer beads, were observed as a matter of an increase in the CP concentration from 2 to 3 wt. %. As it could be seen in Table 18, by increasing the cellulose concentration to 4 wt. %, standing fibers were obtained (Figure 72).



**Figure 72.** Image showing standing fibers on the collector from electrospinning of 4 wt. % CP in DBU- $\text{CO}_2$  switchable solvent system (E-spinning conditions: 29 kV-20 cm-0.12 mL/h).

The morphology of the obtained fibers was studied using SEM, and the result is shown in Figure 73. Increasing the CP concentration to 5 wt. % still resulted in standing fibers with a mean diameter of  $560 \pm 30$  nm.



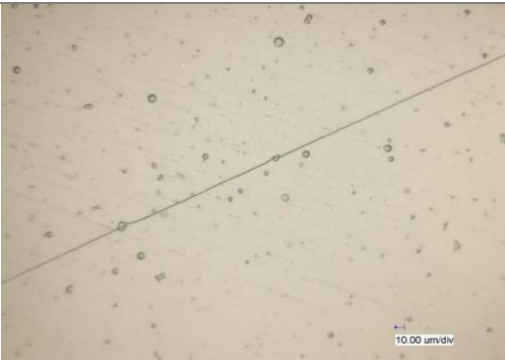
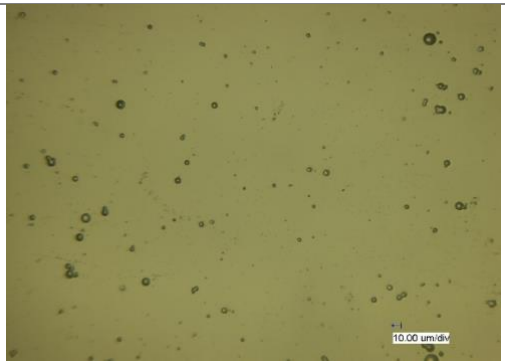
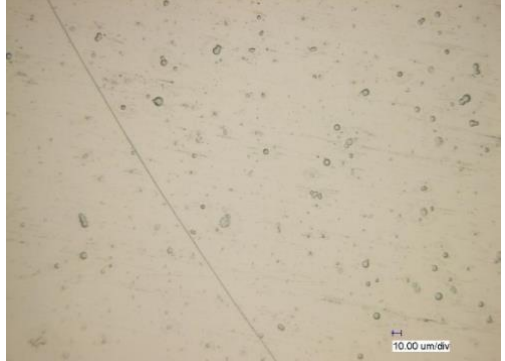
**Figure 73.** SEM image showing electrospun fibers (<1  $\mu\text{m}$ ) produced from electrospinning of 4 wt.% CP in DBU- $\text{CO}_2$  switchable solvent system (E-spinning conditions: 29 kV-20 cm-0.12 mL/h).

#### 2.8.2.1 Use of additives for electrospinning of CP

As explained earlier, the electrospinning of neat CP from the DBU- $\text{CO}_2$  solvent system resulted in standing fibers. Additionally, the non-uniform fibers obtained from this process are not interesting in terms of application. As indicated in Frenot et al. work,<sup>[154]</sup> where they attained almost identical standing fibers, they attributed this phenomenon to the presence of the highly ionic solvent. Consequently, they hypothesized that adding a polymer additive helps to improve the process. This was confirmed when we obtained only beaded fibers when PVA was included as an additive (3 wt. % CP and 5 wt. % PVA at ratio of 56:44, see Expt.3g). Results proved that the addition of PVA contributed to the vanishing of standing fibers, and as a result, a very stable electrospinning process was obtained. Still, rising the CP ratio up to 67 % (experiment 3h) caused beaded fibers. SEM demonstrated that the trend with the morphology of the beaded fibers was very similar to PVA, which was used as an additive in MCC electrospinning (Table 19). Similarly, beaded fibers were acquired by using a higher weight concentration of CP (5 wt. %). The SEM of beaded fibers with 5 wt. % CP at 67:33 ratio with 5 wt. % PVA is represented in Figure 74. The results

further strengthen the earlier hypothesis that the obtained unique beaded morphology of the nanofibers could be mainly attributed to the interaction between the cellulose and polymer additive.

**Table 19.** Different electrospinning conditions of CP.

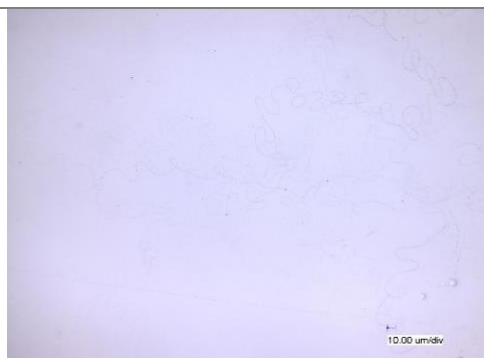
Expt. No.	Electrospinning condition	Optical microscopy
3a	17 kV-15 cm-0.12 mL/h	
3b	25 kV-25 cm-0.24 mL/h	
3c	17 kV-15 cm-0.12 mL/h	

<p><b>3d</b></p> <p>29 kV-15 cm-0.12 mL/h</p>	
<p><b>3e</b></p> <p>29 kV-20 cm-0.12 mL/h</p>	
<p><b>3f</b></p> <p>29 kV-20 cm-0.12 mL/h</p>	
<p><b>3g</b></p> <p>8 kV-20 cm-0.12 mL/h</p>	



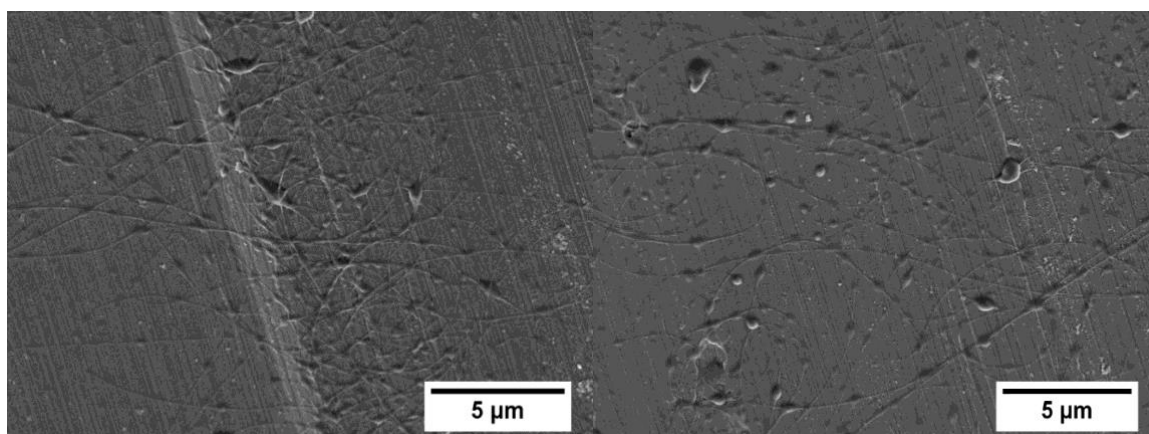
**3h**

7 kV-20 cm-0.12 mL/h



**3i**

8.5 kV-20 cm-0.12 mL/h



**Figure 74.** SEM image showing electrospun fibers (<2μm) produced from electrospinning of 5 wt. % CP and 5 wt. % PVA in a ratio 67/33 respectively in DBU-CO<sub>2</sub> switchable solvent system (E-spinning conditions: 8.5 kV-20 cm-0.12 mL/h).

# **Chapter 3**

## **Experimental part**

## 3 Experimental part

### 3.1 Materials

$\epsilon$ -Caprolactone (CL) was purchased from Alfa Aesar and was dried using calcium hydride (Merck Co.) for 24 h and purified by distillation under vacuum.  $\alpha$ -Hydroxy- $\omega$ -methoxy-poly (ethylene glycol) (mPEG, Mw: 5000) from Aldrich Co. was dried in a vacuum oven at 40 °C for 2 h. Stannous octoate [Sn(Oct)<sub>2</sub>] and Tween 80 were bought from Sigma-Aldrich. PLGA 50:50 Poly (DL-lactide-co-glycolide) resomer RG 503 (Molecular weight 27000 - 38000 Da) was obtained from Evonik. Artemisone was donated by CIPLA and used without further purification. Acetone and acetonitrile were purchased from Sigma-Adrich, p.a. grade and were used as received. PEO (poly (ethylene oxide)) (Mw: 900000) was purchased from ACROS Organics and was dried in vacuum oven at 40 °C for 2 h. Polyethylene glycole (PEG) (MW 20000) was bought from Merck. Pluronic F-68 was purchased from Applichem.

MCC was provided from Sigma-Aldrich. Cellulose pulp was bought from Rayonier Advanced Materials Company (Tartas Biorefinery, France) and was produced by ammonium sulphite cooking and bleached with an elementary chlorine free (ECF) process (purity in alpha-cellulose is 94 %). All cellulose samples were dried at 100 °C for 24 h under vacuum to remove free water before using. Dimethyl sulfoxide (DMSO) 99% was purchased from VWR. Diazabicyclo [5.4.0] undec-7-ene (DBU, >98%) was bought from TCI and used without further purification. PVA 98 - 99% hydrolyzed (MW 31000 - 50000 g/mol) was obtained from Sigma-Aldrich. Polyethyleneoxide, PEO (MW 900,000 g/mol) was purchased from Alfa Aesar. Vivaspin 20 centrifugal concentrator (MW 10 KDa) was purchased from GE Healthcare.

## 3.2 Methods

### 3.2.1 Characterizations

The morphology of micro and nanoparticles was examined by SEM using Zeiss electron microscope model LEO 1530. The average nanofiber diameter was determined by means of at least 100 random measurements using ImageJ software based on SEM images. EDX analysis was done in order to characterize the presence of ART in micro and nanoparticles.

X-ray diffraction analysis (XRD) analysis was done in order to determine the crystallinity of the ART, PLGA and ART-loaded PLGA micro and nanoparticles. Different samples containing the pure drug, pure polymer and drug-loaded micro and nanoparticles were evaluated using analytical empyrean XRD diffractometer with Cu K $\alpha$  radiation (1.5418 Å).

TEM was performed using Zeiss EM922 Omega EFTEM (Zeiss NTS GmbH, Oberkochen, Germany) electron microscope operated at an acceleration voltage of 200 kV. The samples were diluted with water, and then drop-coated onto a carbon-coated copper grid lying on a filter paper. After drying in a vacuum oven at room temperature and a pressure of 2 mbar, the samples were stained with RuO<sub>4</sub> vapor, which is known to selectively stain.

Asymmetric flow-field flow fractionation (AF4) was carried out in order to measure the particle size in a dispersion using NEW AF2000 ELECTRICAL FLOW FFF (Postnova). AF4 measurements were conducted on an AF2000 FFF system with a Smart Stream Splitter from Postnova with channel thickness of 350  $\mu$ m and a NovaRC 10 kDa membrane. Detection was carried out by a UV detector with a maximum absorption of 525 nm and additionally by MALS and DLS. Water was selected as an eluent with a flow rate of 0.5 mL/min. The samples were dispersed with a concentration of 1 mg/mL in the corresponding solvent (water).

In case of spray-dried particles, first particles were redispersed in water using tween 80 (1 % w/v) as a surfactant. And subsequently, the characterization was done.

The mean particle size and particle size distribution were assessed by means of dynamic light scattering (DLS) at 25 °C. DLS measurements were conducted using a LS spectrometer of LS Instruments AG (Fribourg, Switzerland) with HeNe laser (max. 35 mW constant output at 632.8 nm) as a source of light. The scattered light was detected using two APD detectors in pseudo-cross correlation, the time average scattering intensities were measured at scattering angle of 90 °. Samples were diluted in water. The temperature was set with a stability of  $\pm 100$  mK by a heat controlled decalin bath. A PT100 thermoelement located close to the sample position in the decalin bath was utilized for monitoring the temperature. High-performance liquid chromatography analysis (HPLC) was used in order to not only determining the amount of ART in nano and microparticles as well as nanofibers, but also characterizing the ART release from micro and nanoparticles. This was accomplished using HPLC instrument Eclipse XDB-C18, 4.6 x 150 mm, 5  $\mu$ m column Waters system equipped with autosampler AS100 and waters 2489 as UV detector. The injection volume was 20  $\mu$ l. The mobile phase consisted of acetonitrile/water (60:40). The experiments were done at the wavelength of 200 nm with a flow rate of 0.8 mL/min.

A confocal WITec alpha 300 RA+ imaging system equipped with a UHTS 300 spectrometer and a back-illuminated Andor Newton 970 EMCCD camera was employed for Raman imaging of spray-dried particles. Raman spectra was obtained using an excitation wavelength of  $\lambda = 532$  nm, a step size of 10 pixels/ $\mu$ m and integration times of 0.1 – 0.5 s/pixel (100 $\times$  objective, NA = 0.9, software WITec Control FOUR 4.1). All spectra were exposed to a cosmic ray removal routine and baseline correction.

For Differential scanning calorimetry (DSC), a DSC 821e (Mettler Toledo) with 40  $\mu$ L aluminum crucibles was used. 5 – 10 mg of sample was measured with heating rate of 10 K/min under nitrogen atmosphere.

Thermogravimetric analysis (TGA) was conducted with Libra F1 TG 209 from Netzsch with gas flow of 50 mL/min. 5 – 10 mg of sample were weighted in an aluminium oxide crucible and heated from 25 – 1100 °C with heating rate of 10 ° K/min.

Gel permeation chromatography analysis (GPC) was carried out in chloroform using a PSS-SDV pre- column (8 mm  $\times$  50 mm) and a PSS-SDV column (linear XL, 5  $\mu$ m, 8 mm  $\times$  300 mm) at 40 °C with a flow rate of 1 mL/min and Win GPC Unity (build 6807) for evaluation. The standard calibration was applied by using polystyrene as the standards.

Nuclear magnetic resonance (NMR) spectroscopy was conducted in  $\text{CDCl}_3$  as a solvent using a Bruker ARX300 spectrometer and MestReNova software for evaluation.

Optical microscope images were taken with a Smartzoom5 (Zeiss). To be able to initially characterize morphology of each sample, which was electrospun and to conduct optimizations for electrospinning, every sample was firstly observed under optical microscopy. The smooth bead free nanofibers were selected for SEM measurement.

### **3.2.2 Preparation of nanoparticles through solvent displacement method**

Different amounts of PLGA and ART were dissolved in organic phase consisting of acetone as a water-miscible solvent. The organic phase was then added to

aqueous phase drop by drop under continuous stirring thereby forming milky colloidal suspension. Afterwards, the organic solvent was eliminated from the colloidal suspension using rotary evaporator. The resultant dispersion was then centrifuged three times at 8000 rpm for 30 min in order to separate the nanoparticles from aqueous phase as well as unreacted drug. In order to establish a correlation between the influence of different processing parameters on the particle size of the nanoparticles as well as drug encapsulation and loading efficiency. The parameters which were assessed are PLGA and ART concentration, organic to aqueous ratio, organic phase addition rate, stirrer rate and temperature. The aforementioned parameters along with the amounts are indicated in Table 20.

**Table 20.** Different processing parameters for solvent displacement method.

Parameter	Amount
PLGA concentration (mg)	30,35,40
ART concentration (wt. %)	10,15,20
Organic to aqueous ratio (-)	1:2,1:3,1:4
Stirring rate (rpm)	250,500,750

### 3.2.3 Preparation of ART-loaded microparticles using spray drying technique

ART-loaded micro and nanoparticles were fabricated using spray dryer. Different concentrations of PLGA and ART were accurately weighed and dissolved in acetone. The resultant organic solutions were then spray dried using Büchi mini spray dryer B-290 (Büchi, Switzerland). Various parameters such as PLGA concentration, ART concentration, feed rate and inlet temperature were

optimized to get the highest loading and encapsulation efficiencies as well as homogeneous size distribution. Operating conditions are shown in Table 21.

**Table 21.** Different processing parameters for spray drying technique.

Parameter	Amount
PLGA concentration (wt. %)	1,1.5,2
ART concentration (wt. %)	10,15,20
Feed rate (ml/min)	1.5,3,4.5
Inlet Temperature (°C)	61,66,71

### 3.2.4 Determining calibration curve of ART for validating HPLC for determining the amount of ART

Validation of method was conducted preparing different concentrations of ART in aqueous medium containing different concentrations of tween 80. The lowest concentration which was detected by HPLC was 3.125 µg/mL. Seven different concentrations of drug in methanol/PBS 1 wt. % were prepared. These are as following:

(3.125, 6.25, 12.5, 25, 50, 100 and 200 µg/mL). HPLC was used to determine the amount of drug at 200 nm, 0.8 mL/h and 35 °C. Acetonitrile (ACN)/water 60:40 was used as a mobile phase. The lowest amount of ART which was detected was 3.125 µg/mL. The experiment was repeated 3 times.

### 3.2.5 Determination of drug loading and encapsulation efficiency

The drug encapsulation and loading efficiency were determined as explained below. For ART-loaded particles, accurately weighed dried particles were put in volumetric flask, then the appropriate solvent (acetonitrile/water) (60%v/40%v)



was added and the obtained mixture was vortexed for 5 min. Afterwards the flasks were put on shaker for the next 45 min. Then the mixture was filtered using syringe filter 0.2  $\mu\text{m}$ . The dissolved ART was then injected to HPLC at a flow rate of 0.8 mL/min. Detection wavelength was set at 200 nm. The temperature of the column was kept at 35 °C. Each experiment was repeated 3 times. All results have been reported as mean  $\pm$  SD. Drug encapsulation and drug loading of the particles could be calculated using following equations 1 and 2.

$$\text{Drug encapsulation efficiency} = \frac{\text{amount of drug in nanoparticles}}{\text{initial amount of drug}} \times 100$$

**Equation 1.** Determining drug encapsulation efficiency of micro and nanoparticle.

$$\text{Drug loading efficiency} = \frac{\text{amount of drug in nanoparticles}}{\text{weight of the nanoparticles}} \times 100$$

**Equation 2.** Determining drug encapsulation efficiency of micro and nanoparticle.

### 3.2.6 Release behavior of ART-loaded micro and nanoparticles using HPLC

For release tests, a weighed amount of ART-loaded micro and particles were put in a PBS medium containing 1 wt. % tween 80 with pH value of  $7.4 \pm 0.05$ . Particle dispersion was placed in an incubator at 37 °C. At different time intervals, the dispersions were taken out and centrifuged at 10000 rpm for 10 min. The pellets were then replaced with the same amount of solution in order to maintain the sink condition. The supernatants were evaluated for determining the amount of ART released in the medium using HPLC. All experiments were carried out in triplicate.

### 3.2.7 Synthesis of PCL<sub>15000</sub>-b-MPEG<sub>5000</sub>

The biodegradable diblock copolyester PCL<sub>15000</sub>-b-MPEG<sub>5000</sub> (the subscript shows the Mn of the polycaprolactone (PCL) block and MPEG according to NMR analysis) (PCL-mPEG) was synthesized by ring-opening of  $\epsilon$ -caprolactone catalyzed by stannous octoate in the presence of  $\alpha$ -methoxy- $\omega$ -hydroxy-poly(ethylene glycol) (MPEG) as a macroinitiator. The reaction was started with 13.95 g caprolactone and 4.65 g mPEG. The mixture was then heated up to 130 °C, and afterwards 30  $\mu$ L catalyst was added to the mixture. Ultimately, the mixture viscosity started to increase, which was cooled down to room temperature after 3 h of reaction time. For purification of the polymer, after precipitation in n-pentane, the polymer was extracted with water to remove the water-soluble parts of the product, like the oligo PCL-b-mPEG and unreacted mPEG.

### 3.2.8 Preparation of ART-loaded electrospun nanofibers immobilized with ART-loaded nanoparticles

Green electrospinning was used in order to fabricate drug-loaded PCL-mPEG nanofibers. The preparation of PCL-mPEG dispersion in water was done based on Sun's work.<sup>[17]</sup> Briefly, PCL-mPEG in water was heated up to 80°C so that micelles would be formed. Then ART-loaded PLGA nanoparticle dispersion, which was synthesized in our work using solvent-displacement method, was up concentrated using ultrafiltration centrifugal concentrator and added to the PCL-mPEG dispersion. In order to make the viscosity appropriate for electrospinning, PEO was added to the mixture. The electrospinning condition is brought in Table 22.

**Table 22.** Electrospinning composition for nanofibers loaded with ART-loaded nanoparticles.

<b>PCL-mPEG</b>	<b>PEO</b>	<b>Wasser</b>	<b>ART</b>	<b>PLGA</b>
<b>(g)</b>	<b>(g)</b>	<b>(g)</b>	<b>(mg)</b>	<b>(mg)</b>
0.15	0.025	0.825	10	40

### 3.2.9 Preparation of ART-loaded electrospun nanofibers

Accordingly, PCL-mPEG was heated up to 80 °C. Subsequently, ART was dissolved in acetone and was added drop by drop to the PCL-mPEG dispersion. Furthermore, PEO was added to the dispersion to obtain a suitable viscosity for electrospinning. The electrospinning conditions are listed in Table 23.

**Table 23.** Electrospinning composition for ART-loaded nanofibers.

<b>PCL-mPEG</b>	<b>PEO</b>	<b>Wasser</b>	<b>ART</b>
<b>(g)</b>	<b>(g)</b>	<b>(g)</b>	<b>(mg)</b>
0.15	0.025	0.825	10

### 3.2.10 Quantification of ART in ART-loaded PLGA nanoparticles and electrospun nanofibers immobilized with ART-loaded PLGA nanoparticles

HPLC was exploited in order to quantitatively determine the amount of drug in ART-loaded PLGA micro and nanoparticles (Equation 3) and electrospun nanofibers immobilized with ART-loaded PLGA nanoparticles (Equation 4). To meet the goal, nanoparticles and nanofibers were put in a mobile phase comprised of ACN (60 % v)/water (40 % v), in which the drug is readily dissolved.

For this purpose, three different batches of nanoparticles and three nanofiber samples, immobilized with ART-loaded nanoparticles were chosen and analyzed at 200 nm with a flow rate of 0.8 mL/min. The values were obtained by comparing the data from the samples and the standard solution. The assay amounts were obtained by comparing the data achieved from ART-loaded electrospun nanofibers and the standard solutions. Each experiment was repeated three times.

$$\text{Assay: } \frac{\text{experimental amount of ART in nanoparticle}}{\text{theoretical amount of ART in nanoparticle}}$$

**Equation 3.** Calculation of ART amount in nanoparticles.

$$\text{Assay: } \frac{\text{experimental amount of ART in nanofiber}}{\text{theoretical amount of ART in nanofiber}}$$

**Equation 4.** Calculation of ART amount in nanofiber.

### **3.2.11 Release behavior of different electrospun nanofibers using HPLC**

A specific amount of fiber was cut and weighed. Then they were incubated at 37 °C in aqueous medium including 1 wt. % Tween 80. After certain time intervals, 1 mL of the medium was taken out and replaced with 1 mL fresh medium. The cumulative released amount of ART was quantified using HPLC medium.

### **3.2.12 Preparation of suspension electrospinning immobilized with ART-loaded PLGA micro and nanoparticles**

First of all, PLGA and ART are dissolved in chloroform. Afterwards, Pluronic F-68 is added to water and dissolved and subsequently PCL-mPEG is added to the mixture is heated up to 80 ° C. The PLGA/ART solution is added to the PCL-mPEG

dispersion drop by drop under stirring. In the next step, to make different particle sizes (micro and nanoparticles) in nanofiber, two emulsification methods were used namely ultrasonic and ultrasonifier. The suspensions were under these emulsification methods for 1 min. Then PEO is added to make the viscosity suitable for electrospinning. Electrospinning was done using vertical electrospinning apparatus under the voltage of 30 kV, electrospinning distance of 20 cm and the feed rate of 0.5 mL/h. The electrospinning condition could be observed in Table 24.

**Table 24.** Suspension electrospinning conditions containing 15 wt. % particle in fiber and 15 wt. % ART in particle.

PLGA	ART	PCL-mPEG	Pluronic F-68	PEO
1 % w/v	10 wt. %	15 wt. %	5 % w/v	2.5 wt. %

### 3.2.13 Core-shell electrospinning

15 wt. % PCL-mPEG and 10 wt. % ART were dissolved in dichloromethane separately. Pyridinium formate was added to the previous solution in order to reduce the amount of beads. PEG 20000 was added to the ART in order to increase the spinnability of the ART solution. Different electrospinning conditions were used (Table 25, 26 and 27). Rhodamine B was used to dye the core solution. The electrospinning conditions are shown in Table 28.

**Table 25.** ART/PCL-mPEG core-shell electrospinning condition.

PCL-mPEG	ART
15 wt. %	10 wt. %
(DCM)	(DCM)

**Table 26.** ART-PEG/PCL-mPEG core-shell electrospinning condition in DCM.

PCL-mPEG	ART	PEG
15 wt. % (DCM)	10 wt. % (DCM)	10 % w/w (DCM)

**Table 27.** ART-PEG (in DCM)/PCL-mPEG (in water) core-shell electrospinning condition.

PCL-mPEG	ART	PEG
15 wt. % (water)	10 wt. % (DCM)	10 % w/w (DCM)

**Table 28.** Electrospinning condition of core-shell electrospun nanofiber.

Voltage	Feed rate (core)	Feed rate (shell)	distance
25 kV	0.2 mL/h	0.8 mL/h	20 cm

### 3.2.14 Solubilization of MCC and CP

The solubilization of MCC & CP was done based on a previous report done by Onwukamike et al. [176] Briefly, cellulose was stirred in DMSO, which was followed by addition of DBU (3 eq. per anhydroglucose unit). The cloudy suspension was then transferred to a steel pressure reactor, where 5 bar CO<sub>2</sub> was applied at 30 °C for 15 min. The solubilized and clear cellulose solution was carefully transferred to a syringe, making sure that the trapped CO<sub>2</sub> does not escape, and is ready to be used for the electrospinning process. Equally, PVA & PEO were separately dissolved in DMSO and were added to the cellulose solution in different ratios depending on the target wt. %.

### **3.2.15      Electrospinning of cellulose solutions**

The prepared solutions were electrospun under different electrospinning conditions. The parameters including (cellulose concentration, applied voltage, feed rate and electrospinning distance) were optimized to gain smooth bead-free fibers. Different concentrations of PVA in DMSO were prepared and were added subsequently to the cellulose solutions.

# **Chapter 4**

## **Summary**



## 4 Summary

Electrospinning has been introduced as an efficient technique for the fabrication of polymeric nanofibers. Electrospun nanofibrous structures have gained an unprecedented application among other nanostructures in drug delivery owing to their high surface area, which enable drugs to be adhered on the surface of the nanofibers. Our concept was to fabricate electrospun nanofibers and then immobilize drug-loaded polymeric micro- and nanoparticles into electrospun nanofibers. In our studies, artemisone (ART) as an antiparasitic anti-inflammatory medication was used. By immobilizing ART into micro and nanocarriers, we aimed at increasing the stability as well as protecting the drug from degradation in aqueous medium and more importantly reducing the amount of burst release along with prolonging the release rate.

We developed different carriers such as ART-loaded micro and nanoparticles synthesized by spray drying and solvent-displacement method. We were aiming at optimizing the governing parameters, which substantially influences particle size and encapsulation efficiency. It is important to produce particles with an efficient amount of drug and achieve the highest encapsulation efficiencies especially in case of ART, which is an expensive drug. Our concept was to immobilize these ART-loaded nanoparticles in electrospun nanofibers to evaluate whether we can merit from both advantages of nanoparticle and nanofiber. Our results proved our concept that the electrospun nanofibers immobilized with ART-loaded nanoparticles showed less burst release and more sustained release compared to nanoparticles and nanofibers itself. In other work, we tried to immobilize ART-loaded micro and nanoparticle in electrospun nanofibers simultaneously by conducting suspension electrospinning to have an understanding of how the particle size impacts the ART release from electrospun

nanofibers. Using this concept, the ART-loaded micro and nanoparticles immobilized in electrospun nanofibers revealed a less burst release and a more sustained release compared to fibers without particles. We also employed core-shell electrospinning as a concept to encapsulate ART into electrospun nanofibers. We achieved the core-shell structure, which resulted in a sustained release as well as less burst release compared to other systems. Lastly, we electrospun two types of cellulose namely MCC and CP, which resulted in obtaining nanofibers with a unique structure. The obtained nanofiber could be loaded with ART and find application for drug delivery.

# **Chapter 5**

## **Zusammenfassung**

## 5 Zusammenfassung

Das Elektrosponnen wurde als effiziente Technik für die Herstellung von polymeren Nanofasern eingeführt. Elektrogesponnene Nanofaserstrukturen haben aufgrund ihrer großen Oberfläche, die es ermöglicht, Arzneimittel auf der Oberfläche der Nanofasern anzuheften, eine beispiellose Anwendung unter anderen Nanostrukturen für die Arzneimittelverabreichung gefunden. Unser Konzept bestand darin, elektrogesponnene Nanofasern herzustellen und dann mit Medikamenten beladene polymere Mikro- und Nanopartikel in den elektrogesponnenen Nanofasern zu immobilisieren. In unseren Studien wurde Artemisinin (ART), ein entzündungshemmendes Medikament gegen Plasmodium, verwendet. Durch die Immobilisierung von ART in Mikro- und Nanocarrier wollten wir die Stabilität erhöhen und das Medikament vor dem Abbau in wässrigem Medium schützen, und, was noch wichtiger ist, die Freisetzungsrate verlängern und die Menge des Freisetzungstoßes verringern.

Wir entwickelten verschiedene Träger wie ART-beladene Mikro- und Nanopartikel, die durch Sprühtrocknung und Lösungsmittelverdrängung hergestellt wurden. Unser Ziel war es, die maßgeblichen Parameter zu optimieren, die die Partikelgröße und die Verkapselungseffizienz wesentlich beeinflussen. Es ist wichtig, Partikel mit einer effizienten Menge an Medikamenten herzustellen und die höchste Verkapselungseffizienz zu erreichen, insbesondere im Falle von ART, einem teuren Medikament. Unser Konzept bestand darin, diese mit ART beladenen Nanopartikel in elektrogesponnenen Nanofasern zu immobilisieren, um zu prüfen, ob wir die Vorteile von Nanopartikeln und Nanofasern nutzen können. Unsere Ergebnisse bestätigten unser Konzept, dass die elektrogesponnenen Nanofasern, die mit ART-beladenen Nanopartikeln immobilisiert wurden, im Vergleich zu den

Nanopartikeln und den Nanofasern selbst eine geringere sprunghafte und nachhaltigere Freisetzung zeigten. In einer anderen Arbeit haben wir versucht, ART-beladene Mikro- und Nanopartikel gleichzeitig in elektrogesponnenen Nanofasern zu immobilisieren, indem wir Suspensions-Elektrospinnen durchgeführt haben, um zu verstehen, wie die Partikelgröße die ART-Freisetzung aus elektrogesponnenen Nanofasern beeinflusst. Mit diesem Konzept zeigten die mit ART beladenen Mikro- und Nanopartikel, die in elektrogesponnenen Nanofasern immobilisiert waren, eine geringere Freisetzung und eine nachhaltigere Freisetzung im Vergleich zu Fasern ohne Partikel. Wir verwendeten auch das Konzept des Kern-Schale-Elektrospinnens, um ART in elektrogesponnene Nanofasern einzukapseln. Wir erreichten eine Kern-Schale-Struktur, die im Vergleich zu anderen Systemen zu einer anhaltenden Freisetzung und einer geringeren Freisetzung in Schüben führte. Schließlich haben wir zwei Arten von Zellulose, nämlich MCC und CP, elektrogesponnen, wodurch wir Nanofasern mit einer einzigartigen Struktur erhalten haben. Die erhaltenen Nanofasern könnten mit ART beladen werden und für die Verabreichung von Medikamenten eingesetzt werden.

# **Chapter 6**

## **Acknowledgements**

## 6 Acknowledgements

I would like to express my gratitude to all those who supported and helped me during my doctoral thesis.

The practical work of my thesis was done at the department of Macromolecular Chemistry II (MCII) at the University of Bayreuth.

First and foremost, I would like to express my deepest gratitude to Professor Greiner for accepting me as a PhD student in his group, for his brilliant and invaluable guidance, support and kindness during these years. He was not only my supervisor, but also he always went out of his way to help me in different ways within these years.

My gratitude to Dr. Amirreza Bagheri for the introduction and helping me at the beginning.

I would also like to thank all my colleagues, especially Rika Schneider, Christian Hils, Thomas Schmitt and Adrian Wambach for their friendship, help and their scientific discussions.

I would like to thank Prof. Jacob Golenser for his kindness and meticulous reviewing of my manuscripts.

I would like to say thank you to my cooperation partners Dr Johanna Zech and Dr Kelechukwu Onwukamike for nice discussions and friendly atmosphere during the work.

My great gratitude to Professor Seema Agarwal for her support and proofreading my manuscripts.

And from the bottom of my heart, I am grateful to my mother, for her love, sense of humor (especially to me) and her endless support. Whatever I achieved in my life, is because of her. I am grateful to my siblings for their support and love,

especially my sister Mojdeh, for her continuous support, encouragement and for always being there for me as a friend.



# **Chapter 7**

## **References**

## 7 References

- [1] Balan P, Indrakumar J, Murali P and Korrapati P S 2020 Bi-faceted delivery of phytochemicals through chitosan nanoparticles impregnated nanofibers for cancer therapeutics *Int. J. Biol. Macromol.* **142** 201–11
- [2] Balagangadharan K, Trivedi R, Vairamani M and Selvamurugan N 2019 Sinapic acid-loaded chitosan nanoparticles in polycaprolactone electrospun fibers for bone regeneration in vitro and in vivo *Carbohydr. Polym.* **216** 1–16
- [3] Naeimirad M, Zadhoush A, Kotek R, Esmaeely Neisiany R, Nouri Khorasani S and Ramakrishna S 2018 Recent advances in core/shell bicomponent fibers and nanofibers: A review *J. Appl. Polym. Sci.* **135** 46265
- [4] Bagheri A R, Golenser J and Greiner A 2020 Controlled and manageable release of antimalarial Artemisone by encapsulation in biodegradable carriers *Eur. Polym. J.* **129** 109625
- [5] Zupančič Š, Sinha-Ray S, Sinha-Ray S, Kristl J and Yarin A L 2016 Controlled Release of Ciprofloxacin from Core–Shell Nanofibers with Monolithic or Blended Core *Mol. Pharm.* **13** 1393–404
- [6] Bhattarai R, Bachu R, Boddu S and Bhaduri S 2018 Biomedical Applications of Electrospun Nanofibers: Drug and Nanoparticle Delivery *Pharmaceutics* **11** 5
- [7] Jiang S, Lv L-P, Landfester K and Crespy D 2016 Nanocontainers in and onto Nanofibers *Acc. Chem. Res.* **49** 816–23
- [8] Günday C, Anand S, Gencer H B, Munafò S, Moroni L, Fusco A, Donnarumma G, Ricci C, Hatir P C, Türeli N G, Türeli A E, Mota C and Danti S 2020 Ciprofloxacin-loaded polymeric nanoparticles incorporated electrospun fibers for drug delivery in tissue engineering applications *Drug Deliv. Transl. Res.* **10** 706–20
- [9] Balaji A, Vellayappan M V, John A A, Subramanian A P, Jaganathan S K, Supriyanto E and Razak S I A 2015 An insight on electrospun-nanofibers-inspired modern drug delivery system in the treatment of deadly cancers *RSC Adv.* **5** 57984–8004
- [10] Wang C, Wang J, Zeng L, Qiao Z, Liu X, Liu H, Zhang J and Ding J 2019 Fabrication of Electrospun Polymer Nanofibers with Diverse Morphologies *Molecules* **24** 834
- [11] Yu D-G, Yang C, Jin M, Williams G R, Zou H, Wang X and Annie Bligh S W 2016 Medicated Janus fibers fabricated using a Teflon-coated side-by-side spinneret *Colloids Surf. B Biointerfaces* **138** 110–6
- [12] Hu J, Prabhakaran M P, Tian L, Ding X and Ramakrishna S 2015 Drug-loaded emulsion electrospun nanofibers: characterization, drug release and in vitro biocompatibility *RSC Adv.* **5** 100256–67
- [13] Zhang C, Feng F and Zhang H 2018 Emulsion electrospinning: Fundamentals, food applications and prospects *Trends Food Sci. Technol.* **80** 175–86
- [14] Agarwal S, Burgard M, Greiner A and Wendorff J H 2016 *Electrospinning: a practical guide to nanofibers* (Berlin Boston: De Gruyter)
- [15] El Fawal G 2019 Polymer nanofibers electrospinning: A review *Egypt. J. Chem.* **0** 0–0
- [16] Agarwal S and Greiner A 2011 On the way to clean and safe electrospinning-green electrospinning: emulsion and suspension electrospinning: On the way to clean and safe electrospinning *Polym. Adv. Technol.* **22** 372–8
- [17] Sun J, Bubel K, Chen F, Kissel T, Agarwal S and Greiner A 2010 Nanofibers by Green Electrospinning of Aqueous Suspensions of Biodegradable Block Copolyesters for Applications in Medicine, Pharmacy and Agriculture: Nanofibers by Green Electrospinning of Aqueous Suspensions ... *Macromol. Rapid Commun.* **31** 2077–83

- [18] Beck-Broichsitter M, Thieme M, Nguyen J, Schmehl T, Gessler T, Seeger W, Agarwal S, Greiner A and Kissel T 2010 Novel ‘Nano in Nano’ Composites for Sustained Drug Delivery: Biodegradable Nanoparticles Encapsulated into Nanofiber Non-Wovens *Macromol. Biosci.* **10** 1527–35
- [19] Sun Z, Zussman E, Yarin A L, Wendorff J H and Greiner A 2003 Compound Core–Shell Polymer Nanofibers by Co-Electrospinning *Adv. Mater.* **15** 1929–32
- [20] Moghe A K and Gupta B S 2008 Co-axial Electrospinning for Nanofiber Structures: Preparation and Applications *Polym. Rev.* **48** 353–77
- [21] Pant B, Park M and Park S-J 2019 Drug Delivery Applications of Core-Sheath Nanofibers Prepared by Coaxial Electrospinning: A Review *Pharmaceutics* **11** 305
- [22] He M, Jiang H, Wang R, Xie Y and Zhao C 2017 Fabrication of metronidazole loaded poly ( $\epsilon$ -caprolactone)/zein core/shell nanofiber membranes via coaxial electrospinning for guided tissue regeneration *J. Colloid Interface Sci.* **490** 270–8
- [23] Yarin A L, Zussman E, Wendorff J H and Greiner A 2007 Material encapsulation and transport in core–shell micro/nanofibers, polymer and carbon nanotubes and micro/nanochannels *J Mater Chem* **17** 2585–99
- [24] Qin X 2017 Coaxial electrospinning of nanofibers *Electrospun Nanofibers* (Elsevier) pp 41–71
- [25] He C, Huang Z, Han X, Liu L, Zhang H and Chen L 2006 Coaxial Electrospun Poly(L -Lactic Acid) Ultrafine Fibers for Sustained Drug Delivery *J. Macromol. Sci. Part B* **45** 515–24
- [26] Jiang H, Hu Y, Li Y, Zhao P, Zhu K and Chen W 2005 A facile technique to prepare biodegradable coaxial electrospun nanofibers for controlled release of bioactive agents *J. Controlled Release* **108** 237–43
- [27] Zhang Y Z, Venugopal J, Huang Z-M, Lim C T and Ramakrishna S 2005 Characterization of the Surface Biocompatibility of the Electrospun PCL–Collagen Nanofibers Using Fibroblasts *Biomacromolecules* **6** 2583–9
- [28] Song T, Zhang Y Z and Zhou T J 2006 Fabrication of magnetic composite nanofibers of poly( $\epsilon$ -caprolactone) with FePt nanoparticles by coaxial electrospinning *J. Magn. Magn. Mater.* **303** e286–9
- [29] Ranjbar-Mohammadi M, Zamani M, Prabhakaran M P, Bahrami S H and Ramakrishna S 2016 Electrospinning of PLGA/gum tragacanth nanofibers containing tetracycline hydrochloride for periodontal regeneration *Mater. Sci. Eng. C* **58** 521–31
- [30] Indurkha A, Patel M, Sharma P, Abed S N, Shnoudeh A, Maheshwari R, Deb P K and Tekade R K 2018 Influence of Drug Properties and Routes of Drug Administration on the Design of Controlled Release System *Dosage Form Design Considerations* (Elsevier) pp 179–223
- [31] Fredenberg S, Wahlgren M, Reslow M and Axelsson A 2011 The mechanisms of drug release in poly(lactic-co-glycolic acid)-based drug delivery systems—A review *Int. J. Pharm.* **415** 34–52
- [32] Jain D, Raturi R, Jain V, Bansal P and Singh R 2011 Recent technologies in pulsatile drug delivery systems *Biomatter* **1** 57–65
- [33] Wong H M, Wang J J and Wang C-H 2001 In Vitro Sustained Release of Human Immunoglobulin G from Biodegradable Microspheres *Ind. Eng. Chem. Res.* **40** 933–48
- [34] Kim H K, Chung H J and Park T G 2006 Biodegradable polymeric microspheres with “open/closed” pores for sustained release of human growth hormone *J. Controlled Release* **112** 167–74
- [35] Sun Y, Wang J, Zhang X, Zhang Z, Zheng Y, Chen D and Zhang Q 2008 Synchronic release of two hormonal contraceptives for about one month from the PLGA microspheres: In vitro and in vivo studies *J. Controlled Release* **129** 192–9
- [36] Bishara A and Domb A J 2005 PLA stereocomplexes for controlled release of

- somatostatin analogue *J. Controlled Release* **107** 474–83
- [37] Shah S S, Cha Y and Pitt C G 1992 Poly (glycolic acid-co-dl-lactic acid): diffusion or degradation controlled drug delivery? *J. Controlled Release* **18** 261–70
- [38] Jonnalagadda S and Robinson D H 2000 A bioresorbable, polylactide reservoir for diffusional and osmotically controlled drug delivery *AAPS PharmSciTech* **1** 26–34
- [39] Mochizuki A, Niikawa T, Omura I and Yamashita S 2008 Controlled release of argatroban from PLA film—Effect of hydroxyesters as additives on enhancement of drug release *J. Appl. Polym. Sci.* **108** 3353–60
- [40] Fonseca C, Simões S and Gaspar R 2002 Paclitaxel-loaded PLGA nanoparticles: preparation, physicochemical characterization and in vitro anti-tumoral activity *J. Controlled Release* **83** 273–86
- [41] Manuela Gaspar M, Blanco D, Cruz M E M and José Alonso M 1998 Formulation of l-asparaginase-loaded poly(lactide-co-glycolide) nanoparticles: influence of polymer properties on enzyme loading, activity and in vitro release *J. Controlled Release* **52** 53–62
- [42] Zhu G, Mallery S R and Schwendeman S P 2000 Stabilization of proteins encapsulated in injectable poly (lactide- co-glycolide) *Nat. Biotechnol.* **18** 52–7
- [43] Gagliardi M, Silvestri D, Cristallini C, Guadagni M, Crifaci G and Giusti P 2010 Combined drug release from biodegradable bilayer coating for endovascular stents *J. Biomed. Mater. Res. B Appl. Biomater.* **93B** 375–85
- [44] Park T G 1995 Degradation of poly(lactic-co-glycolic acid) microspheres: effect of copolymer composition *Biomaterials* **16** 1123–30
- [45] Matsumoto A, Matsukawa Y, Horikiri Y and Suzuki T 2006 Rupture and drug release characteristics of multi-reservoir type microspheres with poly(dl-lactide-co-glycolide) and poly(dl-lactide) *Int. J. Pharm.* **327** 110–6
- [46] Friess W and Schlapp M 2002 Release mechanisms from gentamicin loaded poly(lactic-co-glycolic acid) (PLGA) microparticles *J. Pharm. Sci.* **91** 845–55
- [47] Kamaly N, Yameen B, Wu J and Farokhzad O C 2016 Degradable Controlled-Release Polymers and Polymeric Nanoparticles: Mechanisms of Controlling Drug Release *Chem. Rev.* **116** 2602–63
- [48] Siepmann J, Siegel R A and Siepmann F 2012 Diffusion Controlled Drug Delivery Systems *Fundamentals and Applications of Controlled Release Drug Delivery* ed J Siepmann, R A Siegel and M J Rathbone (Boston, MA: Springer US) pp 127–52
- [49] Blasi P, D’Souza S S, Selmin F and DeLuca P P 2005 Plasticizing effect of water on poly(lactide-co-glycolide) *J. Controlled Release* **108** 1–9
- [50] Chen X, Ooi C P and Lim T H 2006 Effect of Ganciclovir on the Hydrolytic Degradation of Poly(lactide-co-glycolide) Microspheres *J. Biomater. Appl.* **20** 287–302
- [51] Zolnik B S, Leary P E and Burgess D J 2006 Elevated temperature accelerated release testing of PLGA microspheres *J. Controlled Release* **112** 293–300
- [52] Chung T-W, Tsai Y-L, Hsieh J-H and Tsai W-J 2006 Different ratios of lactide and glycolide in PLGA affect the surface property and protein delivery characteristics of the PLGA microspheres with hydrophobic additives *J. Microencapsul.* **23** 15–27
- [53] Wang L, Venkatraman S and Kleiner L 2004 Drug release from injectable depots: two different in vitro mechanisms *J. Controlled Release* **99** 207–16
- [54] Faisant N, Siepmann J and Benoit J P 2002 PLGA-based microparticles: elucidation of mechanisms and a new, simple mathematical model quantifying drug release *Eur. J. Pharm. Sci.* **15** 355–66
- [55] Aderibigbe B 2017 Design of Drug Delivery Systems Containing Artemisinin and Its Derivatives *Molecules* **22** 323
- [56] Ekladios I, Colson Y L and Grinstaff M W 2019 Polymer–drug conjugate therapeutics: advances, insights and prospects *Nat. Rev. Drug Discov.* **18** 273–94
- [57] Cai H, Wang X, Zhang H, Sun L, Pan D, Gong Q, Gu Z and Luo K 2018 Enzyme-

sensitive biodegradable and multifunctional polymeric conjugate as theranostic nanomedicine *Appl. Mater. Today* **11** 207–18

[58] Wang D, Li H, Gu J, Guo T, Yang S, Guo Z, Zhang X, Zhu W and Zhang J 2013 Ternary system of dihydroartemisinin with hydroxypropyl- $\beta$ -cyclodextrin and lecithin: Simultaneous enhancement of drug solubility and stability in aqueous solutions *J. Pharm. Biomed. Anal.* **83** 141–8

[59] Torchilin V P 2006 *Nanoparticulates as drug carriers* (London : Hackensack, N.J: Imperial College Press ; Distributed by World Scientific Pub)

[60] Wang Z, Yu Y, Ma J, Zhang H, Zhang H, Wang X, Wang J, Zhang X and Zhang Q 2012 LyP-1 Modification To Enhance Delivery of Artemisinin or Fluorescent Probe Loaded Polymeric Micelles to Highly Metastatic Tumor and Its Lymphatics *Mol. Pharm.* **9** 2646–57

[61] Mvango S, Matshe W M R, Balogun A O, Pilcher L A and Balogun M O 2018 Nanomedicines for Malaria Chemotherapy: Encapsulation vs. Polymer Therapeutics *Pharm. Res.* **35** 237

[62] Isacchi B, Arriguucci S, Marca G la, Bergonzi M C, Vannucchi M G, Novelli A and Bilia A R 2011 Conventional and long-circulating liposomes of artemisinin: preparation, characterization, and pharmacokinetic profile in mice *J. Liposome Res.* **21** 237–44

[63] Chen Y, Lin X, Park H and Greever R 2009 Study of artemisinin nanocapsules as anticancer drug delivery systems *Nanomedicine Nanotechnol. Biol. Med.* **5** 316–22

[64] Xiao X and Hong Z 2010 Firstborn microcrystallization method to prepare nanocapsules containing artesunate *Int. J. Nanomedicine* 483

[65] Soppimath K S, Aminabhavi T M, Kulkarni A R and Rudzinski W E 2001 Biodegradable polymeric nanoparticles as drug delivery devices *J. Controlled Release* **70** 1–20

[66] Gathirwa J W, Omwoyo W, Ogutu B, Oloo F, Swai H, Kalombo L, Melariri P and Maroa G 2014 Preparation, characterization, and optimization of primaquine-loaded solid lipid nanoparticles *Int. J. Nanomedicine* 3865

[67] Dwivedi A, Mazumder A, du Plessis L, du Preez J L, Haynes R K and du Plessis J 2015 In vitro anti-cancer effects of artemisone nano-vesicular formulations on melanoma cells *Nanomedicine Nanotechnol. Biol. Med.* **11** 2041–50

[68] Murakami H, Kobayashi M, Takeuchi H and Kawashima Y 1999 Preparation of poly(dl-lactide-co-glycolide) nanoparticles by modified spontaneous emulsification solvent diffusion method *Int. J. Pharm.* **187** 143–52

[69] Martínez Rivas C J, Tarhini M, Badri W, Miladi K, Greige-Gerges H, Nazari Q A, Galindo Rodríguez S A, Román R Á, Fessi H and Elaissari A 2017 Nanoprecipitation process: From encapsulation to drug delivery *Int. J. Pharm.* **532** 66–81

[70] Golenser J, Buchholz V, Bagheri A, Nasereddin A, Dzikowski R, Guo J, Hunt N H, Eyal S, Vakruk N and Greiner A 2017 Controlled release of artemisone for the treatment of experimental cerebral malaria *Parasit. Vectors* **10** 117

[71] Nguyen H T, Tran T H, Kim J O, Yong C S and Nguyen C N 2015 Enhancing the in vitro anti-cancer efficacy of artesunate by loading into poly-d,l-lactide-co-glycolide (PLGA) nanoparticles *Arch. Pharm. Res.* **38** 716–24

[72] Tsuchida K and Murakami T 2008 Recent Advances in Inorganic Nanoparticle-Based Drug Delivery Systems *Mini-Rev. Med. Chem.* **8** 175–83

[73] Chen J, Guo Z, Wang H-B, Zhou J-J, Zhang W-J and Chen Q-W 2014 Multifunctional mesoporous nanoparticles as pH-responsive Fe<sup>2+</sup> reservoirs and artemisinin vehicles for synergistic inhibition of tumor growth *Biomaterials* **35** 6498–507

[74] Ding C and Li Z 2017 A review of drug release mechanisms from nanocarrier systems *Mater. Sci. Eng. C* **76** 1440–53

[75] Sahoo N G, Abbas A, Judeh Z, Li C M and Yuen K-H 2009 Solubility Enhancement of a Poorly Water-Soluble Anti-Malarial Drug: Experimental Design and Use of a Modified

Multifluid Nozzle Pilot Spray Drier *J. Pharm. Sci.* **98** 281–96

[76] Fessi H, Puisieux F, Devissaguet J Ph, Ammoury N and Benita S 1989 Nanocapsule formation by interfacial polymer deposition following solvent displacement *Int. J. Pharm.* **55** R1–4

[77] Pinto Reis C, Neufeld R J, Ribeiro, A J and Veiga F 2006 Nanoencapsulation I. Methods for preparation of drug-loaded polymeric nanoparticles *Nanomedicine Nanotechnol. Biol. Med.* **2** 8–21

[78] Avgoustakis K 2004 Pegylated Poly(Lactide) and Poly(Lactide-Co-Glycolide) Nanoparticles: Preparation, Properties and Possible Applications in Drug Delivery *Curr. Drug Deliv.* **1** 321–33

[79] Badri W, Miladi K, Nazari Q A, Fessi H and Elaissari A 2017 Effect of process and formulation parameters on polycaprolactone nanoparticles prepared by solvent displacement *Colloids Surf. Physicochem. Eng. Asp.* **516** 238–44

[80] Mora-Huertas C E, Fessi H and Elaissari A 2011 Influence of process and formulation parameters on the formation of submicron particles by solvent displacement and emulsification–diffusion methods *Adv. Colloid Interface Sci.* **163** 90–122

[81] Budhian A, Siegel S J and Winey K I 2007 Haloperidol-loaded PLGA nanoparticles: Systematic study of particle size and drug content *Int. J. Pharm.* **336** 367–75

[82] Draheim C, de Crécy F, Hansen S, Collnot E-M and Lehr C-M 2015 A Design of Experiment Study of Nanoprecipitation and Nano Spray Drying as Processes to Prepare PLGA Nano- and Microparticles with Defined Sizes and Size Distributions *Pharm. Res.*

[83] Hans M L and Lowman A M 2002 Biodegradable nanoparticles for drug delivery and targeting *Curr. Opin. Solid State Mater. Sci.* **6** 319–27

[84] Hernández-Giottonini K Y, Rodríguez-Córdova R J, Gutiérrez-Valenzuela C A, Peñuñuri-Miranda O, Zavala-Rivera P, Guerrero-Germán P and Lucero-Acuña A 2020 PLGA nanoparticle preparations by emulsification and nanoprecipitation techniques: effects of formulation parameters *RSC Adv.* **10** 4218–31

[85] Ali H, Kalashnikova I, White M A, Sherman M and Rytting E 2013 Preparation, characterization, and transport of dexamethasone-loaded polymeric nanoparticles across a human placental in vitro model *Int. J. Pharm.* **454** 149–57

[86] Şimşek S, Eroğlu H, Kurum B and Ulubayram K 2013 Brain targeting of Atorvastatin loaded amphiphilic PLGA-b-PEG nanoparticles *J. Microencapsul.* **30** 10–20

[87] Dong Y and Feng S-S 2007 In vitro and in vivo evaluation of methoxy polyethylene glycol–polylactide (MPEG–PLA) nanoparticles for small-molecule drug chemotherapy *Biomaterials* **28** 4154–60

[88] Chorny M, Fishbein I, Danenberg H D and Golomb G 2002 Lipophilic drug loaded nanospheres prepared by nanoprecipitation: effect of formulation variables on size, drug recovery and release kinetics *J. Controlled Release* **83** 389–400

[89] Khayata N, Abdelwahed W, Chehna M F, Charcosset C and Fessi H 2012 Preparation of vitamin E loaded nanocapsules by the nanoprecipitation method: From laboratory scale to large scale using a membrane contactor *Int. J. Pharm.* **423** 419–27

[90] Govender T 1999 PLGA nanoparticles prepared by nanoprecipitation: drug loading and release studies of a water soluble drug *J. Controlled Release* **57** 171–85

[91] Stainmesse S, Orecchioni A-M, Nakache E, Puisieux F and Fessi H 1995 Formation and stabilization of a biodegradable polymeric colloidal suspension of nanoparticles *Colloid Polym. Sci.* **273** 505–11

[92] Nehilla B, Bergkvist M, Popat K and Desai T 2008 Purified and surfactant-free coenzyme Q10-loaded biodegradable nanoparticles *Int. J. Pharm.* **348** 107–14

[93] Limayem Blouza I, Charcosset C, Sfar S and Fessi H 2006 Preparation and characterization of spironolactone-loaded nanocapsules for paediatric use *Int. J. Pharm.* **325** 124–31

- [94] Guhagarkar S A, Malshe V C and Devarajan P V 2009 Nanoparticles of Polyethylene Sebacate: A New Biodegradable Polymer *AAPS PharmSciTech* **10** 935
- [95] Asadi H, Rostamizadeh K, Salari D and Hamidi M 2011 Preparation of biodegradable nanoparticles of tri-block PLA–PEG–PLA copolymer and determination of factors controlling the particle size using artificial neural network *J. Microencapsul.* **28** 406–16
- [96] Galindo-Rodríguez S A, Puel F, Briançon S, Allémann E, Doelker E and Fessi H 2005 Comparative scale-up of three methods for producing ibuprofen-loaded nanoparticles *Eur. J. Pharm. Sci.* **25** 357–67
- [97] Chacón M, Molpeceres J, Berges L, Guzmán M and Aberturas M R 1999 Stability and freeze-drying of cyclosporine loaded poly(D,L lactide–glycolide) carriers *Eur. J. Pharm. Sci.* **8** 99–107
- [98] Li X, Anton N, Arpagaus C, Belleiteix F and Vandamme T F 2010 Nanoparticles by spray drying using innovative new technology: The Büchi Nano Spray Dryer B-90 *J. Controlled Release* **147** 304–10
- [99] Mu L and Feng S S 2001 Fabrication, characterization and in vitro release of paclitaxel (Taxol®) loaded poly (lactic-co-glycolic acid) microspheres prepared by spray drying technique with lipid/cholesterol emulsifiers *J. Controlled Release* **76** 239–54
- [100] Salama A H 2020 Spray drying as an advantageous strategy for enhancing pharmaceuticals bioavailability *Drug Deliv. Transl. Res.* **10** 1–12
- [101] Schafroth N, Arpagaus C, Jadhav U Y, Makne S and Douroumis D 2012 Nano and microparticle engineering of water insoluble drugs using a novel spray-drying process *Colloids Surf. B Biointerfaces* **90** 8–15
- [102] Tonon R V, Grosso C R F and Hubinger M D 2011 Influence of emulsion composition and inlet air temperature on the microencapsulation of flaxseed oil by spray drying *Food Res. Int.* **44** 282–9
- [103] Rattes A L R and Oliveira W P 2007 Spray drying conditions and encapsulating composition effects on formation and properties of sodium diclofenac microparticles *Powder Technol.* **171** 7–14
- [104] Ré M-I 2006 Formulating Drug Delivery Systems by Spray Drying *Dry. Technol.* **24** 433–46
- [105] Yamamoto H, Hoshina W, Kurashima H, Takeuchi H, Kawashima Y, Yokoyama T and Tsujimoto H 2007 Engineering of poly(DL-lactic-co-glycolic acid) nanocomposite particles for dry powder inhalation dosage forms of insulin with the spray-fluidized bed granulating system *Adv. Powder Technol.* **18** 215–28
- [106] Fatnassi M, Jacquart S, Brouillet F, Rey C, Combes C and Girod Fullana S 2014 Optimization of spray-dried hyaluronic acid microspheres to formulate drug-loaded bone substitute materials *Powder Technol.* **255** 44–51
- [107] Rivera P A, Martinez-Oharriz M C, Rubio M, Irache J M and Espuelas S 2004 Fluconazole encapsulation in PLGA microspheres by spray-drying *J. Microencapsul.* **21** 203–11
- [108] Ho H and Lee J 2012 Redispersible drug nanoparticles prepared without dispersant by electro-spray drying *Drug Dev. Ind. Pharm.* **38** 744–51
- [109] Linke A, Linke T, Hinrichs J and Kohlbus R 2021 Factors determining the surface oil concentration of encapsulated lipid particles—impact of the spray drying conditions *Dry. Technol.* **39** 173–86
- [110] Fu Y-J, Shyu S-S, Su F-H and Yu P-C 2002 Development of biodegradable copoly(D,L-lactic/glycolic acid) microspheres for the controlled release of 5-FU by the spray drying method *Colloids Surf. B Biointerfaces* **25** 269–79
- [111] Islam Shishir M R, Taip F S, Aziz N Ab, Talib R A and Hossain Sarker Md S 2016 Optimization of spray drying parameters for pink guava powder using RSM *Food Sci. Biotechnol.* **25** 461–8

- [112] Marconi G, Monti S, Manoli F, Degli Esposti A and Mayer B 2004 A circular dichroism and structural study of the inclusion complex artemisinin- $\beta$ -cyclodextrin *Chem. Phys. Lett.* **383** 566–71
- [113] Steyn J D, Wiesner L, du Plessis L H, Grobler A F, Smith P J, Chan W-C, Haynes R K and Kotzé A F 2011 Absorption of the novel artemisinin derivatives artemisone and artemiside: Potential application of Pheroid™ technology *Int. J. Pharm.* **414** 260–6
- [114] Huang G 2017 Inclusion Complex of Artemether with 2-Hydroxypropyl - $\beta$ -Cyclodextrin for the Treatment of Malaria: Preparation, Characterization and Evaluation *MOJ Bioequivalence Bioavailab.* **3**
- [115] Gemma S, Travagli V, Savini L, Novellino E, Campiani G and Butini S 2010 Malaria Chemotherapy: Recent Advances in Drug Development *Recent Patents Anti-Infect. Drug Disc.* **5** 195–225
- [116] Lung, Chung Man *Decomposition of current clinically-used artemisinin derivatives and preparation of polar artemisinin derivatives*
- [117] Anon CDC - Malaria - About Malaria - Where Malaria Occurs. Available online: <https://www.cdc.gov/malaria/about/distribution.html> (accessed on 22 June 2021).
- [118] Anon Anopheles Stechmücke - Überträger der Malaria. Available online: <https://www.malaria.info/anopheles/> (accessed on 22 June 2021).
- [119] Waknine-Grinberg J H, Hunt N, Bentura-Marciano A, McQuillan J A, Chan H-W, Chan W-C, Barenholz Y, Haynes R K and Golenser J 2010 Artemisone effective against murine cerebral malaria *Malar. J.* **9** 227
- [120] Guo Z 2016 Artemisinin anti-malarial drugs in China *Acta Pharm. Sin. B* **6** 115–24
- [121] Haynes R K, Fugmann B, Stetter J, Rieckmann K, Heilmann H-D, Chan H-W, Cheung M-K, Lam W-L, Wong H-N, Croft S L, Vivas L, Rattray L, Stewart L, Peters W, Robinson B L, Edstein M D, Kotecka B, Kyle D E, Beckermann B, Gerisch M, Radtke M, Schmuck G, Steinke W, Wollborn U, Schmeer K and Römer A 2006 Artemisone—A Highly Active Antimalarial Drug of the Artemisinin Class *Angew. Chem. Int. Ed.* **45** 2082–8
- [122] Septembre-Malaterre A, Lalarizo Rakoto M, Marodon C, Bedoui Y, Nakab J, Simon E, Hoarau L, Savriama S, Strasberg D, Guiraud P, Selambarom J and Gasque P 2020 *Artemisia annua*, a Traditional Plant Brought to Light *Int. J. Mol. Sci.* **21** 4986
- [123] Li Z, Li Q, Wu J, Wang M and Yu J 2016 Artemisinin and Its Derivatives as a Repurposing Anticancer Agent: What Else Do We Need to Do? *Molecules* **21** 1331
- [124] van Zyl L, Viljoen J M, Haynes R K, Aucamp M, Ngwane A H and du Plessis J 2019 Topical Delivery of Artemisone, Clofazimine and Decoquinat Encapsulated in Vesicles and Their In vitro Efficacy Against Mycobacterium tuberculosis *AAPS PharmSciTech* **20** 33
- [125] Bagheri A R, Agarwal S, Golenser J and Greiner A 2017 Unlocking Nanocarriers for the Programmed Release of Antimalarial Drugs *Glob. Chall.* **1** 1600011
- [126] Anon Wu, W.K. *Preparation of polar artemisinins for cerebral malaria and model mechanistic studies*, 2010
- [127] Sosnik A and Seremeta K P 2015 Advantages and challenges of the spray-drying technology for the production of pure drug particles and drug-loaded polymeric carriers *Adv. Colloid Interface Sci.* **223** 40–54
- [128] Kohane D S 2007 Microparticles and nanoparticles for drug delivery *Biotechnol. Bioeng.* **96** 203–9
- [129] Klemm D, Heublein B, Fink H-P and Bohn A 2005 Cellulose: Fascinating Biopolymer and Sustainable Raw Material *Angew. Chem. Int. Ed.* **44** 3358–93
- [130] Delidovich I, Hausoul P J C, Deng L, Pfützenreuter R, Rose M and Palkovits R 2016 Alternative Monomers Based on Lignocellulose and Their Use for Polymer Production *Chem. Rev.* **116** 1540–99
- [131] Putro J N, Soetaredjo F E, Lin S-Y, Ju Y-H and Ismadji S 2016 Pretreatment and conversion of lignocellulose biomass into valuable chemicals *RSC Adv.* **6** 46834–52



- [132] Rose M and Palkovits R 2011 Cellulose-Based Sustainable Polymers: State of the Art and Future Trends: Cellulose-Based Sustainable Polymers ... *Macromol. Rapid Commun.* **32** 1299–311
- [133] Dwyer R and Abel S 1986 The Efficiencies of Cellulose Acetate Filters *Beitr. Zur Tab. Int. Tob. Res.* **13** 243–53
- [134] Edgar K J, Buchanan C M, Debenham J S, Rundquist P A, Seiler B D, Shelton M C and Tindall D 2001 Advances in cellulose ester performance and application *Prog. Polym. Sci.* **26** 1605–88
- [135] Doshi J and Reneker D H 1995 Electrospinning process and applications of electrospun fibers *J. Electrostat.* **35** 151–60
- [136] McCormick C L and Dawsey T R 1990 Preparation of cellulose derivatives via ring-opening reactions with cyclic reagents in lithium chloride/N,N-dimethylacetamide *Macromolecules* **23** 3606–10
- [137] Fink H-P, Weigel P, Purz H J and Ganster J 2001 Structure formation of regenerated cellulose materials from NMMO-solutions *Prog. Polym. Sci.* **26** 1473–524
- [138] Hasegawa M, Isogai A, Onabe F and Usuda M 1992 Dissolving states of cellulose and chitosan in trifluoroacetic acid *J. Appl. Polym. Sci.* **45** 1857–63
- [139] Ohkawa K, Hayashi S, Nishida A, Yamamoto H and Ducreux J 2009 Preparation of Pure Cellulose Nanofiber via Electrospinning *Text. Res. J.* **79** 1396–401
- [140] Thomas Heinze, René Dicke, Andreas Koschella, Arne Henning Kull, Erik-Andreas Klohr, Wolfgang Koch Effective preparation of cellulose derivatives in a new simple cellulose solvent
- [141] Kim C-W, Kim D-S, Kang S-Y, Marquez M and Joo Y L 2006 Structural studies of electrospun cellulose nanofibers *Polymer* **47** 5097–107
- [142] Kim C-W, Frey M W, Marquez M and Joo Y L 2005 Preparation of submicron-scale, electrospun cellulose fibers via direct dissolution *J. Polym. Sci. Part B Polym. Phys.* **43** 1673–83
- [143] Welton T 1999 Room-Temperature Ionic Liquids. Solvents for Synthesis and Catalysis *Chem. Rev.* **99** 2071–84
- [144] Hallett J P and Welton T 2011 Room-Temperature Ionic Liquids: Solvents for Synthesis and Catalysis. 2 *Chem. Rev.* **111** 3508–76
- [145] Swatloski R P, Spear S K, Holbrey J D and Rogers R D 2002 Dissolution of Cellose with Ionic Liquids *J. Am. Chem. Soc.* **124** 4974–5
- [146] Freire M G, Teles A R R, Ferreira R A S, Carlos L D, Lopes-da-Silva J A and Coutinho J A P 2011 Electrospun nanosized cellulose fibers using ionic liquids at room temperature *Green Chem.* **13** 3173
- [147] Viswanathan G, Murugesan S, Pushparaj V, Nalamasu O, Ajayan P M and Linhardt R J 2006 Preparation of Biopolymer Fibers by Electrospinning from Room Temperature Ionic Liquids *Biomacromolecules* **7** 415–8
- [148] Xu S, Zhang J, He A, Li J, Zhang H and Han C C 2008 Electrospinning of native cellulose from nonvolatile solvent system *Polymer* **49** 2911–7
- [149] Clough M T, Geyer K, Hunt P A, Son S, Vagt U and Welton T 2015 Ionic liquids: not always innocent solvents for cellulose *Green Chem.* **17** 231–43
- [150] Gericke M, Fardim P and Heinze T 2012 Ionic Liquids — Promising but Challenging Solvents for Homogeneous Derivatization of Cellulose *Molecules* **17** 7458–502
- [151] Ebner G, Schiehser S, Potthast A and Rosenau T 2008 Side reaction of cellulose with common 1-alkyl-3-methylimidazolium-based ionic liquids *Tetrahedron Lett.* **49** 7322–4
- [152] Anon Formhals A (1938) Electrical spinning of fibers from solutions (U.S. Patent 2123992)
- [153] Son W K, Youk J H, Lee T S and Park W H 2004 Electrospinning of ultrafine cellulose acetate fibers: Studies of a new solvent system and deacetylation of ultrafine

- cellulose acetate fibers *J. Polym. Sci. Part B Polym. Phys.* **42** 5–11
- [154] Frenot A, Henriksson M W and Walkenström P 2007 Electrospinning of cellulose-based nanofibers *J. Appl. Polym. Sci.* **103** 1473–82
- [155] Jessop P G, Heldebrant D J, Li X, Eckert C A and Liotta C L 2005 Reversible nonpolar-to-polar solvent *Nature* **436** 1102–1102
- [156] Onwukamike K N, Tassaing T, Grelier S, Grau E, Cramail H and Meier M A R 2018 Detailed Understanding of the DBU/CO<sub>2</sub> Switchable Solvent System for Cellulose Solubilization and Derivatization *ACS Sustain. Chem. Eng.* **6** 1496–503
- [157] Söyler Z, Onwukamike K N, Grelier S, Grau E, Cramail H and Meier M A R 2018 Sustainable succinylation of cellulose in a CO<sub>2</sub>-based switchable solvent and subsequent Passerini 3-CR and Ugi 4-CR modification *Green Chem.* **20** 214–24
- [158] Onwukamike K N, Grelier S, Grau E, Cramail H and Meier M A R 2018 Sustainable Transesterification of Cellulose with High Oleic Sunflower Oil in a DBU-CO<sub>2</sub> Switchable Solvent *ACS Sustain. Chem. Eng.* **6** 8826–35
- [159] Heidari M, Bahrami H and Ranjbar-Mohammadi M 2017 Fabrication, optimization and characterization of electrospun poly(caprolactone)/gelatin/graphene nanofibrous mats *Mater. Sci. Eng. C* **78** 218–29
- [160] Tan T B, Yussof N S, Abas F, Mirhosseini H, Nehdi I A and Tan C P 2016 Forming a lutein nanodispersion via solvent displacement method: The effects of processing parameters and emulsifiers with different stabilizing mechanisms *Food Chem.* **194** 416–23
- [161] Yu H, Zhao X, Zu Y, Zhang X, Zu B and Zhang X 2012 Preparation and Characterization of Micronized Artemisinin via a Rapid Expansion of Supercritical Solutions (RESS) Method *Int. J. Mol. Sci.* **13** 5060–73
- [162] Anwer K, Mohammad M, Ezzeldin E, Fatima F, Alalaiwe A and Iqbal M 2019 Preparation of sustained release apremilast-loaded PLGA nanoparticles: in vitro characterization and in vivo pharmacokinetic study in rats *Int. J. Nanomedicine* **Volume 14** 1587–95
- [163] Blanco-Prieto M J, Besseghir K, Zerbe O, Andris D, Orsolini P, Heimgartner F, Merkle H P and Gander B 2000 In vitro and in vivo evaluation of a somatostatin analogue released from PLGA microspheres *J. Controlled Release* **67** 19–28
- [164] Toro-Sierra J, Schumann J and Kulozik U 2013 Impact of spray-drying conditions on the particle size of microparticulated whey protein fractions *Dairy Sci. Technol.* **93** 487–503
- [165] Lavanya M N, Kathiravan T, Moses J A and Anandharamakrishnan C 2020 Influence of spray-drying conditions on microencapsulation of fish oil and chia oil *Dry. Technol.* **38** 279–92
- [166] Blanco M D, Sastre R L, Teijón C, Olmo R and Teijón J M 2005 5-Fluorouracil-loaded microspheres prepared by spray-drying poly(D,L-lactide) and poly(lactide-co-glycolide) polymers: Characterization and drug release *J. Microencapsul.* **22** 671–82
- [167] Lebhardt T, Roesler S, Uusitalo H P and Kissel T 2011 Surfactant-free redispersible nanoparticles in fast-dissolving composite microcarriers for dry-powder inhalation *Eur. J. Pharm. Biopharm.* **78** 90–6
- [168] Heidari M, Bahrami S H, Ranjbar-Mohammadi M and Milan P B 2019 Smart electrospun nanofibers containing PCL/gelatin/graphene oxide for application in nerve tissue engineering *Mater. Sci. Eng. C* **103** 109768
- [169] Rengifo A F C, Stefanos N M, Toigo J, Mendes C, Argenta D F, Dotto M E R, Santos da Silva M C, Nunes R J, Caon T, Parize A L and Minatti E 2019 PEO-chitosan nanofibers containing carboxymethyl-hexanoyl chitosan/dodecyl sulfate nanoparticles loaded with pyrazoline for skin cancer treatment *Eur. Polym. J.* **119** 335–43
- [170] Liu W, Wei J and Chen Y 2014 Electrospun poly(L-lactide) nanofibers loaded with paclitaxel and water-soluble fullerenes for drug delivery and bioimaging *New J Chem* **38** 6223–9

- [171] Okuda T, Tominaga K and Kidoaki S 2010 Time-programmed dual release formulation by multilayered drug-loaded nanofiber meshes *J. Controlled Release* **143** 258–64
- [172] Xie H, Yu X, Yang Y and Zhao Z K 2014 Capturing CO<sub>2</sub> for cellulose dissolution *Green Chem* **16** 2422–7
- [173] Ku, Min Kyung, Park, Hyunkyu and Kim, Hyungsup 2013 전기분무 기술을 이용한 셀룰로스 입자 제조 한국섬유공학회지 **50** 187–92
- [174] Chin S F, Jimmy F B and Pang S C 2018 Size controlled fabrication of cellulose nanoparticles for drug delivery applications *J. Drug Deliv. Sci. Technol.* **43** 262–6
- [175] Heidari M, Onwukamike K N, Grau E, Grelier S, Cramail H, Meier M A R and Greiner A 2021 Direct electrospinning of cellulose in the DBU-CO<sub>2</sub> switchable solvent system *Cellulose*
- [176] Onwukamike K N, Tassaing T, Grelier S, Grau E, Cramail H and Meier M A R 2018 Detailed Understanding of the DBU/CO<sub>2</sub> Switchable Solvent System for Cellulose Solubilization and Derivatization *ACS Sustain. Chem. Eng.* **6** 1496–503
- [177] Jacobs V, Anandjiwala R D and Maaza M 2010 The influence of electrospinning parameters on the structural morphology and diameter of electrospun nanofibers *J. Appl. Polym. Sci.* **115** 3130–6
- [178] Liu Y, He J-H, Yu J and Zeng H 2008 Controlling numbers and sizes of beads in electrospun nanofibers *Polym. Int.* **57** 632–6
- [179] Zuo W, Zhu M, Yang W, Yu H, Chen Y and Zhang Y 2005 Experimental study on relationship between jet instability and formation of beaded fibers during electrospinning *Polym. Eng. Sci.* **45** 704–9

## **(Eidesstattliche) Versicherungen und Erklärungen**

(§ 9 Satz 2 Nr. 3 PromO BayNAT)

*Hiermit versichere ich eidesstattlich, dass ich die Arbeit selbstständig verfasst und keine anderen als die von mir angegebenen Quellen und Hilfsmittel benutzt habe (vgl. Art. 64 Abs. 1 Satz 6 BayHSchG).*

(§ 9 Satz 2 Nr. 3 PromO BayNAT)

*Hiermit erkläre ich, dass ich die Dissertation nicht bereits zur Erlangung eines akademischen Grades eingereicht habe und dass ich nicht bereits diese oder eine gleichartige Doktorprüfung endgültig nicht bestanden habe.*

(§ 9 Satz 2 Nr. 4 PromO BayNAT)

*Hiermit erkläre ich, dass ich Hilfe von gewerblichen Promotionsberatern bzw. -vermittlern oder ähnlichen Dienstleistern weder bisher in Anspruch genommen habe noch künftig in Anspruch nehmen werde.*

(§ 9 Satz 2 Nr. 7 PromO BayNAT)

*Hiermit erkläre ich mein Einverständnis, dass die elektronische Fassung meiner Dissertation unter Wahrung meiner Urheberrechte und des Datenschutzes einer gesonderten Überprüfung unterzogen werden kann.*

(§ 9 Satz 2 Nr. 8 PromO BayNAT)

*Hiermit erkläre ich mein Einverständnis, dass bei Verdacht wissenschaftlichen Fehlverhaltens Ermittlungen durch universitätsinterne Organe der wissenschaftlichen Selbstkontrolle stattfinden können.*

.....  
Ort, Datum, Unterschrift